Exploiting Potential Inversion for Photoinduced Charge-Accumulation in Molecular Systems

Inauguraldissertation

zur Erlangung der Würde eines Doktors der Philosophie

vorgelegt der Philosophisch-Naturwissenschaftlichen Fakultät

der Universität Basel

von

Julia Nomrowski

aus Hildesheim, Deutschland

Basel, 2018

Originaldokument gespeichert auf dem Dokumentenserver

der Universität Basel edoc.unibas.ch

Genehmigt von der Philosophisch-Naturwissenschaftlichen Fakultät auf Antrag von

Fakultätsverantwortlicher/Dissertationsleiter: Prof. Dr. Oliver S. Wenger
Koreferentin: Prof. Dr. Catherine E. Housecroft

Basel, den 14.11.2017

Prof. Dr. Martin Spiess, Dekan

Für Maurice

Acknowledgments

First of all, I would like to thank **Prof. Dr. Oliver S. Wenger** for his continuous support and encouragement throughout my PhD studies. I am grateful for the opportunity to work on such an interesting topic and I greatly appreciate the guidance and help he offered whenever needed. I could not have imagined having a better Doktorvater.

Special thanks are given to **Prof. Dr. Catherine E. Housecroft** for kindly agreeing to be my co-referee.

I sincerely thank **Prof. Dr. Christof Sparr** for chairing my examination.

Sylvie Mittelheisser and **Dr. Heinz Nadig** are thanked for measuring elemental analysis and high resolution mass spectra, respectively.

Many thanks are given to the whole **Werkstatt-team** for soldering cables, constructing LED and snap-cap vial holders, repairing pumps and everything else they take care of. I also thank **Oli Ilg** for doing such a great job. **Beatrice Erismann** and especially **Brigitte Howald** are thanked for their help in organizational and administrative matters.

Furthermore, I want to thank all past and present members of the **AK Wenger** for the terrific working atmosphere.

Special thanks are given to **Martin**, **Chris** and **Xingwei** for the helpful discussions we had, and for proof-reading my thesis, especially to **Chris,** who probably had the hardest job.

I thank **Hauke** for his company from our common first day in Basel until now, but especially during the last weeks, according to the motto 'Geteiltes Leid, ist halbes Leid'.

Michael is thanked for being such a decent and calm 'desk neighbor' for the last years.

Many thanks are given to **Mirj** for organizing BBQs, game nights, group fondue and so on, in summary, for being the 'gute Seele' of our group.

Also many thanks are given to **Svenja** for the great time we had in the lab, but also outside the university. I much enjoyed our shopping tours or T-bow sessions, and of course your delicious cakes and cookies.

Last but not least, I thank everyone who joined our fabulous Skull King breaks!

I would like to thank **Franzi**, **Karo**, **Sabrina** and **Janine** for the great time we had in Göttingen. Many thanks are given to **Clara** for everything we have experienced together during school years and on various unforgettable W:O:As. Special thanks are also given to **Maren** for her unconditional friendship for more than 25 years.

Desweiteren möchte ich mich bei den **Nordstemmern** bedanken. Mit Euch wurden die Wochenenden in der Heimat nie langweilig: Sei es auf diversen Feiern, Festivals, Hochzeiten, Straßenfesten, legendären St. Peter Urlauben, Rocknächten, Weihnachtsmärkten oder einfach beim Grillen und Wikinger-Schach spielen. Dabei danke ich natürlich auch meinen Lieblingsschwägern in spe: Zum einen **Alex** für die wunderbaren Tage auf *seinem* Garten und **Phillip** für die wunderbaren Tage auf s*einem* Garten!

Von Herzen danke ich meiner Familie für ihre uneingeschränkte Unterstützung in allem was ich tue und für ihre Motivation und Bestärkung, vor allem während der letzten Jahre. **Mom**, **Klaus**, **Isi** und **Kiki,** danke, dass ihr immer für mich da seid.

Ganz besonders bedanke ich mich bei **Maurice** für seine Liebe und Unterstützung. Danke dafür, dass Du stets hinter mir stehst und ich mich immer auf Dich verlassen kann.

Abstract

In view of the steadily growing global population and concomitant increasing energy demand, the use of alternative energy sources becomes more and more important. Although the energy demand of the next few decades could in principle be met from fossil fuels, their supply progressively decreases. Moreover, the use of fossil fuels should be decreased because their combustion has devastating consequences for the environment. Aside from threatening human heath, the release of CO_2 and other greenhouse gases contributes to global warming. For these reasons, the conversion of sunlight into useful and environmentally friendly energy has received significant attention in recent years and many research groups investigate the formation of so called solar fuels, especially from water. A major challenge of the light-driven water oxidation, or CO_2 reduction, is the transfer and accumulation of multiple redox equivalents, which are required for successful conversion.

The focus of this thesis is the development of a purely molecular system, in which multiple charges can be accumulated without the use of sacrificial agents. Dibenzo[*c*,*e*][1,2]dithiin was used as a central two-electron acceptor, the reduction of which with potential inversion should facilitate electron-accumulation. This acceptor was covalently linked to two ruthenium trisbipyridyl photosensitizers and the electron-accumulation investigated. Furthermore, this triad was extended to a pentad by attaching triarylamine groups to the bipyridine ligands of the sensitizers, which act as internal electron donors. Upon irradiation with visible light, two electrons were successfully accumulated in the triad in the presence of a sacrificial electron donor, whereas the twofold charge-separated state of the pentad is formed without the use of external reductants. The lifetime of the charge-accumulated pentad was determined to be ~100 ns. Investigations of the pentad in the presence of acid revealed that upon protonation of the thiolate groups, a stable photoproduct is formed, which does not undergo charge-recombination to the ground state. Furthermore, it was shown that both the triad and pentad can be used as multi-electron photoredox catalysts. Twofold reduction of the substrate disulfide occurs via thiol-disulfide interchange with the catalyst, and can be performed catalytically in the presence of a sacrificial agent.

Contents

1 General Introduction **1**

2 Theoretical Background and Motivation **5**

2.1 Natural Photosynthesis . . . 5
2.2 The Excited State . . . 9
2.3 Electron-Transfer . . . 12
2.4 Accumulative Charge-Separation . . . 15
2.5 Potential Inversion . . . 21
  2.5.1 Potential Inversion in Bipyridine Disulfide and Biphenyl Disulfide . 22
2.6 Thiol-Disulfide Interchange . . . 23

3 Exploiting Potential Inversion for Photoinduced Charge-Accumulation in Molecular Systems **27**

3.1 Ref-SS and the Ligand . . . 29
  3.1.1 Synthesis of Ref-SS and the Ligand . . . 29
  3.1.2 Optical Absorption Spectroscopy . . . 32
  3.1.3 Electrochemistry . . . 33
  3.1.4 Spectro-Electrochemistry . . . 36
  3.1.5 Summary . . . 37
3.2 Charge-Accumulation in a Molecular Triad . . . 39
  3.2.1 Synthesis of Ref-Ru-^{t}Bu and the Triad . . . 39
  3.2.2 Optical Absorption Spectroscopy . . . 40
  3.2.3 Electrochemistry . . . 41
  3.2.4 Spectro-Electrochemistry . . . 45
  3.2.5 Time-Resolved Emission Spectroscopy . . . 46
  3.2.6 Transient Absorption Spectroscopy . . . 47
  3.2.7 Continuous Irradiation Measurements . . . 48
  3.2.8 Summary . . . 50
3.3 Charge-Accumulation in a Molecular Pentad . . . 53
  3.3.1 Synthesis of Ref-Ru-TAA and the Pentad . . . 54
  3.3.2 Optical Absorption Spectroscopy . . . 55

3.3.3 Electrochemistry . . . 56
3.3.4 Spectro-Electrochemistry . . . 58
3.3.5 Transient and Time Resolved Absorption Measurements . . . 60
3.3.6 Continuous Irradiation Measurements . . . 63
3.3.7 Summary . . . 65
3.4 Multi-Electron Photoredox Catalysis via Thiolate-Disulfide Interchange . . . 69
3.4.1 Results and Discussion . . . 71
3.4.2 Summary . . . 75
3.4.3 Outlook . . . 76

4 General Summary 79

5 Experimental Section 83
5.1 Analytical Methods . . . 83
5.2 Synthesis of Ref-SS . . . 87
5.3 Synthesis of the Ligand . . . 89
5.4 Synthesis of Ref-Ru-^{t}Bu and the Triad . . . 95
5.5 Synthesis of Ref-Ru-TAA and the Pentad . . . 98

6 Appendix 103

Bibliography 130

Abbreviations

δ	chemical shift
A	acceptor
ATP	adenosine triphosphate
bpy	2,2'-bipyridine
BDE	bond dissociation energy
Bu	butyl
CPET	concerted proton-coupled electron-transfer
Cyt	cytochrome
D	donor
dba	dibenzylideneacetone
DCM	dichloromethane
DFT	density functional theory
DMF	N,N'-dimethylformamide
DMSO	dimethylsulfoxide
DTT	dithiothreitol
ε	extinction coefficient
e	elementary charge
Et_2O	diethyl ether
EtOAc	ethyl acetate
EtOH	ethanol
Fc	ferrocene
FD	ferredoxin
FNR	ferredoxin-NADP$^+$ reductase
ΔG	free energy
$HAsc^-$	ascorbate
HOMO	highest occupied molecular orbital
IC	internal conversion
IR	infrared
ISC	intersystem crossing
k	rate constant
LC	ligand-centered
LMCT	ligand to metal charge-transfer
LUMO	lowest unoccupied molecular orbital

M	molar, mol·L^{-1}
m/z	mass per charge
MC	metal-centered
MeCN	acetonitrile
MeOH	methanol
MLCT	metal-to-ligand charge transfer
NADP	nicotinamide adenine dinucleotide phosphate
Nd:YAG	neodymium-doped yttrium aluminum garnet
NHE	normal hydrogen electrode
NMR	nuclear magnetic resonance
OD	optical density
OEC	oxygen evolving complex
p	*para*
P	photosensitizer
PCET	proton-coupled electron-transfer
Pheo	pheophytin photosystem
PS	photosystem
PPh_3	triphenylphosphine
ppm	parts per million
ref	reference
rt	room temperature
SCE	saturated calomel electrode
SOMO	single occupied molecular orbital
t	tertiary
τ	excited state lifetime
TAA	triarylamine
$TBAPF_6$	tetrabutylammonium hexafluorophosphate
TEA	triethylamine
THF	tetrahydrofuran
TMS	trimethylsilyl
TON	turnover number
TsOH	*para*-toluenesulfonic acid
Tyr_Z	tyrosine Z
UV	ultraviolet
vis	visible
xy	*para*-xylyl

1 General Introduction

The generation of renewable energy is one of the most important topics in the 21st century. Due to population and economic growth, it is assumed that the worldwide energy requirement will increase by more than twofold by 2050.[1] The International Energy Agency reported a total energy consumption of $5.71 \cdot 10^{20}$ J or 18.1 TW in 2015.[2] As presented in Figure 1.1, more than 80% of the energy was generated from fossil fuels, i.e. coal, oil and natural gas, and only a small percentage from sustainable resources. The advantages of fossil fuels are their easy conversion into useful energy and that there is well-established technology for their storage and distribution. Furthermore, fossil fuels have a higher energy density compared to many other fuels. For these reasons, they are broadly used; mainly for transportation, but also for electricity generation, heating and industrial processes. The main disadvantage of fossil fuels is the pollutant emission by its combustion. The harmful pollution threatens human health and the increasing emission of CO_2 and other greenhouse gases contributes to global warming. Besides, fossil fuels are finite energy sources, progressively decreasing.[3] Therefore, it is important to promote the expansion of renewable energies.

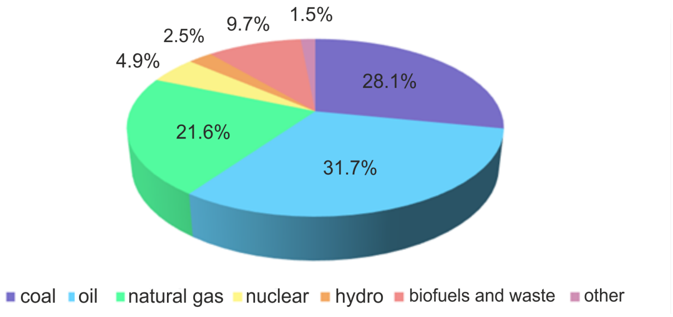

Figure 1.1: World total primary energy supply by fuel.[2]

The sun is the most promising renewable energy source. Annually, the earth surface is irradiated by 120,000 TW solar energy, which is almost four orders of magnitude greater than the present combustion of fossil fuels.[4] Furthermore, the sun is abundant, inexhaustible and geographically fairly distributed. But unfortunately, solar energy cannot be used until it is converted into a useful energy form, which is the major challenge.

Moreover, storage of the energy needs to considered, since due to the diurnal cycles and varying intensity dependent on season and weather conditions, solar energy is not always and everywhere available.

Solar energy can be converted into heat or electricity, but the most useful is the conversion into fuels in the form of energy rich chemicals. The principle of converting sunlight into energy rich molecules was already developed by nature million years ago. In natural photosynthesis, H_2O is split into O_2 and the liberated electrons and protons are used to reduce CO_2 to carbohydrates.[3] As well as sunlight, H_2O is an abundant substance on earth. Therefore, light-induced water splitting into O_2 and H_2 is a promising approach to solve the global energy problem. H_2 could be directly used as a fuel. It is very environmentally friendly, since the only waste product of its combustion is H_2O. Besides, H_2 could be used to convert CO_2 to energy rich chemicals like CH_4 or methanol (MeOH). In comparison to H_2, they can be much more easily be stored and distributed. Although the combustion of these molecules releases CO_2, it would be a carboneutral fuel if the CO_2 that is converted was taken from the atmosphere.[1, 5]

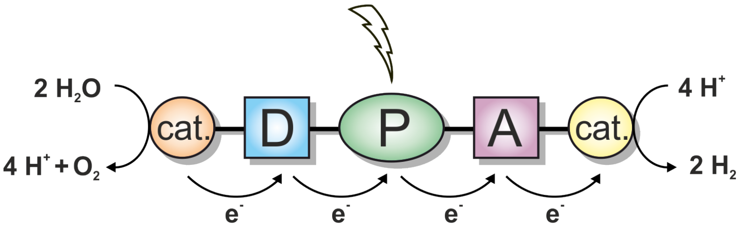

Figure 1.2: Schematic representation of a molecular system converting H_2O to O_2 and H_2.

Successful water oxidation requires the development a molecular system that mimics the essential steps of natural photosynthesis. The structure of such a system, being composed of five important parts, is schematically represented in Figure 1.2. To absorb the sunlight, a light-harvesting complex is required, a so called photosensitizer (P). The absorbed photon then induces an electron-transfer from the donor (D) to the acceptor (A), such that a charge-separated state is formed. Furthermore, two suitable catalysts (cat.) that are able perform the oxidation and reduction reactions, respectively, are necessary. Consequently, the generated positive and negative charge, i.e. the hole and the electron, need to be transferred from D and A to the corresponding catalyst. A crucial aspect of water splitting and H_2 generation is the requirement of multiple holes and electrons, respectively. Therefore, these redox equivalents have to be accumulated before a reaction can occur. This work will focus on this aspect of artificial photosynthesis, photoinduced charge-accumulation.

In the following chapter, the essential reaction steps of natural photosynthesis are briefly summarized. Relevant theoretical background about excited states and electron-transfer is provided and the problems associated with charge-accumulation are discussed. Subsequently, there is a short overview of potential inversion, especially regarding disulfides, and general aspects of thiol-disulfide interchange reactions are introduced. This is followed by the investigation of photoinduced charge-accumulation in a molecular triad and pentad, both containing a two-electron acceptor that is reduced with potential inversion. Finally, multi-electron photoredox catalysis using these systems as catalysts is investigated.

2 Theoretical Background and Motivation

2.1 Natural Photosynthesis

Solar-to-chemical energy conversion is one of the most important goals for many of today's scientists. An ingenious way to perform this reaction was established by nature - photosynthesis. That is, the sunlight-driven conversion of H_2O into O_2, which is performed in the chloroplasts of green plants, algae and cyanobacteria. Moreover, the energy poor substrates nicotinamide adenine dinucleotide phosphate ($NADP^+$), adenosine diphosphate (ADP) and phosphate are converted into energy rich NADPH and adenosine triphosphate (ATP) that are required to convert CO_2 to carbohydrates. The key protein complexes involved in the conversion of light into chemical energy are the light-harvesting complexes, ATP synthase, cytochrome b_6f (Cyt b_6f), and photosystems I (PSI) and II (PSII). All of these proteins are located in the thylakoid membrane, which is a folded lipid bilayer separating the inner (lumen) and the outer (stroma) part of the thylakoids (see Figure 2.1). In PS II, four electrons and protons are extracted from water, induced by four photons. Each sequentially generated electron in PSII is then excited in PSI, such that altogether four additional photons are required. Finally, the electrons are used to reduce CO_2. In contrast to the preceding light reactions, CO_2 fixation is independent of light, and therefore called a dark reaction.[6] The light reactions of photosynthesis are represented in more detail in the Z-scheme in Figure 2.2.[7]

Light is absorbed by light-harvesting complexes, which transfer the absorbed energy within 100 fs to both photosystems.[6] Both PSII and PSI are composed of central chlorophyll α dimers that are called P680 and P700, respectively. Upon excitation of P680, an electron is transferred to pheophytin (Pheo), and within a few picoseconds, the charge-separated state $P680^{\bullet+}$-$Pheo^{\bullet-}$ is formed.[8] To overcome energetically highly-favorable charge-recombination, the electron is then transferred to a quinone acceptor (Q_A). The formed charge-separated state has a lifetime of 200 µs. Hence, there is more than enough time for the following reactions to occur.[9]

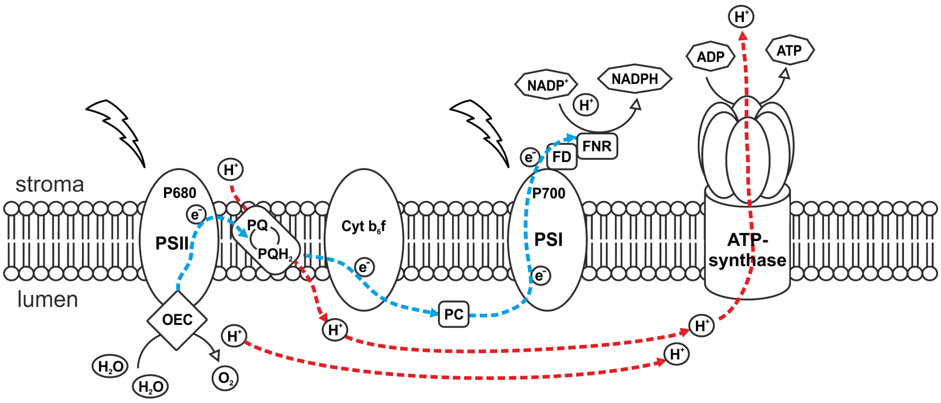
stroma
lumen
P680
PSII
e^-
OEC
H_2O
H_2O
O_2
H^+
H^+
PQ
PQH_2
H^+
Cyt b_6f
e^-
PC
H^+
P700
PSI
e^-
e^-
FD
FNR
$NADP^+$
H^+
NADPH
ADP
ATP
H^+
ATP-synthase
H^+
H^+

Figure 2.1: Schematic representation of the thylakoid membrane, including some key proteins involved in photosynthesis.

The electron is then transferred from $Q_A^{\bullet -}$ to a second plastoquinone (Q_B). With the absorption of the next photon, Q_B is reduced a second time followed by protonation with protons from the stroma side to Q_BH_2, which is then released into the plastoquinone pool (PQ) in the thylakoid membranes. The protons are then carried to the lumen side during transfer of the two electrons of Q_BH_2 to Cyt b_6f (see Figure 2.1). This results in a proton gradient that drives the synthesis of ATP. Cyt b_6f passes the electron to plastocyanin (PC), which transfers it to P700. Upon excitation of P700, the electron is transferred over an electron-transport chain consisting of chlorophyll A_0, phylloquinone A_1, and three separated iron sulfur clusters (F_x, F_B, F_A) to ferredoxin (F_D), which passes it to ferredoxin NADP reductase (FNR). This enzyme catalyses the reduction of $NADP^+$ to NADPH.[8]

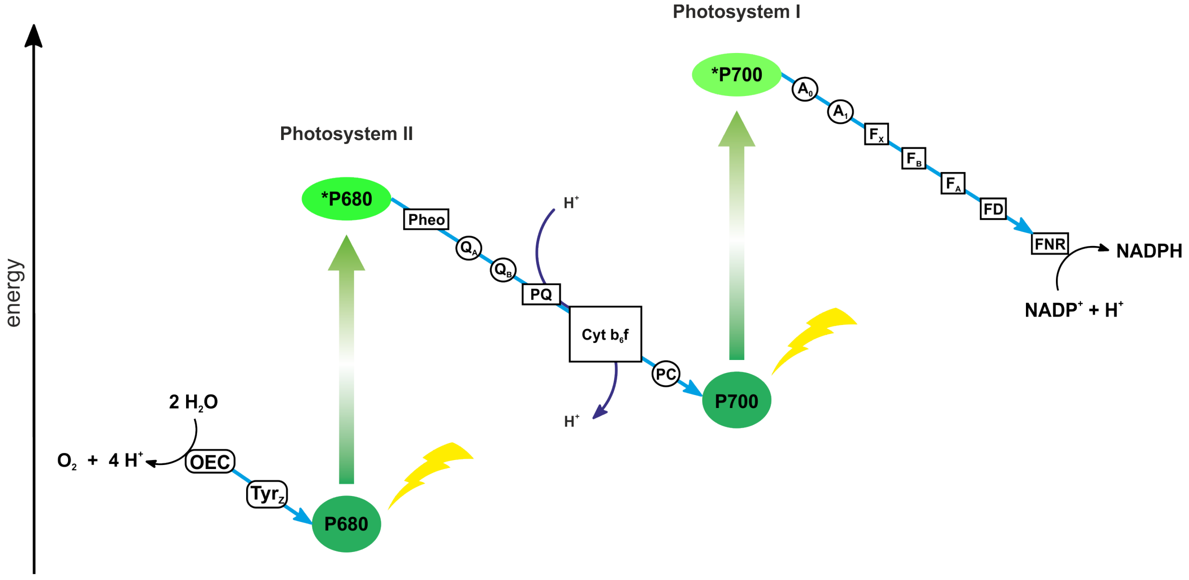
energy
Photosystem II
Photosystem I
*P680
Pheo
Q_A
Q_B
PQ
H^+
Cyt b_6f
H^+
PC
P700
*P700
A_0
A_1
F_X
F_B
F_A
FD
FNR
NADPH
$NADP^+ + H^+$
2 H_2O
O_2 + 4 H^+
OEC
Tyr_Z
P680

Figure 2.2: Schematic representation of the light reactions in PSII and PSI.

The part of PSII responsible for water oxidation is called the oxygen evolving complex (OEC). It contains a Mn_4CaO_5 cluster, the crystal structure of which was recently measured with a resolution of 1.9 Å.[10] Three of the manganese atoms and the calcium atom occupy the corners of a cubane-like structure together with four oxygen atoms. The fourth manganese atom is located outside of this cubane and is connected by the fifth oxygen atom to a manganese atom and to one oxygen of the cubane (see Figure 2.3). Hence, every manganese atom is connected to the adjacent manganese by a di-μ-dioxo bridge. The cluster is surrounded by amino acids, providing ligands for the metal ions. Furthermore, it is assumed that the amino acids play a crucial role in the deprotonation of the substrate water molecules.[11]

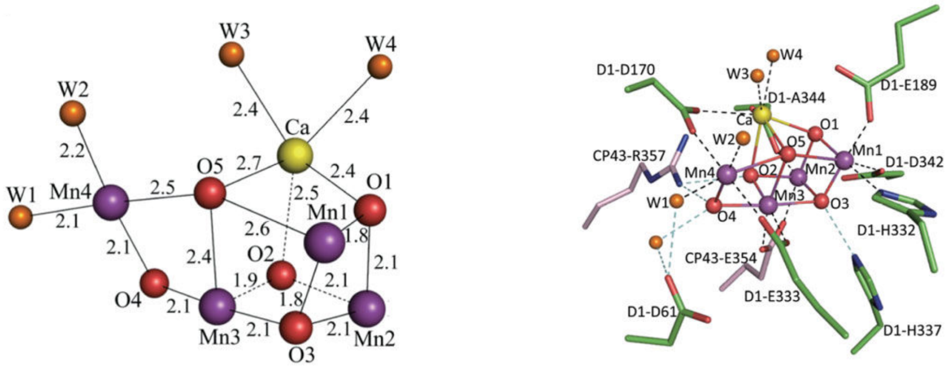

Figure 2.3: Crystal structure of the Mn_4CaO_5 cluster with a resolution of 1.9 Å, with and without the surrounding amino acid. Adapted by permission from Macmillan Publishers Ltd: NATURE,[10] copyright 2011.

As described above, the excitation of PSII generates highly oxidizing $P680^{\bullet+}$ (+1.2 V vs NHE)[11], which is then reduced by adjacent tyrosine Z (Tyr_Z). The latter is deprotonated by an adjacent histidine, resulting in the formation of a stable tyrosine radical $Tyr_Z^{\bullet}$, which is re-reduced by electron-transfer from the Mn_4CaO_5 cluster. The excitation of PSII and the oxidation of Mn_4CaO_5 by $Tyr_Z^{\bullet}$ are repeated three additional times until the four charges required for catalytic water splitting are accumulated. Thus, Mn_4CaO_5 cycles through five different redox states during the charge-accumulation. Electron-transfer from Mn_4CaO_5 to $Tyr_Z^{\bullet}$, induced by four short flashes of light, was first summarized by Kok in a S-state cycle.[12] In this model the S-states S_0-S_4 describe the different oxidation states of the OEC. A more extended cycle was proposed by Dau and Hauman (see Figure 2.4).[13, 14] This cycle contains the oxidation states from S_0 to S_4 and S'_4, which represents a hypothetical intermediate, i.e. the fourfold oxidized complex including the two substrate water molecules. Furthermore, it also takes into account proton liberation. The cycle starts with the dark-stable S_1 state, which is oxidized with the first photon. Upon the second excitation of PSII, S_2 is oxidized, coupled with the release of a proton.

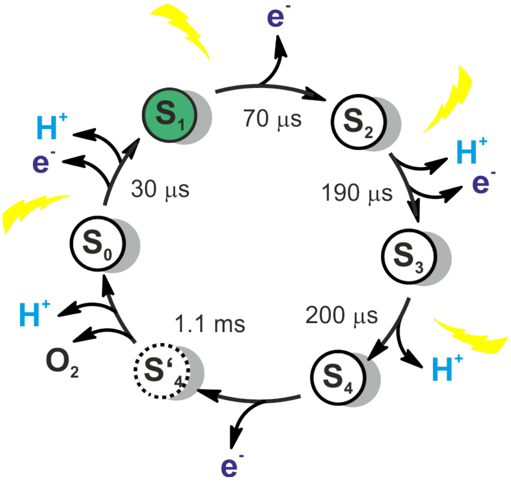

Figure 2.4: Extended S-state cycle according to Dau and Hauman, representing the light-induced electron and proton release in the OEC and the different oxidation states of the Mn_4CaO_5 cluster during the oxidation from H_2O to O_2. The dark-stable S_1 state is marked in green and is starting point of the catalytic cycle. The times correspond to the halftimes of the S-state transitions.[14]

Upon the third photon, there is a cascade reaction from S_3 over S_4 and S'_4 to S_0, resulting in the release of O_2. The fourth photon closes the cycle. However, neither the exact mechanism of this catalytic cycle, nor how the O-O bond is formed, are known. One proposed mechanism implies the conversion of the manganese-bound water molecule into a highly electrophilic Mn(IV)-oxo species that is then nucleophilically attacked by the other substrate water, located at the calcium atom.[15–17] An alternative mechanism proposed by Siegbahn suggests the formation of an oxyl-radical that forms the O-O-bond by attacking an oxygen bridging unit of the cubane.[18–20]

2.2 The Excited State

The first step of a photochemical reaction is the absorption of a photon, leading to the excitation of an electron. Typical energies for electronic transitions are in the range of a few electron volts (eV). Hence, the photons involved in such transitions have wavelengths in the near-infrared, visible and ultraviolet range.

Depending on the structure of a molecule, different transitions can occur. Which of these transitions are allowed is determined by various selection rules.[21, 22] The Laporte rule strictly applies for centrosymmetric molecules, i.e. molecules with an inversion center. It states that only transitions between states of the converse symmetry are allowed. A symmetry forbidden transition can be allowed when the inversion center is disrupted by an asymmetric vibration or Jahn-Teller distortion. Furthermore, transitions between states of different spins are forbidden, but these restrictions can be eased when there is a sufficient spin-orbit coupling. Spin-orbit coupling arises from the interaction of the spin magnetic moment with the magnetic moment due to the orbital motion of the electron and increases with increasing the nuclear charge.[23] For this reason, transitions to a state of different multiplicity are allowed in complexes with heavy atoms. In general, a forbidden transition can occur but is less probable, which is also reflected in molar extinction coefficients (ε). Whereas for Laporte and spin forbidden transitions $\varepsilon < 1$ L mol^{-1} cm^{-1}, ε increases up to 10^6 L mol^{-1} cm^{-1} for Laporte and spin allowed transitions.

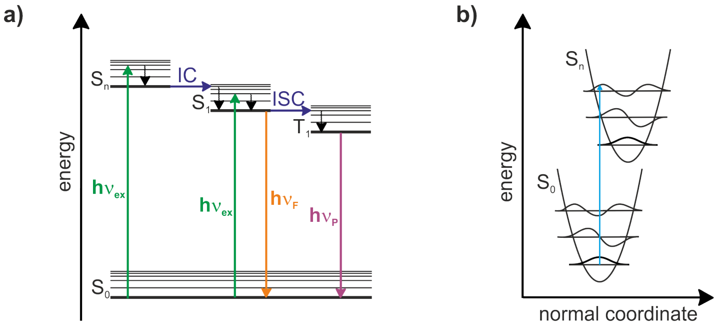

Figure 2.5: a) Simplified Jablonski diagram; b) schematic representation of a vertical electronic transition from the lowest vibrational energy level of S_0 into a higher vibrational level of S_n.

Upon excitation of a molecule by light, excess energy can be either released as heat or emitted as light. All possible radiative and non-radiative decay pathways are summarized in a Jablonski diagram presented in Figure 2.5a. The Born-Oppenheimer approximation states that the position of nuclei may be considered to be fixed whilst electrons move in their field, due to the light mass of electrons compared to nuclei and consequent rapidity of electronic motion compared to nuclear.[24, 25] As a result, nuclear geometry does not change during an electronic transition, and therefore occurs vertically on a potential energy diagram. According to the Franck-Condon principle, the probability of an electronic transition is related to wavefunction overlap.[24, 26] Due to different electronic structures of excited states compared to the ground state, the excited-state potential energy curves are shifted on the normal coordinate (see Figure 2.5b). To achieve the greatest wavefunction overlap, the vertical transition from the lowest vibrational level of the ground state (S_0) to the excited state (S_n) has therefore to occur into a higher energy vibrational level of S_n (see Figure 2.5b). The excited electron then rapidly relaxes to the lowest vibrational energy level of S_n. From there, transition into a higher vibrational level of the first excited state (S_1) occurs, followed once again by rapid relaxation to the lowest vibrational level of S_1. The non-radiative transition between states of the same multiplicity are called internal conversion (IC). The whole process typically occurs within 1 ps, such that other processes cannot compete with it. Hence, the following transitions occur from the lowest vibrational level of S_1. From there, the electron can relax non-radiatively to the ground state, or the excess energy is emitted by a photon, which is called fluorescence ($h\nu_F$). The non-radiative transition to a state of different multiplicity (e.g. S_1-T_1) is called intersystem crossing (ISC). Phosphorescence ($h\nu_P$) describes the transition to a state of different multiplicity under emission of a photon. As this is a spin forbidden transition, which is only allowed when there is sufficient spin-orbit coupling (see above), the radiative decay to the ground state is normally slower compared to fluorescence.[6] Each transition has a certain rate (k_i), and each state a certain lifetime (τ). The lifetime is defined as the inverse sum of the radiative and non-radiative decay rates of this state (Equation 2.1).[27]

$$\tau = 1/\textstyle\sum_i k_i \tag{2.1}$$

In metal complexes, there are generally four different types of transitions. Transitions between molecular orbitals mainly localized on the metal are called d-d or metal-centered (MC) transitions. Since this a symmetry forbidden transition, its intensity in an optical absorption spectrum is only weak (ε < 1000 L mol^{-1}cm^{-1}). Furthermore, there are ligand-centered (LC) transitions, which are transitions between molecular orbitals mainly localized on the ligand. There is also the possibility of transitions between metal and ligand. Depending on the orbitals in which the excited electron is initially located, it is a ligand-to-metal or metal-to-ligand charge-transfer (LMCT and MLCT, respectively).[21]

In octahedral complexes, the d-orbitals are split into three t_{2g}- and two e_g-orbitals, where the extent of the splitting is dependent on the metal and the ligands. $[Ru(bpy)_3]^{2+}$, which is used as photosensitizer in this work, has a d^6 low-spin configuration, i.e. the

t_{2g}-orbitals are completely occupied and the e_g-orbitals are unoccupied (see Figure 2.6). The lowest unoccupied orbital (LUMO) of the bipyridine ligand, a π*-orbital, is lower in energy than the e_g-orbital, such that the lowest excited state is a MLCT state. Hence, upon photoexcitation, the ^{1}MLCT state is formed. Due to strong spin-orbit coupling, there is 100% conversion of the ^{1}MLCT to the ^{3}MLCT state via ISC.[28, 29] As mentioned above, the transition of this state to the ground state is spin forbidden, and therefore relatively long-living. This is important for electron- or energy-transfer to occur from this state.

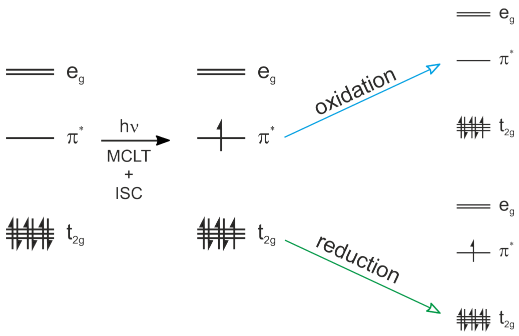

Figure 2.6: Simplified representation of molecular orbitals of $[Ru(bpy)_3]^{2+}$ before and after photoexcitation; and after oxidation and reduction.

The excitation of an electron from the t_{2g}- to the π*-orbitals has two effects. Firstly, the complex becomes a stronger reductant compared to the ground state, because there is a higher-energy electron that can be transferred from the π*- orbital. Secondly, the photoexcited complex is also a stronger oxidant, because a lower-energy hole in the t_{2g}-orbital is generated that can accept an electron (see Figure 2.6). This is also reflected by the redox potentials of the excited complex. The ground state and excited state redox potentials of $[Ru(bpy)_3]^{2+}$ are summarized in the LATIMER diagram in Figure 2.7. The energy difference between the ^{3}MLCT and ground state is given by the zero-zero excitation energy (E^{00}). By adding this energy to the ground state reduction potential or by subtracting it from the oxidation potential, the corresponding excited state potentials are estimated.

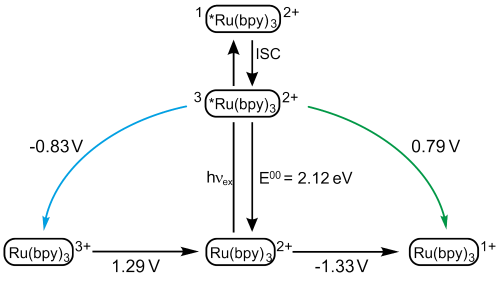

Figure 2.7: LATIMER diagram representing the ground and excited state redox potentials of $[Ru(bpy)_3]^{2+}$ (V vs SCE) in MeCN.[30],[31]

2.3 Electron-Transfer

In 1956, Rudolph A. Marcus developed a theory to explain the rates of electron-transfer reactions. It originally referred to outer-sphere self-exchange reactions, but was extended to inner-sphere electron-transfer by Noel Hush.[32–37]

In outer-sphere electron-transfer reactions, the electron donor (D) and acceptor (A) form a so-called outer-sphere complex without the cleavage or formation of bonds. To transfer an electron, the redox centers come close, but they are not covalently linked, such that there is only weak electronic coupling (H_{DA}). Due to the Frank-Condon principle, bond lengths and angles of the reactants need to adjust before electron-transfer can occur. The same holds true for the surrounding molecules, which also need to rearrange. These reorganizations increase the activation barrier for electron-transfer, and therefore influence the rate of electron-transfer (k_{ET}).

When the formation of the encounter complex results in the linkage of D and A by a bridging ligand, through which the electron is transferred, it is called an inner-sphere reaction. Due to the covalent linkage, H_{DA} between the redox centers increases. As a consequence, not only the internal rearrangement and the reorganization of the solvent shell, but also the H_{DA} between D and A, need to be considered when estimating k_{ET}.

$$k_{ET} = \tfrac{2\pi}{\hbar} \cdot {H_{DA}}^2 \cdot \sqrt{\tfrac{\pi}{\lambda K_B T}} \cdot e^{\left(-\frac{(\lambda+\Delta G^0)^2}{4\lambda K_B T}\right)} \tag{2.2}$$

The Marcus-Hush theory is commonly described by the semi-classical Equation 2.2.[38] Accordingly, k_{ET} depends on H_{DA}, the reorganization energy (λ), and the reaction free energy (ΔG^0). These factors are explained in more detail below. The potential energy curves of an exergonic redox process from D–A to D^{+}–A^{-} as a function of the normal coordinate are presented in Figure 2.8. Electron-transfer can only take place at the point of intersection between the parabolas. It is distinguished between adiabatic and non-adiabatic processes. In the case of adiabatic electron-transfer, H_{DA} is large and the free energy curves split into a upper and lower part (black traces) and the reaction from D-A to D^{+}-A^{-} occurs along the lower potential well. When the electronic coupling is small, the parabolas only slightly split (red traces), and the reaction from the ground to the charge-separated state requires a certain activation energy ($\Delta G^{\ddagger}$). Equation 2.2 is only applicable to the latter case, i.e for non-adiabatic electron-transfer.

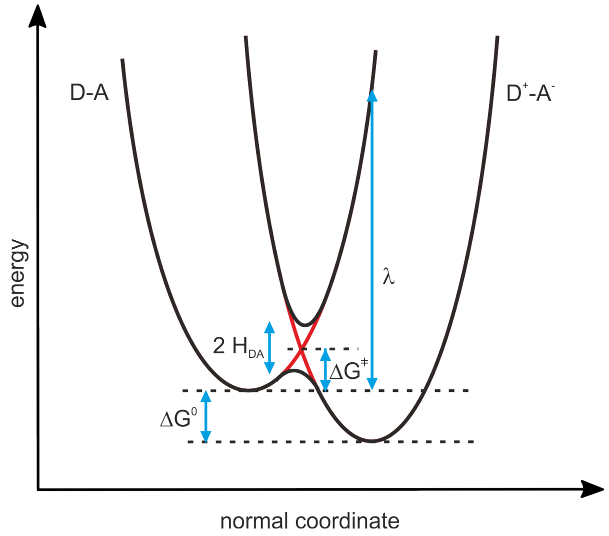

Figure 2.8: Schematic representation of the potential energy of D-A and D^{+}-A^{-} states as a function of the normal coordinate.

Electronic coupling

As mentioned above, k_{ET} is influenced by the electronic coupling, H_{DA}. With increasing H_{DA}, the splitting of the energy curves at the intersection (see Figure 2.8) increases, and with this the probability of electron-transfer also increases. H_{DA} reaches its maximum value when the distance of the reactants corresponds to the sum of their van-der-Waals radii (σ), then $H_{\mathrm{DA}} = H_{\mathrm{DA,0}}$.

In the case of weak electronic coupling, i.e. non-adiabatic electron-transfer, H_{DA} can be described with Equation 2.3.[39] Thus, the electronic coupling exponentially decays with increasing distance between donor and acceptor. How strong H_{DA} depends on the distance is determined by the distance-decay constant β.

$$H_{DA}{}^{2} = H_{DA,0}{}^{2} \cdot e^{(-\beta(r_{DA}-\sigma))} \tag{2.3}$$

Reorganization Energy

The overall energy, which is necessary to rearrange D–A to D^{+}–A^{-}, is called the reorganization energy λ. It is composed of the inner-sphere (λ_{in}) and outer-sphere (λ_{out}) reorganization energies. As mentioned above, bond lengths and angles need to change prior to electron-transfer. λ_{in} describes the energetic barrier that is associated with the structural change. The intramolecular movements can be described as linear combinations of vibrational normal modes, such that λ_{in} can be calculated with Equation 2.4. This equation includes the normal mode force constants in the reactants and products (f_j^R, f_j^P) and the change in the equilibrium value of the normal mode (Δq_j).[38]

$$\lambda_{in} = \sum_j \frac{f_j^R \cdot f_j^P}{f_j^R + f_j^P} (\Delta q_j)^2 \tag{2.4}$$

$$\lambda_{out} = (\Delta e)^2 \cdot \left(\frac{1}{2r_D} + \frac{1}{2r_A} - \frac{1}{r_{DA}} \right) \cdot \left(\frac{1}{D_{op}} - \frac{1}{D_s} \right) \tag{2.5}$$

Furthermore, a reorientation of the solvents molecules is required, since the transfer of an electron also leads to a different electronic structure. As well as the inner-sphere reorganization, the solvation shell needs to adjust before the electron-transfer. To estimate λ_{out}, the solvent is usually treated as dielectric continuum, and a linear change of the dielectric polarization outside of the coordination sphere with the change in charge distribution is assumed (see Equation 2.5).[38] The reactants are treated as hard spheres with radii r_D and r_A, and a center-to-center distance r_{DA}. Δe is the charge which is transferred from D to A. λ_{out} decreases with increasing r_D and r_A because of the lower polarization effect on solvent molecules. It increases with increasing r_{DA}, as there is a larger difference in charge distribution before and after electron-transfer. Furthermore, the optical and static dielectric constants of the solvents D_{op} and D_s need to be considered.

Reaction Free Energy

The reaction free energy, ΔG^0, is also called the driving force, and describes the energy difference between D–A in the ground state and in the charge-separated state D^+–A^-. To transfer the electron from D to A, an activation barrier needs to be overcome. This activation energy ($\Delta G^\ddagger$) is dependent on both λ and ΔG^0 (see Equation 2.6).

$$\Delta G^\ddagger = \frac{\left(\Delta G^0 + \lambda\right)^2}{4\lambda} \tag{2.6}$$

The upper part of Figure 2.9 illustrates that an increasing driving force shifts the potential energy curve of D^+–A^- downwards such that $\Delta G^\ddagger$ decreases, which consequently leads to faster electron-transfer. The quadratic dependence of $\Delta G^\ddagger$ on ΔG^0 results in increasing k_{ET} with increasingly negative driving force, until $-\Delta G^0 = \lambda$. At this point, electron-transfer is activationless, and k_{ET} reaches its maximum. When a reaction is strongly exergonic, such that $-\Delta G^0 > \lambda$, the activation barrier increases again and electron-transfer becomes slower. The dependence of k_{ET} on ΔG^0 is schematically presented in the lower part of Figure 2.9. In the normal region, where $-\Delta G^0 < \lambda$, k_{ET} increases with increasing driving force, and decreases in the inverted region, where $-\Delta G^0 > \lambda$.

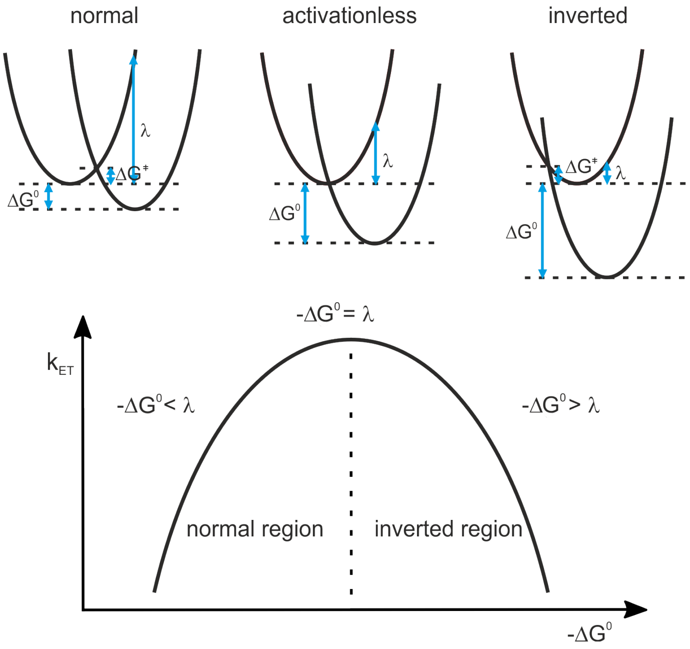

Figure 2.9: Simplified dependence of the rate constant for electron-transfer, k_{ET}, on the driving force, ΔG^0.[40]

2.4 Accumulative Charge-Separation

As already discussed in Section 1, the generation of solar fuels is an important topic, but the design of molecular systems that convert solar into chemical energy is challenging. Water splitting and the generation of H_2, CH_4 or MeOH, for example, require several redox equivalents (see Equations 2.7 - 2.10), but with each absorbed photon, only one electron-hole pair is generated. Therefore, the redox equivalents need to be accumulated by the sequential absorption of several photons, before a catalytic redox reaction can take place. An additional problem is that the multiply charge-separated state needs to be sufficiently long-living for catalytic applications. One reason for the formation of a (long-living) charge-accumulated state being much more difficult compared to single electron-transfer is the increased number of undesired decay pathways.

$$2\,H_2O \rightarrow O_2 + 4\,H^+ + 4\,e^- \tag{2.7}$$

$$2\,H^+ + 2\,e^- \rightarrow H_2 \tag{2.8}$$

$$CO_2 + 6\,H^+ + 6\,e^- \rightarrow CH_3OH + H_2O \tag{2.9}$$

$$CO_2 + 8\,H^+ + 8\,e^- \rightarrow CH_4 + 2\,H_2O \tag{2.10}$$

The energies of the different species formed during charge-accumulation in a donor-photosensitizer-acceptor (D-P-A) assembly and their decay pathways are presented in Scheme 2.1.[41]

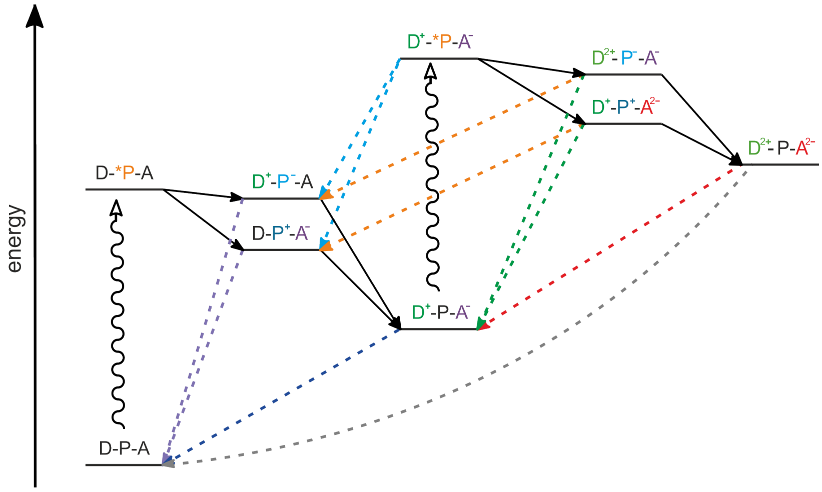

Scheme 2.1: Schematic energy scheme for the formation of the charge-separated states in a D-P-A assembly and their decay pathways.[41]

Upon absorption of the first photon, the excited photosensitizer can be reductively or oxidatively quenched, yielding D$^+$-P$^-$-A or D-P$^+$-A$^-$, respectively. These states can either decay to the ground state (purple arrows), or undergo electron-transfer to afford the singly charge-separated state D$^+$-P-A$^-$. This state needs to be sufficiently long-living to be excited by a second photon before recombination to the ground state occurs (blue arrow).

Another problem in accumulative electron-transfer, playing no role in single charge-separation, is the typically strong reducing, as well as oxidizing, power of the excited photosensitizer. When D$^+$-P-A$^-$ is excited, there is a strong driving force to reduce D$^+$ or oxidize A$^-$, yielding D-P$^+$-A$^-$ or D$^+$-P$^-$-A (cyan arrows). These states can also decay to the ground state (purple arrows) or, once again undergo electron-transfer, forming the singly charge-separated state D$^+$-P-A$^-$.

When there is a successful second excitation followed by electron-transfer to form D^{2+}-P$^-$-A$^-$ or D$^+$-P$^+$-A^{2-}, further decay pathways arise. On the one hand, charge-recombination between donor and acceptor (orange arrows) is possible, and on the other hand, between the photosensitizer and donor or acceptor, respectively, to form D$^+$-P-A$^-$ (green arrows). The productive pathways result in the formation of D^{2+}-P$^+$-A^{2-}, which may also rapidly decay to D$^+$-P-A$^-$ (red arrow) or to the ground state (grey arrow).

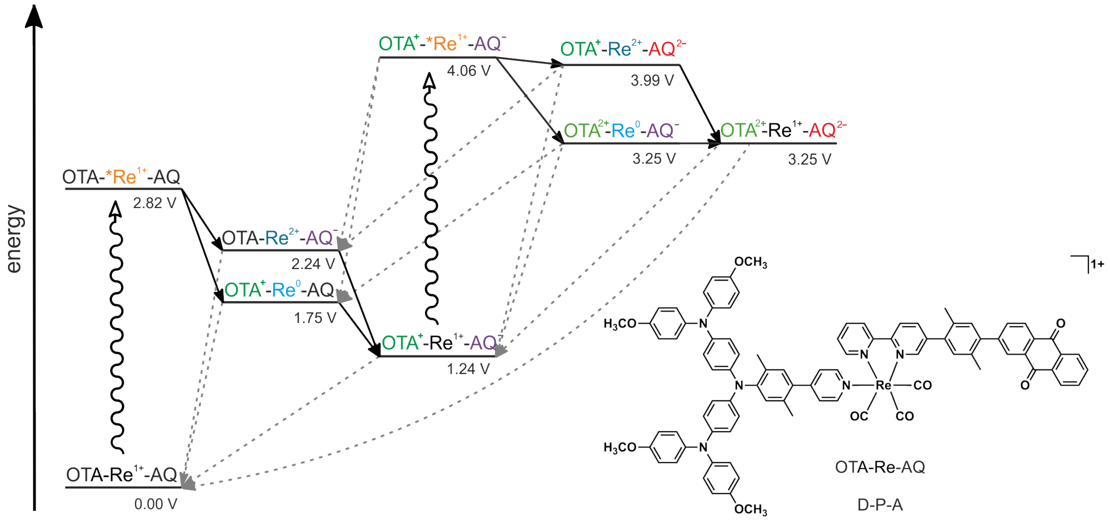
energy
OTA•+-*Re1+-AQ•-
4.06 V
OTA•+-Re2+-AQ2-
3.99 V
OTA2+-Re0-AQ•-
3.25 V
OTA2+-Re1+-AQ2-
3.25 V
OTA-*Re1+-AQ
2.82 V
OTA-Re2+-AQ•-
2.24 V
OTA•+-Re0-AQ
1.75 V
OTA•+-Re1+-AQ•-
1.24 V
OTA-Re1+-AQ
0.00 V
OCH3
H3CO
N
OCH3
H3CO
N
N
N
N
N
Re
CO
OC
CO
O
O
1+
OTA-Re-AQ
D-P-A

Scheme 2.2: Energy scheme of the formation and decay pathways for the possible charge-separated states in OTA-Re-AQ in MeCN.[42]

Our group recently reported a D-P-A assembly, theoretically able to perform twofold charge-separation, presented in Scheme 2.2.[43] It is composed of oligo-triarylamine (OTA) as a two-electron donor, a rhenium photosensitizer (Re) and anthraquinone (AQ) as a two-electron acceptor. Upon photoexcitation at 355 nm with laser pulses of 10 ns duration, the singly charge-separated state ($AQ^{\bullet -}$-Re-$OTA^{\bullet +}$) is formed within the laser pulse. It has a lifetime of 205 ns in dry, de-oxygenated MeCN, and its further excitation is expected to be possible. However, the twofold charge-separated state could not be observed. The main problem with this system was a relatively low photo-degradation threshold at the excitation wavelength.[44] However, the energy scheme of this system is a good example to illustrate how strong the driving forces of unproductive pathways are, competing with the formation of the desired photoproduct.

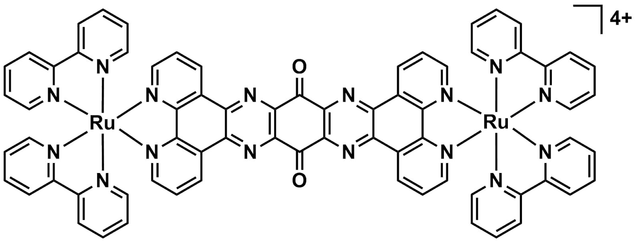

Figure 2.10: Structure of a dinuclear ruthenium triad with TATPQ as a four electron acceptor. In the presence of a sacrificial donor, four electrons are sequentially transferred to the acceptor upon excitation with visible light, each step is coupled with its protonation.[45]

By using a sacrificial oxidant or reductant, the productive pathways can become more competitive. MacDonnell and co-workers investigated electron-accumulation in a dinuclear ruthenium complex with a central tetra-n-butylammonium (TATPQ) moiety as an electron acceptor (see Figure 2.10).[45, 46] Upon excitation of one of the ruthenium photosensitizers, it transfers an electron to TATPQ. The oxidized sensitizer is then reduced to the ground state by triethylamine (TEA), preventing charge-recombination of the singly charge-separated state. The reduced acceptor is then protonated by the released proton from oxidized TEA. This reaction sequence can be repeated three additional times, such that altogether four electrons and protons can be stored in this system. However, such approaches, using sacrificial reagents, are not compatible with sustainable solar fuel production, and they should therefore be avoided.

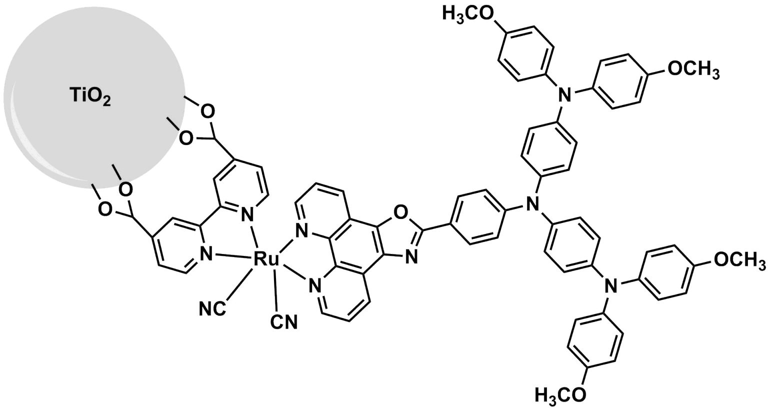

Figure 2.11: Structure of a triad with a TiO_2 nanoparticle as an electron acceptor, able to form a twofold charge-separated state upon excitation with visible light.[47]

An approach for successful charge-accumulation without the use of sacrificial agents is the use of nanoparticles as electron acceptors. The system presented in Figure 2.11 was developed by Hammarström and co-workers.[47, 48] It is composed of OTA as the two-electron donor, a ruthenium photosensitizer, and a TiO_2 nanoparticle that can accept multiple electrons. The key feature of this system is the rapid electron injection from the excited sensitizer and slow back electron-transfer. The oxidized sensitizer is then re-reduced by OTA, forming the singly-charge-separated state, which has a lifetime of at least 10 µs. Upon excitation with a second laser pulse, the twofold charge-separated state is formed in the same way.

The first molecular system able to perform light-induced charge-accumulation independent of sacrificial agents or nanoparticles was developed by Wasielewski and co-workers in 1992.[49] It consists of a central perylene bis(carboxyimide) (PBDCI) electron acceptor that is covalently connected to two free base porphyrin photosensitizer (see Figure 2.12, top). This system was excited at 585 nm by 160 fs laserpulses, generating the singlet excited state of both sensitizers. Then, each excited sensitizer successively transfers an electron to PBDCI. The twofold charge-separated state was found to be relatively short living at approximately 5 ns. However, its lifetime is longer than that of the singly charge-separated state (∼120 ps).

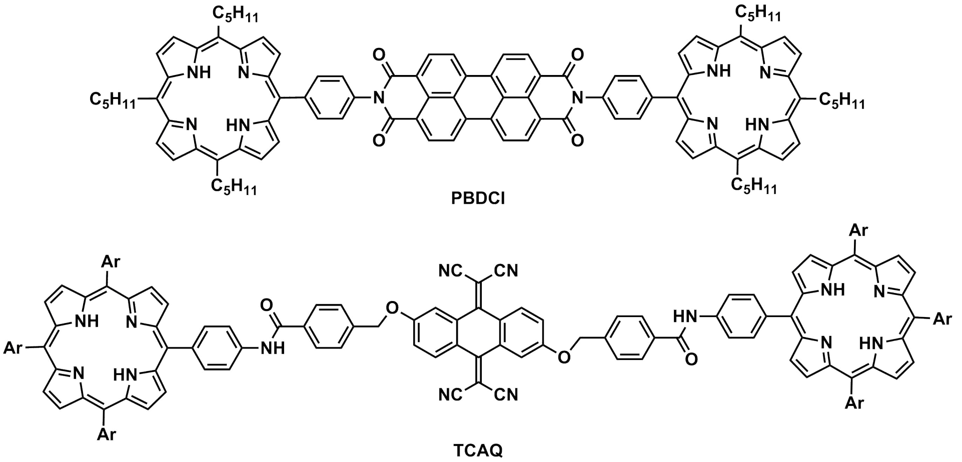

Figure 2.12: Structure of two molecular systems with porphyrin photosensitizers and PBDCI and TCAQ, respectively, as electron acceptors, able to form a short-lived twofold charge-separated state upon excitation with visible light.[49, 50]

In 1998, Imahori and co-workers published a similar system that also contains two free base porphyrin sensitizers, but instead of PBDCI, tetracyanoanthraquinomethane (TCAQ) was used as the acceptor (see Figure 2.12, bottom).[50] This triad was excited by two independent, delayed laser pulses. The excitation of the first sensitizer occurred at 532 nm and the second at 555 nm 233 ps later, resulting in electron-transfer to TCAQ, i.e. the formation of the twofold charge-separated state. Although the spectral features of singly and doubly reduced TCAQ are relatively similar, the rate constants for the formation of the singly and twofold charge-separated states and their decays could be determined. Both states have a lifetime of approximately 1 ns.

With these two molecular systems, photoinduced charge-accumulation was achieved in the absence of sacrificial agents. However, with regard to solar fuel production, their lifetimes are too short to perform a catalytic reaction, hence the formation of a longer-living charge-accumulated state is desirable.

In 2016, a purely molecular pentad was developed in our group that has a significantly increased lifetime compared to the two systems presented above.[51] It is composed of a central AQ moiety that can accept two electrons, two ruthenium trisbipyridyl photosensitizers (Ru), and two triarylamine (TAA) groups acting as electron donors (see Figure

2.13). Upon excitation of both sensitizers at 415 nm with laser pulses of ~100 ps duration, they are rapidly reductively quenched by TAA, followed by electron- transfer from the reduced sensitizers to AQ. The formation of the twofold charge-separated state was confirmed by transient IR-spectroscopy. Although there is a strong driving force for charge-recombination, it has a lifetime of 870 ns, which can be increased to 4.7 µs in the presence of para-toluenesulfonic acid.[52] It was found that upon excitation with femtosecond laser pulses, the twofold charge-separated is formed, followed by protonation of AQ^{2-} to AQH_2. In contrast to the formation of the this state via sequential electron and proton transfers, charge recombination occurs via concerted proton-coupled electron-transfer.

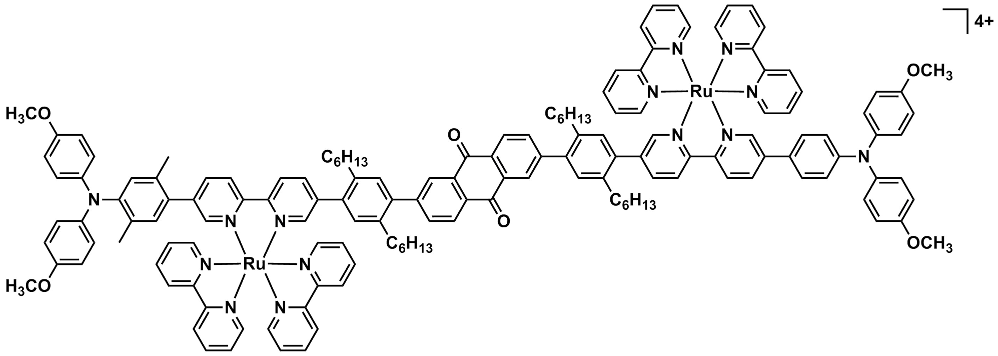

Figure 2.13: Structure of a molecular pentad with AQ as the two electron acceptor, accumulating two electrons upon excitation at 415 nm.[51, 52]

Aside from the competing decay pathways occurring in the separation of multiple charges, an additional drawback of charge-accumulation in small molecules is coulombic repulsion. Once a molecule is reduced or oxidized, it is normally significantly more difficult to reduce or oxidize it a second time. Since the redox potential of the excited photosensitizer is fixed, the difference in first and second redox potentials of donor or acceptor, should be relatively low, as for example in PBDCI or AQ. The span of redox potentials can be decreased by delocalizing the charge on a greater molecule or by coupling electron-transfer with deprotonation or protonation, exploited in the systems with TATPQ and AQ as the electron acceptor.[41, 52] Both strategies reduce electrostatic repulsions. A third opportunity to handle this problem is to use an acceptor or donor, the redox potentials of which are inverted, as demonstrated for the first time in this work.

2.5 Potential Inversion

Normally, the first reduction or oxidation potential (E°$_1$), respectively, of a small neutral molecule (A) is more negative or more positive, respectively, compared to the second (E°$_2$, see Equations 2.11 and 2.12). Upon the first redox step, the molecule gets charged, which makes the insertion or removal of the second electron more difficult due to electrostatic repulsions. The case where E°$_1$ - E°$_2$ > 0 V for reduction (or E°$_1$ - E°$_2$ < 0 V for oxidation) is called normal ordering of potentials.[53] But there is also the situation where E°$_1$ - E°$_2$ < 0 V for reduction (or E°$_1$ - E°$_2$ > 0 V for oxidation). In this case, the second reduction or oxidation step is easier to perform than the first, which is described as potential inversion.[53]

$$A + e^- \rightleftharpoons A^{\bullet -} \qquad E°_1 \tag{2.11}$$

$$A^{\bullet -} + e^- \rightleftharpoons A^{2-} \qquad E°_2 \tag{2.12}$$

An early example of reduction occurring with potential inversion was discovered in 1964 by Balch et al.[54] The polarographic investigation of various nitrobenzenes revealed that dinitrodurene (see Figure 2.14) only showed a singly polarographic wave, whereas most of the other tested molecules exhibited normal ordering of potentials with two separated reduction waves. Recently, dinitrodurene was further investigated, and the reduction with potential inversion confirmed and attributed to structural change upon two-electron reduction (see Figure 2.14).[53, 55]

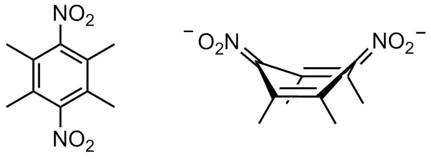

Figure 2.14: Chemical structure of neutral and doubly-reduced dinitrodurene.

In most cases, structural change is the principal cause for potential inversion.[56] Upon reduction or oxidation, changing bond lengths and /or dihedral and twisting angles can affect the energies of the highest occupied (HOMO) and lowest unoccupied molecular orbital (LUMO), such that the redox potentials become compressed or even inverted.[57, 58] Furthermore, changing solvation energies of A, $A^{\bullet -}$ and A^{2-} can influence the redox potentials.[59, 60] Often, both structural change and solvation play a role. Whether the transfer or removal of two electrons occurs stepwise or in a concerted manner depends on the extent of potential inversion. In the case of mild inversion (ΔE° ≤ ±0.3 V), intermediate species can sometimes be detected. A concerted transfer is assumed to be likely to occur when there is a strong inversion, i.e. ΔE° ≤ ±1.0 V.[56]

2.5.1 Potential Inversion in Bipyridine Disulfide and Biphenyl Disulfide

Recently, the reduction of 3,8-diiodo-dibenzo[1,2]dithiin and 4,4´-bipyridyl-3,3´-disulfide (see Figure 2.15) was investigated by Benniston and co-workers, and Glass and Lichtenberger, respectively.[61, 62] It was found that both molecules are reduced with potential inversion.

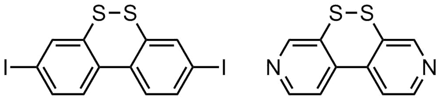

Figure 2.15: Chemical structures of 3,8-diiodo-dibenzo[1,2]dithiin and 4,4´-bipyridyl-3,3´-disulfide.

Cyclic voltammetric measurements of 3,8-diiodo-dibenzo[1,2]dithiin in DCM revealed one reduction half-wave and one re-oxidation half-wave, which are widely separated.[61] Furthermore, the reduction and and re-oxidation peak shift to more negative and positive potentials, respectively, with increasing scan rates. The average separation of the cathodic and anodic peaks was 1.5 V. Calculations and data simulation supported that two-electron reduction occurs with potential inversion, which is attributed to structural change. The dihedral angle between the aromatic rings was calculated as 34°, which changes to 130° upon two-electron reduction. The disulfide bond is assumed to be still intact but elongated upon the uptake of the first electron, and to break with the second. The resulting thiolate groups then rotate away from each other to minimize electrostatic repulsions.

Investigations into 4,4´-bipyridyl-3,3´-disulfide were consistent with these results.[62] The extent of potential inversion, i.e. the difference between reduction and re-oxidation half-waves, was experimentally determined as 0.6 V. DFT calculations confirmed that the first electron goes into the σ*-antibonding orbital of the disulfide bond, which elongates. As a result, the S-C4-C4'-S torsion angle changes from 30° to 40°. Upon the second reduction, the disulfide bond cleaves and the thiolate groups consequently move apart, which is assumed to occur in a concerted manner. Furthermore, the cyclic voltammograms were simulated, and the first and second reduction potentials calculated (-1.35, -0.79 V). They are in very good agreement with the experimentally determined reduction and re-oxidation potentials (-1.4, -0.8 V vs SCE in MeCN).

2.6 Thiol-Disulfide Interchange

Thiol-disulfide interchange describes the reaction of a thiol (RSH) with a disulfide (R'SSR"), leading to the formation a new thiol (R"SH) and disulfide (RSSR') (see Equation 2.13).[63] The reaction is reversible at room temperature and physiological pH, although a strong covalent disulfide bond needs to be cleaved.[64] Thiol-disulfide interchange plays a crucial role in many biological processes, for example in protein folding, where a new disulfide bond is introduced by several subsequent inter- and intramolecular thiol-disulfide interchange reactions.[65, 66] An additional prominent example for this type of reaction in nature is the synthesis of ribonucleotides, intermediates of DNA synthesis, which is catalyzed by ribonucleoreductase. The thiol groups of this enzyme are oxidized during the reaction, and then regenerated by thioredoxin via thiol-disulfide interchange.[67] Furthermore, thiol-disulfide exchange is important for the activation and inhibition of enzymes. Many enzymes contain thiol groups in their active centers, such as thiol proteases, which are inhibited by disulfide bond formation.[68] They can be reactivated by adding strongly reducing thiols, such dithiothreitol (DTT).[69]

$$RSH \ + \ R'SSR'' \rightleftarrows RSSR' \, + \, R''SH \tag{2.13}$$

Thiol-disulfide interchange occurs via a second order nucleophilic substitution (S_N2) reaction.[64, 70] Thiolate (RS^-) acts as nucleophile and attacks the disulfide from the backside, along the disulfide bond axis. A linear "trisulfide-like" transition state (see Figure 2.16) is formed, and the negative charge is delocalized between the sulfur atoms. The reaction follows second-order kinetics, with first-order dependence on the thiol and disulfide concentrations (see Equation 2.14).[71] Since thiolate is the nucleophile, the reaction rate is dependent on its basicity and nucleophilicity, as well as on the pH value of the solution (see Equations 2.15 - 2.17). A low pK_a value is favorable because of the resulting higher thiolate concentration in solution, however, its nucleophilicity consequently decreases. The maximum rate can be achieved if the pK_a value and pH are similar.[72] If the thiol is already fully deprotonated, the reaction is called thiolate-disulfide interchange. In this case, the reaction rate increases with increasing pK_a of the nucleophilic thiolate and decreasing pK_a value of the leaving group. In a mixed disulfide, the cleavage of the thiolate with the lower pK_a value is preferred.[64]

$$\tfrac{d\,[RSSR']}{d\,t} = k\,[RSH]\,[R'SSR''] \tag{2.14}$$

$$RSH \ \rightleftarrows RS^- \, + \, H^+ \ \ (pK_a^{RSH}) \tag{2.15}$$

$$RS^- + R'SSR'' \rightleftarrows RSSR' + R''S^- \tag{2.16}$$

$$R''S^- + H^+ \rightleftarrows R''SH \quad (pK_a^{R''SH}) \tag{2.17}$$

Regarding thiolate-disulfide interchange, reaction rates are higher in polar aprotic solvents, such as DMSO or DMF, than in protic solvents, such as water.[73] In protic solvents, the ground state of the thiolate, as well as the transition state, are stabilized through hydrogen-bonding (see Figure 2.16). However, the transition state is comparatively less stabilized. It is expected to be less influenced by solvation due to delocalization of the negative charge.[73] Hence, the energetic barrier is larger and the rate decreases in protic solvents.

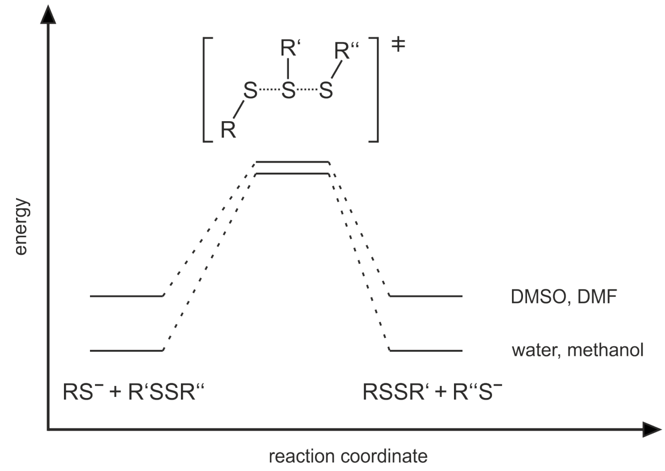

Figure 2.16: Schematic energy profile of Equation 2.16 as a function or the reaction coordinate in protic and polar aprotic solvents.

Substituents in the α-position induce a large steric hindrance when the transition state is formed, and therefore decrease the reaction rate. The substitution of the β-position also influences the rate, but to a lesser extent.[64]

3 Exploiting Potential Inversion for Photoinduced Charge-Accumulation in Molecular Systems

Electron-transfer plays an important role in many biological processes and was intensively studied over the last few decades. In recent years, the accumulation of charges received more attention. It is a crucial aspect of solar fuel production, since the formation of H_2 or the reduction of CO_2 requires the transfer of at least two redox equivalents. Several purely molecular systems have been reported in the literature that are able to accumulate charges, but mostly in the presence of sacrificial agents. There are very few examples capable of storing multiple electrons and holes in the same molecule without using an external electron donor or acceptor.[49–51] However, most of them have very short lifetimes, on the order of a few nanoseconds, except for one system recently developed in our group. In this pentad, a long-living twofold charge-separated state was observed without the use of sacrificial reagents.[51, 52]

In this work, related molecular systems were designed that are theoretically able to accumulate two electrons. In contrast to the previously investigated pentad (see Section 2.4), these systems contain dibenzo[*c*,*e*][1,2]dithiin as a two-electron acceptor. The advantage of this acceptor is that it is reduced with potential inversion, i.e. the second reduction potential is much less negative than the first. Hence, one of the problems of accumulative electron-transfer, a typically more difficult second reduction step, is avoided. Furthermore, there is a strong driving force for the second electron-transfer, making this step potentially more favorable compared to competitive decay pathways. The idea of exploiting potential inversion for charge accumulation is conceptionally novel.

To get first insights into electron-accumulation with potential inversion, a molecular triad was prepared. It contains a central dibenzo[*c*,*e*][1,2]dithiin moiety, which is covalently linked to two ruthenium photosensitizers. This allows the (simultaneous) absorption of two photons. It was assumed that following excitation of the photosensitizers and their subsequent reduction by a sacrificial electron donor, the sensitizers are capable of transferring two electrons to the acceptor. To study charge-accumulation in the absence of sacrificial agents, the triad was extended to a pentad that contains additional triarylamine groups, which act as internal (reversible) electron donors. In the following sections, the synthesis of the triad and pentad and the results of spectroscopic measurements are presented.

Aside from its reduction with potential inversion, dibenzo[*c*,*e*][1,2]dithiin has an additional benefit. Upon two-electron reduction, a dithiolate is formed that can undergo thiol-disulfide interchange reactions. Hence, the electrons stored in the triad and pentad may be used for the two-electron reduction of other disulfides. Results of multi-electron photoredox catalysis are presented in the final section.

3.1 Ref-SS and the Ligand

In Section 2.5.1, previously investigated systems, which are reduced with potential inversion, are presented. Glass and Lichtenberger, and Benniston and co-workers showed that the second reduction step of 4,4´-bipyridyl-3,3´-disulfide and 3,8-diiodo-dibenzo[1,2]dithiin occurs at a much less negative potential than the first.[61, 62] It was found that the disulfide bond breaks upon uptake of the second electron, followed by rotation of the thiolate groups away from each other.

In this work, dibenzo[*c*,*e*][1,2]dithiin (ref-SS) and a more extended ligand, were synthesized. The ligand contains a central dibenzo[*c*,*e*][1,2]dithiin group that is connected on both sides by a *p*-xylene bridging group to 2,2'-bipyridine. The latter moieties make coordination to a photosensitizer possible. To demonstrate that reduction of these molecules also occurs with potential inversion, they were investigated electrochemically. In order to gain insights into their spectroscopic features and how they change upon reduction, UV-vis spectroscopic and spectro-electrochemical measurements were performed.

3.1.1 Synthesis of Ref-SS and the Ligand

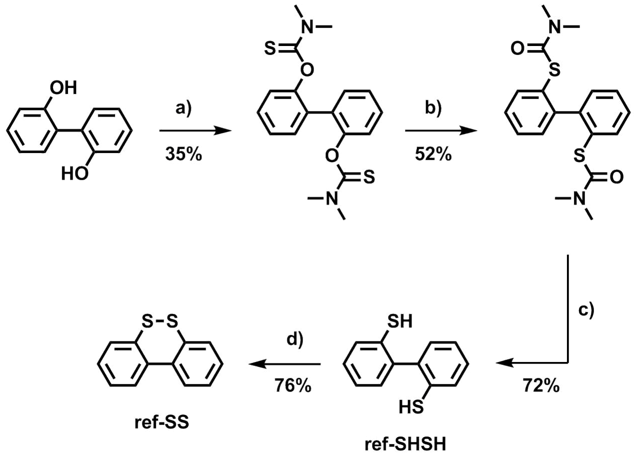

Scheme 3.1: Synthesis of ref-SS: a) NaH, rt, 10 min, dimethylthiocarbamoyl chloride, 85 °C, 3 h; b) tetradecane, 270 °C, 2.3 h; c) $LiAlH_4$, 0 °C, THF, 65 °C, 6.5 h; d) NaHAsc, $MeCN/H_2O$, rt, 6 h.

Ref-SS was synthesized in four steps (see Scheme 3.1). Commercially available biphenyl-2,2'-diol was deprotonated with NaH, followed by thiocarbamoylation. Purification by column chromatography and recrystallization from acetone afforded the desired O-thiocarbamate in 35% yield, but several subsequent recrystallization steps can increase the yield. The S-thiocarbamate was obtained by Newman-Kwart rearrangement at 270 °C in 52%

yield. The starting material and the side product, the singly rearranged species, can be recovered. Reduction with lithium aluminum hydride yielded 2,2'-dimercaptobiphenyl in 72% yield. Subsequent oxidation with sodium ascorbate afforded ref-SS in 76% yield.

To synthesize the ligand, an Ullmann reaction with 4-iodo-3-methoxynitrobenzene and activated copper powder in DMF at 180 °C was performed, affording 2,2‘-dimethoxy-4,4‘-dinitrobiphenyl in 76% yield. The nitro groups were reduced by sodium sulfide in a solvent mixture of toluene and water. Rigorous stirring in the presence of tetra-*n*-butylammonium bromide as a phase-transfer agent afforded 2,2‘-dimethoxy-4,4‘diamino-biphenyl in 82% yield. The amine groups were converted to iodo groups via Sandmeyer reaction in 87% yield. The methoxy groups were deprotected by boron tribromide almost quantitatively. 4,4-Diiodo-2,2-biphenol was deprotonated with NaH, followed by thiocarbamoylation, affording the O-thiocarbamate in 53%, which was rearranged by a Knewman-Kwart reaction in the absence of solvent. Due to the formation of several side products, including the corresponding thiophene and disulfide species, the yield of the S-thiocarbamate was relatively low at 44%. The mono-substituted bipyridine was synthesized via Negishi coupling between 2-iodo-5-bromo-pyridine and 2-pyridylzinc bromide. In the presence of $[Pd(PPh_3)_4]$ as a catalyst, 5-bromo-2,2‘-bipyridine was obtained in 77% yield. The *p*-xylene bridging moiety was attached via Suzuki coupling with 2,5-dimethyl-4-trimethylsilylphenylboronic acid. The TMS-protecting group was converted into a bromo group by addition of $Br_{2.}$ Stirring of the reaction mixture in the absence of light at room temperature for 2.5 h afforded the product in 88% yield. A Miyaura borylation reaction was then performed, affording the boronic acid pinacol ester (bpy-xy-bpin) in 88% yield. Several different catalysts, solvents and bases were tested to find the best reaction conditions to couple bpy-xy-bpin with dimethylthiocarbamic acid O-(2'dimethylthiocarbamoyloxy-4,4'-diiodobiphenyl-2-yl)ester. The best yield (24%) was achieved with $[Pd(PPh_3)_4]$ as a catalyst and Na_2CO_3 as a base in a solvent mixture of THF and water at 85 °C. The formation of the disulfide from the S-thiocarbamate was achieved by alkaline deprotection with NaOH in MeOH and THF, and oxidation of the thiol groups by air. The ligand was obtained in 34% yield.

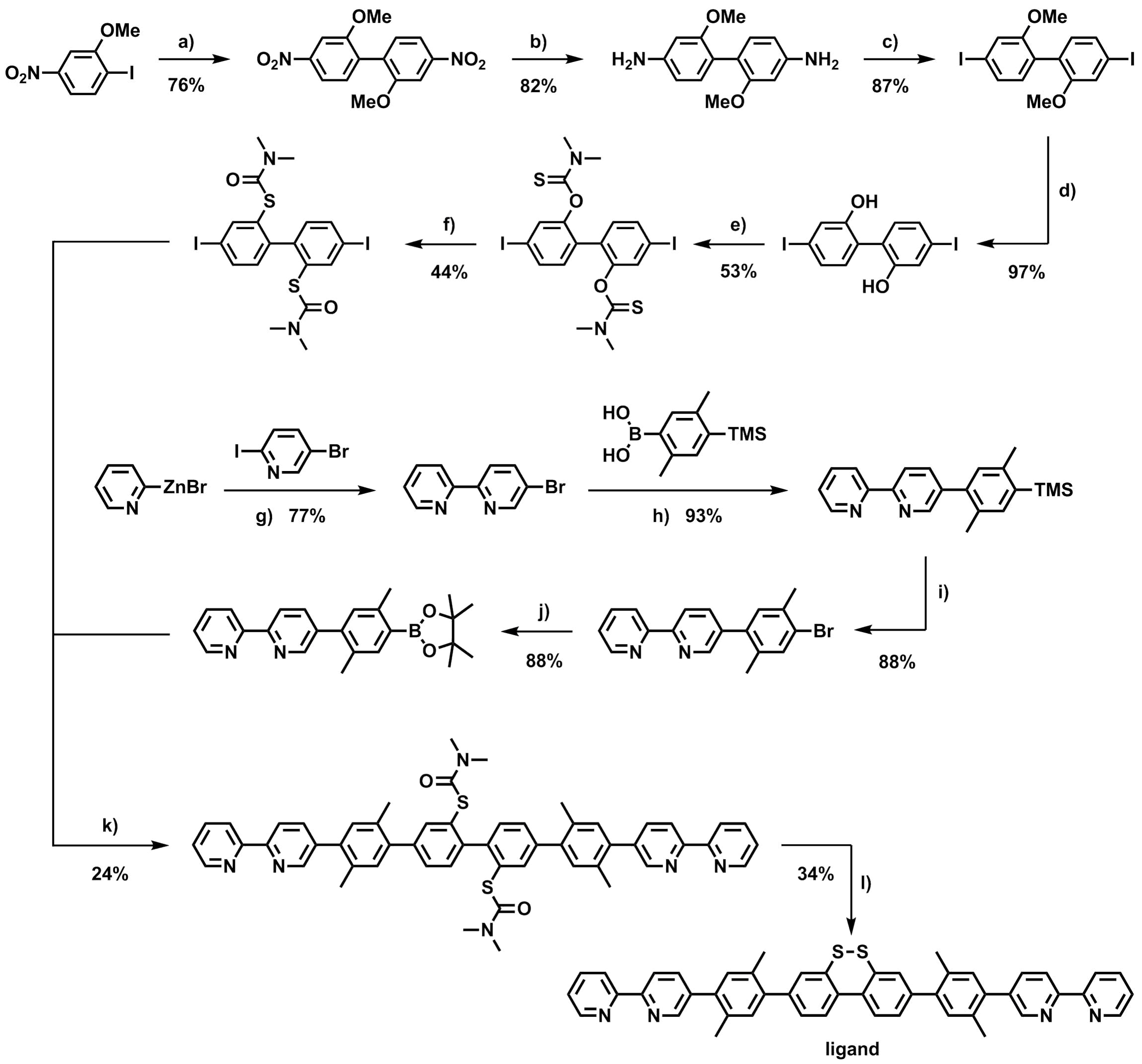

Scheme 3.2: Reaction scheme for the ligand synthesis: a) activated Cu-powder, DMF, 180 °C, 18 h; b) TBABr, $Na_2S \cdot 9\ H_2O$, toluene/H_2O, 95 °C, 16 h; c) HCl, MeCN/H_2O, $NaNO_2$ -10 °C, 15 min, KI, -10 °C, overnight, 80 °C; d) BBr_3, -78 °C, DCM, overnight, rt; e) NaH, rt, 45 min, dimethylthiocarbamoyl chloride, 95 °C, overnight; f) 265 °C, 1.5 h; g) $[Pd(PPh_3)_4]$, THF, 75 °C, 18 h; h) $[Pd(PPh_3)_4]$, Na_2CO_3,THF, 90 °C, 24 h; i) Br_2, KOAc, THF, 2.5 h in the dark, 2.5 h; j) bis(pinacolato)diboron, $[Pd(PPh_3)_4]$, KOAc, DMF, 120 °C, 17 h; k) $[Pd(PPh_3)_4]$, Na_2CO_3, THF/H_2O, 85 °C, 22 h; l) NaOH, MeOH/THF, 80 °C, 2 h.

3.1.2 Optical Absorption Spectroscopy

For spectroscopic characterization, UV-vis absorption spectroscopy of both reference molecules, ref-SS and the ligand, was performed.

Ref-SS

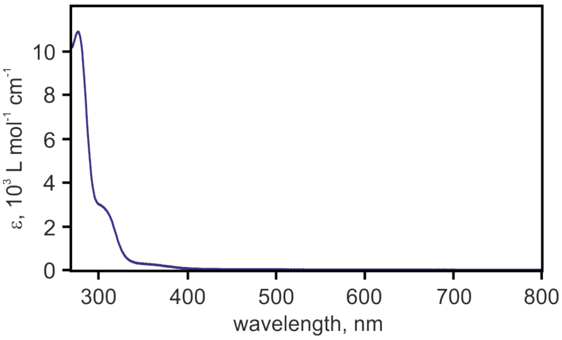

Figure 3.1: UV-vis absorption spectrum of ref-SS in MeCN.

The UV-vis absorption spectrum of ref-SS in dry MeCN is presented in Figure 3.1. The absorption bands observed at 276 nm (ε = 10,900 L mol^{-1} cm^{-1}) and 305 nm (ε = 2,900 L mol^{-1} cm^{-1}) are attributed to $\pi \rightarrow \pi^*$ transitions. They are in good agreement with previously investigated 9,10-dihydrophenanthrene.[74, 75] The absorption band at 355 nm (ε = 300 L mol^{-1} cm^{-1}) can be assigned to the $n \rightarrow \pi^*$ transition associated with the sulfur atoms.

Ligand

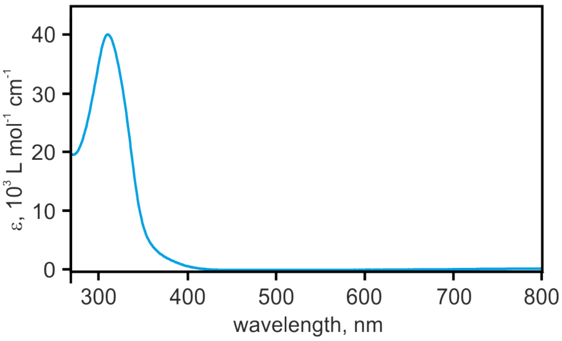

Figure 3.2: UV-vis absorption spectrum of the ligand in DCM.

The UV-vis absorption spectrum of the ligand is presented in Figure 3.2. Because of low solubility in MeCN, dry DCM was used as the solvent. The ligand has an absorption maximum at 310 nm, with an extinction coefficient of 40,000 L mol^{-1} cm^{-1}. In contrast to ref-SS, the π-system of the ligand is more extended resulting in one intense π → π* transition band.

3.1.3 Electrochemistry

In order to investigate the potential inversion of ref-SS and ligand reductions, cyclic voltammetric measurements were performed. Studies of these reference molecules were performed in dry, Ar-purged solvents to minimize the amount of dissolved oxygen. The solutions contained 0.1 M tetra-*n*-butylammonium hexafluorophosphate ($TBAPF_6$) as a supporting electrolyte. The voltammograms were measured against a saturated calomel electrode (SCE). Ref-SS was also studied in the presence of acid.

Ref-SS in the Absence of Acid

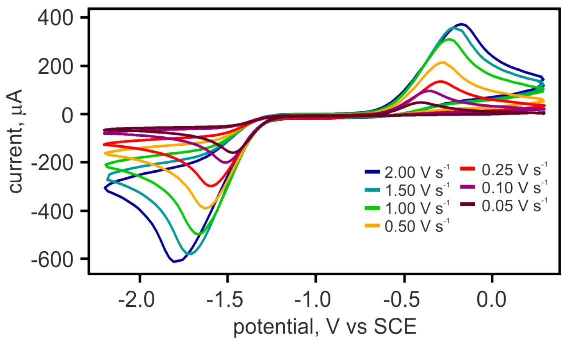

Figure 3.3: Cyclic voltammograms of ref-SS (5.1 mM) in dry, Ar-purged MeCN, containing 0.1 M $TBAPF_6$ as supporting electrolyte. Sweep rates range from 50 mV s^{-1} to 2 V s^{-1} (see inset).

The cyclic voltammograms of ref-SS in dry MeCN measured with different sweep rates are presented in Figure 3.3. On cathodic scans, the peak potentials vary from -1.78 to -1.47 V vs SCE, and on the return scans from -0.45 to -0.17 V vs SCE. Reduction followed by oxidation is chemically reversible, as demonstrated by several subsequent scans. With increasing scan rates, both the reduction potential and current become more negative, while both the peak potential and current of the return oxidation become more positive. The results of these measurements are in good agreement with the previously investigated systems, see Section 2.5.1.[61] The fact that there is just one peak for the two-electron reduction, as well as for the return oxidation, and the wide separation between the peaks indicate that dibenzo[*c*,*e*][1,2]dithiin is reduced with potential inversion. This can be attributed to structural changes, i.e. the disulfide bond breaking upon reduction, and the consequent rotation of the thiolate groups away from each other to minimize the electrostatic repulsion (see Scheme 3.3).

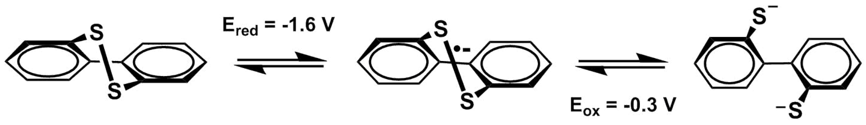

Scheme 3.3: Proposed structural changes upon reduction of ref-SS (V vs SCE).

The average reduction potential of -1.6 V vs SCE can be assigned clearly to the first reduction step. Considering the mechanism proposed in Scheme 3.3, the potential for the second reduction step can be assumed to be the average potential (-0.3 V) of the return oxidation. Investigations with 4,4´-bipyridyl-3,3´-disulfide (see Section 2.5.1) showed that the calculated second reduction potential and experimentally determined return oxidation potential are nearly the same.[62] Therefore, the first and second reduction potentials of ref-SS are proposed to be -1.6 and -0.3 V vs SCE in the following discussions.

Ref-SS in the Presence of Acid

To investigate to what extent the reduction or oxidation of ref-SS is influenced by acid, cyclic voltammetric measurements were performed in the presence of *para*-toluenesulfonic acid (TsOH). The pK$_a$ value of TsOH is 8.6 in MeCN.[76] The pK$_a$ values of the dithiol species (ref-SHSH) of ref-SS have not been reported in the literature. As an approximation, the pK$_a$ value of thiophenol (10.3 in DMSO)[77] was converted into the pK$_a$ in MeCN (22.4) by applying Equation 3.1[76]. In comparison to TsOH, ref-SHSH is a much weaker acid. It is therefore likely that the thiolate groups of doubly reduced ref-SS are protonated, such that the redox potentials may change.

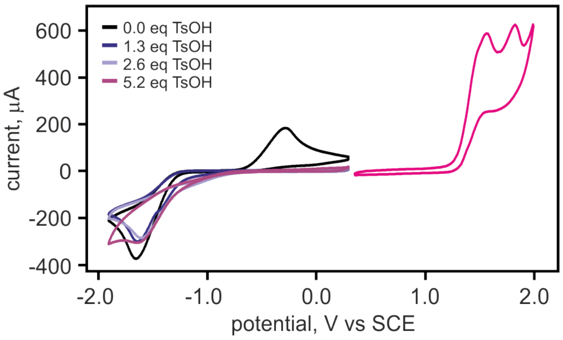

Figure 3.4: Cyclic voltammograms of ref-SS (6.0 mM, left) in the presence of increasing TsOH concentrations (see inset) and of ref-SHSH (6.0 mM, right) in dry, Ar-purged MeCN, containing 0.1 M TBAPF$_6$ as supporting electrolyte, measured at a sweep rate of 0.5 V s^{-1}.

$$pK_a\,(MeCN) = 12.31 + 0.98 \cdot pK_a\,(DMSO) \tag{3.1}$$

The cyclic voltammograms of ref-SS in dry MeCN, in both the absence and presence of TsOH, are presented in Figure 3.4. The two-electron reduction and return oxidation of the disulfide in the absence of TsOH is explained above. Increasing TsOH concentrations, up to 5.2 eq, does not affect the two-electron reduction potential of the disulfide significantly, which shifts by only 50 mV to less negative values. The peak for the two-electron return oxidation at -0.3 V vs SCE disappears after addition of TsOH. In the presence of acid, the dithiolate is protonated, and therefore, the oxidation potential shifts to a more positive value. To obtain the oxidation potentials of the formed dithiol, the cyclic voltammogram of ref-SHSH was measured. There are two irreversible oxidation waves at 1.56 and 1.82 V vs SCE that are assigned to the first and second dithiol oxidations.

Ligand

The cyclic voltammograms of the reduction of the ligand are presented in Figure 3.5. Due to solubility reasons, measurements were performed in DCM instead of MeCN. In contrast to ref-SS (-1.61 V vs SCE in MeCN, at 0.5 V s^{-1}), the peak potential for the two-electron reduction of the ligand is shifted to more negative values (-1.82 V vs SCE in DCM, at 0.5 V s^{-1}). Ref-SS in DCM also showed more negative reduction and more positive re-oxidation potentials in comparison to the measurements performed in MeCN. Hence, these differences can be attributed to a solvent effect.[78] Furthermore, there is no peak for the return oxidation apparent at this sweep rate. That might be explained by the wide potential separation and slow electrode kinetics in DCM leading to the diffusion of the reduced species away from the electrode, before return oxidation can occur.[61] Therefore, the sweep rate was increased to 2.0 V s^{-1}. At faster scan rates, a weak oxidation wave can be observed at -0.13 V vs SCE.

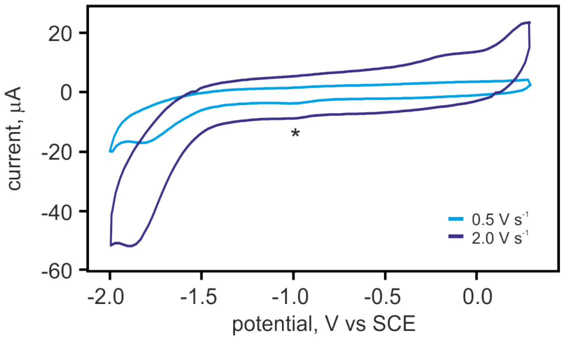

Figure 3.5: Cyclic voltammograms of the ligand (0.43 mM) in dry, Ar-purged DCM, containing 0.1 M $TBAPF_6$ as supporting electrolyte, measured at sweep rates of 0.5 and 2.0 V s^{-1}. *Reproducible impurity at the working electrode.

3.1.4 Spectro-Electrochemistry

In order to investigate how the optical absorption changes upon disulfide reduction, spectro-electrochemical measurements were performed. The ground state UV-vis spectrum was measured as the baseline, followed by applying a certain potential and measuring the absorbance again. On the basis of the cyclic voltammetric studies, potentials of at least -1.8 V vs SCE were applied. Such strongly negative potentials were necessary to ensure the disulfide reduction in both ref-SS and the ligand.

Ref-SS

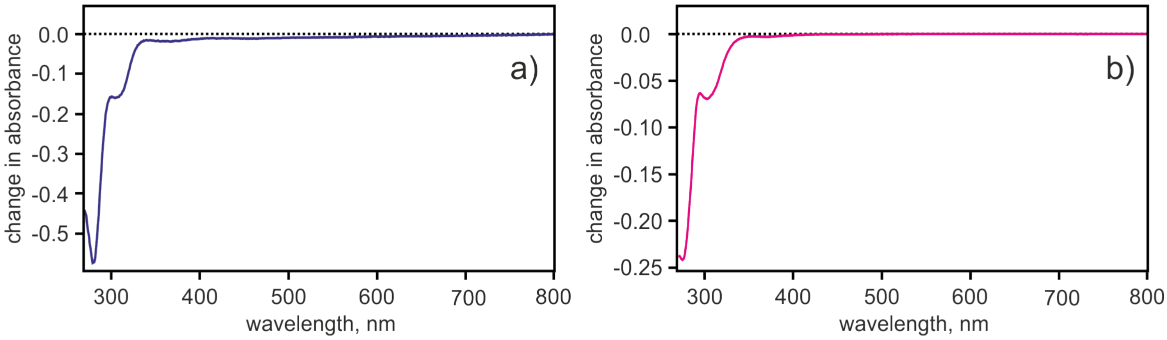

Figure 3.6: a) Difference spectrum of ref-SS (1.0 mM) in dry, Ar-purged DCM, containing 0.1 M TBAPF$_6$ as supporting electrolyte, after applying a potential of -1.8 V (vs SCE); b) calculated difference spectrum of ref-SHSH ($9 \cdot 10^{-5}$ M) and ref-SS (obtained after oxidation of ref-SHSH for 24 h by air) in dry MeCN.

The difference spectrum of ref-SS in DCM after reduction at -1.8 V vs SCE to the dithiolate is presented in Figure 3.6. Due to the reduction, the disulfide bond is cleaved and the thiolate groups rotate away from each other to reduce the electrostatic repulsion. The dihedral angle for the inter-ring connection approximately changes from 34° to 130°.[61] By increasing the dihedral angle, the π-conjugation decreases, leading to a bleach in absorption of the presented bands.[74]

To show how the absorbance changes going from the disulfide to the dithiol, a solution of ref-SHSH in MeCN was prepared. The absorption was measured directly after preparation as well as after oxidation by air. The difference spectrum is presented in Figure 3.6b, calculated by subtracting the absorption spectrum of ref-SS obtained after oxidation for 24 h by air from the spectrum of ref-SHSH. As expected, it is in good agreement with the spectrum of reduced ref-SS, since in both cases the disulfide bond is cleaved and the dihedral angle between phenyl units changes, although probably to a lesser extent in the case of ref-SHSH.

Ligand

The difference spectrum of the ligand in dry DCM after reduction at -2.0 V vs SCE is presented in Figure 3.7. The reduction potential of 2,2'-bipyridine ranges from -2.2 to -2.3 V vs SCE (measured in DMF, THF and MeCN, respectively).[79–81] Hence, the disulfide is the only moiety that is reduced at the applied potential. There is a bleach at 330 nm, whereas a new band arises at 285 nm. As in the case of ref-SS, the disulfide bond of the ligand is cleaved upon reduction and the thiolate groups rotate away from each other. For this reason, the pi-conjugation decreases, resulting in a hypsochromic shift.[82]

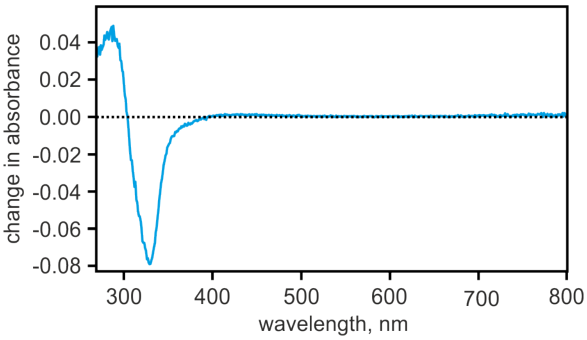

Figure 3.7: Difference spectrum of the ligand ($9.9 \cdot 10^{-5}$ M) in dry, Ar-purged DCM, containing 0.1 M $TBAPF_6$ as supporting electrolyte, after applying a reduction potential of -2.0 V (vs SCE).

3.1.5 Summary

Electrochemical investigations with ref-SS and the ligand revealed that the second reduction potential of both molecules is more than 1.0 V less negative compared to the first. Due to the large potential inversion, there is a strong driving force for the second reduction step. Potential inversion is attributed to disulfide bond cleavage upon the uptake of the second electron, and the consequent rotation of the thiolate groups away from each other. Furthermore, it was demonstrated that the presence of acid does not influence the two-electron reduction of the disulfide (at least not in the tested concentration range), but the thiolate groups are protonated, which shifts the re-oxidation potentials to much more positive values. Spectro-electrochemical measurements showed that the structural change of ref-SS and the ligand upon two electron reduction results in absorption bleaches at 310 nm and 330 nm, respectively.

3.2 Charge-Accumulation in a Molecular Triad

In the following sections, the light-induced electron-accumulation in a molecular triad was investigated. The measurements presented in Section 3.1 already showed that ref-SS and the ligand are reduced with potential inversion. Electrochemical studies showed that the second reduction potential is over 1.0 V less negative than the first. Hence, there is a strong driving force for the second reduction. Furthermore, UV-vis spectroscopic and spectro-electrochemical investigations revealed that both molecules absorb around 310 nm, decreasing upon disulfide bond cleavage and rotation. Hence, a possible disulfide reduction in the triad could be detected by a decreased absorption around 310 nm. With these results in hand, the ligand was coordinated to two ruthenium bipyridine precursors. The bipyridine ligands contain *tert*-butyl groups in the para-positions, which have electron-donating character (+I-effect), increasing the reducing power of the sensitizer. The proposed mechanism for photo-driven electron-accumulation is shown in Figure 3.8. The ruthenium sensitizers are excited by light and reductively quenched by a sacrificial electron donor. Two electrons are then transferred to the disulfide moiety, one from each reduced sensitizer. In comparison to other multi-electron acceptors, the inverted reduction potentials of the disulfide should facilitate electron-accumulation.

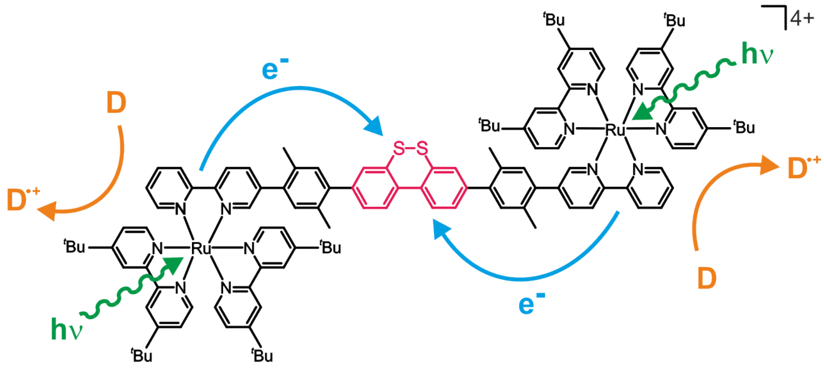

Figure 3.8: Schematic representation of light-induced electron-accumulation in the triad.

3.2.1 Synthesis of Ref-Ru-^{t}Bu and the Triad

The synthesis of the triad and its reference complex [Ru((^{t}Bu)$_2$bpy)$_2$(bpy-xy)](PF$_6$)$_2$ (ref-Ru-^{t}Bu) are presented in Scheme 3.4. To synthesize the ligand of ref-Ru-^{t}Bu, a Grignard reagent from 2,5-dimethylbromobenzene was prepared, followed by its reaction with boric acid to yield xy-B(OH)$_2$ in 69% yield, which was then coupled to 5-bromo-2,2'-bipyridine via Suzuki coupling to afforded bpy-xy-H in 86% yield. Commercially available 4,4'-di-*tert*-butyl-2,2'-bipyridine and RuCl$_3$ · 0.5 H$_2$O were heated to reflux for 6 h and the precursor complex was obtained in 23% yield. Bpy-xy-H was coordinated to the precursor by heating both reactants in a mixture of EtOH and DCM to reflux for 17 h. After purification by column chromatography, the nitrate counterion (obtained from the eluent) was exchanged with hexafluorophosphate (PF_6^-). Ref-Ru-^{t}Bu was isolated in 87% yield. The triad was prepared and purified the same way, but the reaction mixture was stirred for 46 h, yielding 43%.

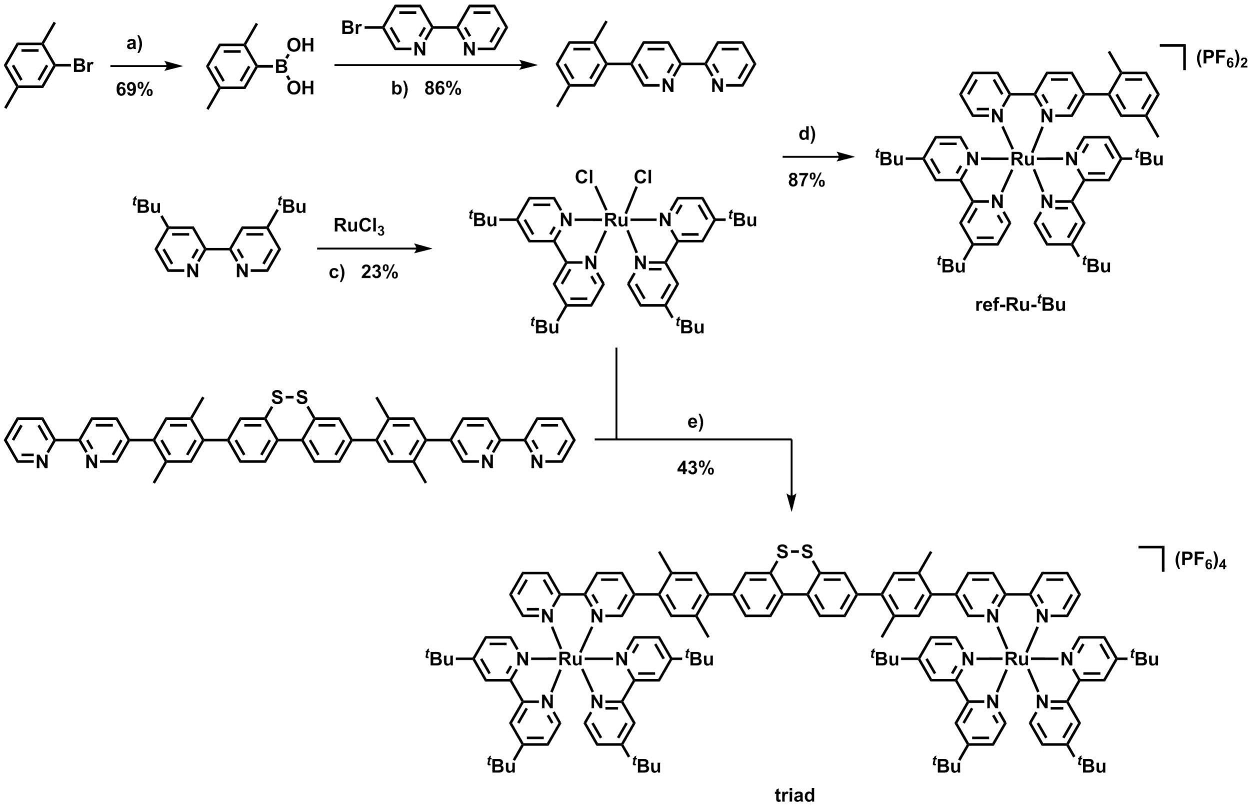

Scheme 3.4: Synthesis of ref-Ru-^{t}Bu and the triad: a) Mg, THF, reflux, 3.5 h, -78 °C, $B(OH)_3$, rt, 2.5 d; b) $[Pd(PPh_3)_4]$, Na_2CO_3, THF/H_2O, 90 °C, 20 h; c) LiCl, DMF, reflux, 6 h; d) EtOH/DCM, reflux, 17 h; e) EtOH/DCM, reflux, 46 h.

3.2.2 Optical Absorption Spectroscopy

For optical characterization, UV-vis spectra of the triad (orange trace) and ref-Ru-^{t}Bu (grey trace) were measured in dry MeCN. As presented in Figure 3.9, both molecules exhibit similar absorption profiles, whereas the absorption of the triad is twice as intense as that of ref-Ru-^{t}Bu. The prominent absorption at 288 nm can be assigned to the $\pi \rightarrow \pi^*$ transition centered on the bipyridine ligands. The broad absorption band at 450 nm arises from a ^{1}MLCT (d_π(Ru) $\rightarrow$ π^*(bpy)) transition. The triad spectrum differs from ref-Ru-^{t}Bu by an additional absorption band at 325 nm. This band is attributed to the dibenzo[*c*,*e*][1,2]dithiin absorption, as this moiety is not present in ref-Ru-^{t}Bu and it is also in agreement with the ligand absorption (see Section 3.1.2).

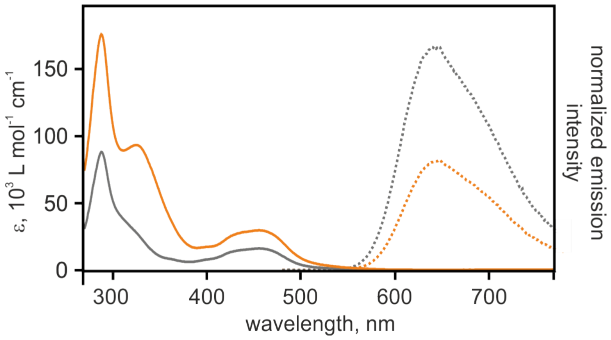

Figure 3.9: UV-vis absorption (solid line) and steady state emission (dashed line) spectra of ref-Ru-^{t}Bu (grey trace) and the triad (orange trace) in dry, de-oxygenated MeCN (λ_{ex} = 450 nm). The emission intensity was normalized against ε_{450}.

The emission intensity of both complexes was normalized against the extinction coefficient at the excitation wavelength (450 nm). Ref-Ru-^{t}Bu exhibits an emission maximum at 642 nm and the triad at 644 nm. It was expected that the normalized emission of the triad has the same intensity as ref-Ru-^{t}Bu, but it is quenched by more than 50%. Compared to ref-Ru-^{t}Bu, the triad may have two different conformations. Hence, it might be possible that in one of the triad conformations the non-radiative decay is enhanced, resulting in the luminescence quenching. Another reason for the decreased emission might be intramolecular electron-transfer to the disulfide.

3.2.3 Electrochemistry

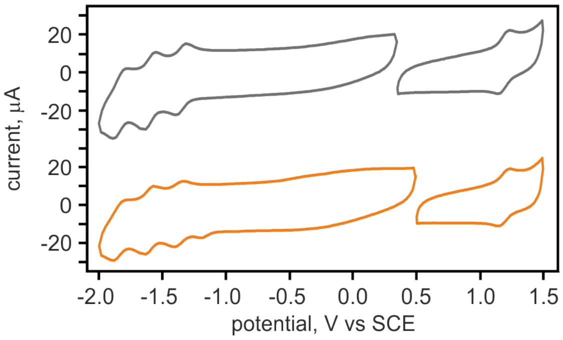

Figure 3.10: Cyclic voltammograms of ref-Ru-^{t}Bu ($1.2 \cdot 10^{-4}$ M, grey trace) and the triad ($6.3 \cdot 10^{-5}$ M, orange trace) in dry, Ar-purged MeCN, containing 0.1 M TBAPF$_6$ as supporting electrolyte, measured at a sweep rate of 0.5 V s^{-1}. The oxidative and reductive sweeps were measured separately to obtain voltammograms of higher quality.

The cyclic voltammograms of ref-Ru-^{t}Bu (grey trace) and the triad (orange trace) are presented in Figure 3.10. Table 3.1 summarizes the redox potentials obtained from the cyclic voltammograms. Additionally, the oxidation and reduction potentials of the excited ruthenium sensitizer ($*[Ru(bpy)_3]^{2+}$) were estimated on the basis of the zero-zero MLCT energy (E^{00} = 2.10 eV)[83] of $[Ru((^tBu)bpy)_2(bpy)]^{2+}$.

Table 3.1: Redox potentials (V vs SCE) of ref-Ru-^{t}Bu and the triad in MeCN extracted from the voltammograms in Figure 3.10, and estimated redox potentials of ^{3}MLCT-excited ref-Ru-^{t}Bu and triad.

	ref-Ru-^{t}Bu	triad
$E(Ru^{3+/2+})$	+1.19	+1.19
$E(bpy_1{}^{0/-1})$	-1.36	-1.36
$E(bpy_2{}^{0/-1})$	-1.60	-1.60
$E(bpy_3{}^{0/-1})$	-1.82	-1.88
$E(*[Ru(bpy)_3]^{3+/2+})$	-0.91	-0.91
$E(*[Ru(bpy)_3]^{2+/1+})$	0.74	0.74

As expected, in both cases three bipyridine reduction waves between -1.36 and -1.88 V are observed, as well as the ruthenium oxidation at 1.19 V vs SCE. In contrast to ref-Ru-^{t}Bu there is an additional peak at -1.21 V vs SCE in the triad voltammogram. This signal may be assigned to the disulfide reduction, although it is less negative compared to the reduction potential obtained from ref-SS (-1.61 V vs SCE) measured at the same sweep rate. A shift to more positive values would be reasonable, because of the spatial proximity of the disulfide to the two positively charged sensitizers. The half wave of the return oxidation is not observed. The reason for this might be a relatively low triad concentration as well as slow electrode kinetics. Due to the wide separation of reduction and return oxidation potential the reduced species may diffuse away from the electrode, before the return oxidation can occur. For the same reason the return oxidation peaks of ref-SS and the ligand are also (much) less intense than the initial reduction peak (see Section 3.1.3).

On the basis of these redox potentials, the energies (E) for the different species involved during the charge-accumulation were estimated with Equation 3.2, and the driving force for electron-transfer (ΔG_{ET}) for the single pathways with Equation 3.3. For the first and second disulfide reduction, the average potentials of ref-SS ($E_{red,1}$ = -1.6 V, $E_{red,2}$ = -0.3 V) were taken. Since it cannot be excluded that the disulfide, bound to the sensitizers, is reduced at -1.21 V, the energies were estimated on the basis of this value, too. They are given in brackets in Scheme 3.5 and Scheme 3.6. The second reduction potential is expected to shift to less negative value to the same extent as the first, but due to the lack of any specific value the average return oxidation potential of ref-SS (-0.3 V) was taken. The calculations were made in the absence and presence of triethylamine (TEA) as an external electron donor. The oxidation potential of TEA is 0.47 V vs Fc$^+$/Fc[84] in MeCN, which was converted into 0.85 V vs SCE by adding 0.38 V[85]. The detailed calculations of the energies of the different states are given in the Appendix. .

$$E = -\, e\, \left(\sum E_{red} - \sum E_{ox}\right) \tag{3.2}$$

$$\Delta G_{ET} = -\, e\, \left(E_{red} - E_{ox}\right) \tag{3.3}$$

The energy level scheme estimated for photoinduced charge-accumulation in the triad in MeCN without the use of TEA is presented in Scheme 3.5. Under these conditions, it is unlikely that, upon mono-excitation, an electron is transferred from the excited photosensitizer to the disulfide, forming Ru^{3+}-[SS]$^{\bullet-}$-Ru^{2+}, due to the strongly endergonic driving force.

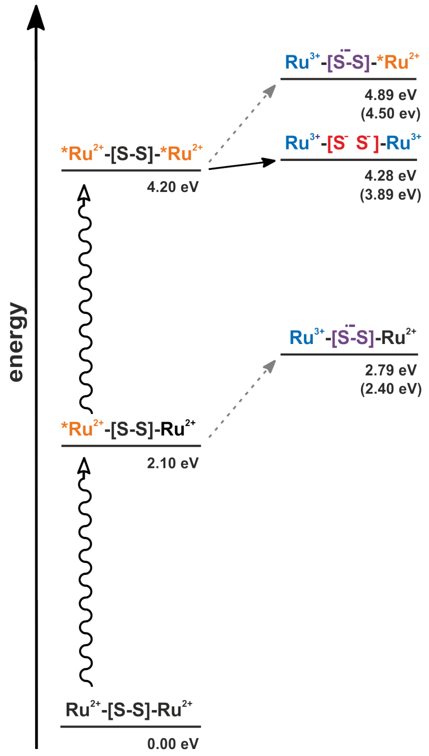
energy
Ru^{3+}-[S$^{\bullet-}$-S]-*Ru^{2+}
4.89 eV
(4.50 ev)
*Ru^{2+}-[S-S]-*Ru^{2+}
4.20 eV
Ru^{3+}-[S$^-$ S$^-$]-Ru^{3+}
4.28 eV
(3.89 eV)
Ru^{3+}-[S$^{\bullet-}$-S]-Ru^{2+}
2.79 eV
(2.40 eV)
*Ru^{2+}-[S-S]-Ru^{2+}
2.10 eV
Ru^{2+}-[S-S]-Ru^{2+}
0.00 eV

Scheme 3.5: Energy scheme for the formation of the charge-separated states in the triad in MeCN in the absence of TEA, based on the redox potentials listed in Table 3.1 and estimated in Section 3.1.3. The energies given in brackets were estimated on the basis of the first reduction potential of the disulfide extracted from the cyclic voltammogram of the triad. Solid and dashed arrows represent likely and unlikely pathways, respectively.

However, in the case of double excitation there is the possibility that two electrons are transferred together, one from each sensitizer, such that Ru^{3+}-[S^- S^-]-Ru^{3+} is formed. Since the first single electron-transfer from the excited photosensitizer to the disulfide is (highly) endergonic, a concerted transfer of two electrons cannot be excluded. The driving force for the latter pathway is either slightly endergonic by +0.08 eV or rather exergonic by -0.31 eV, such that the formation of the charge-separated state Ru^{3+}-[S^- S^-]-Ru^{3+} might be possible.

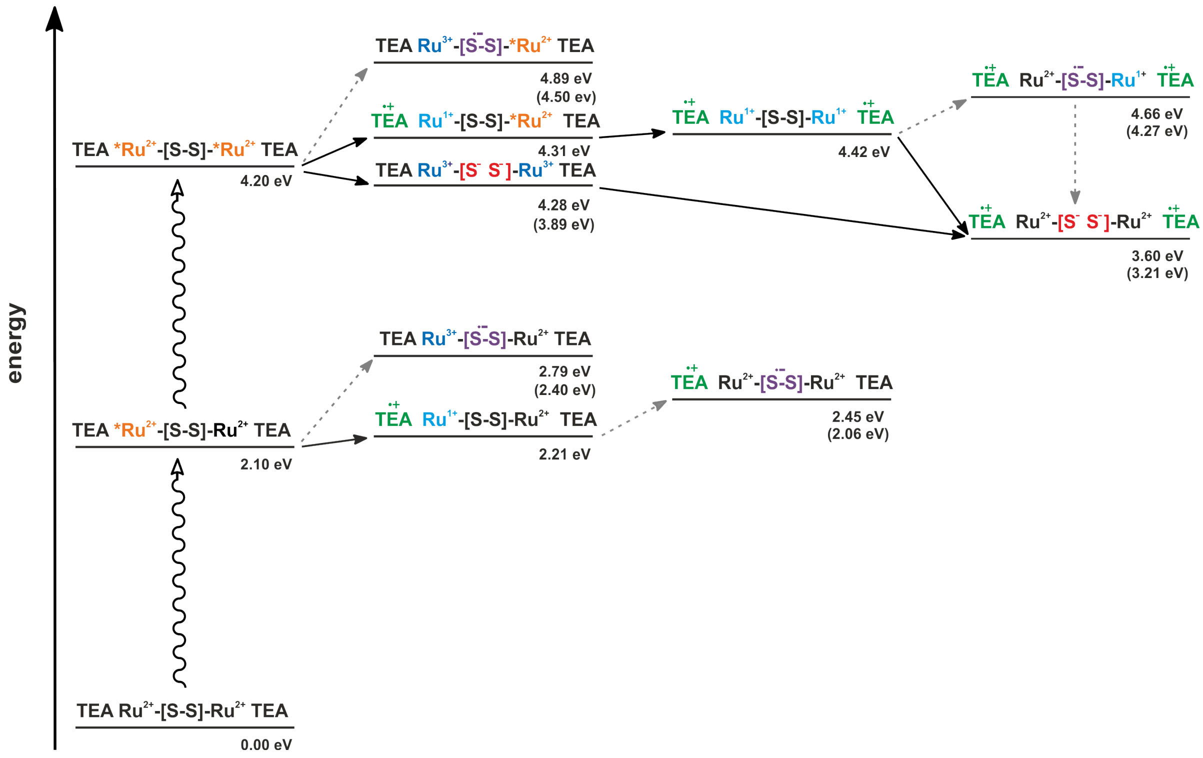
energy
TEA Ru2+-[S-S]-Ru2+ TEA
0.00 eV
TEA *Ru2+-[S-S]-Ru2+ TEA
2.10 eV
TEA *Ru2+-[S-S]-*Ru2+ TEA
4.20 eV
TEA Ru3+-[S•−-S]-Ru2+ TEA
2.79 eV
(2.40 eV)
TEA•+ Ru1+-[S-S]-Ru2+ TEA
2.21 eV
TEA•+ Ru2+-[S•−-S]-Ru2+ TEA
2.45 eV
(2.06 eV)
TEA Ru3+-[S•−-S]-*Ru2+ TEA
4.89 eV
(4.50 ev)
TEA•+ Ru1+-[S-S]-*Ru2+ TEA
4.31 eV
TEA Ru3+-[S- S-]-Ru3+ TEA
4.28 eV
(3.89 eV)
TEA•+ Ru1+-[S-S]-Ru1+ TEA•+
4.42 eV
TEA•+ Ru2+-[S•−-S]-Ru1+ TEA•+
4.66 eV
(4.27 eV)
TEA•+ Ru2+-[S- S-]-Ru2+ TEA•+
3.60 eV
(3.21 eV)

Scheme 3.6: Energy scheme for the formation of the charge-separated states in the triad in MeCN in the presence of TEA, based on the redox potentials listed in Table 3.1 and estimated in Section 3.1.3. The energies given in brackets were estimated on the basis of the first reduction potential of the disulfide extracted from the cyclic voltammogram of the triad. Solid and dashed arrows represent likely and unlikely pathways, respectively.

The energy level scheme estimated for photoinduced electron-accumulation in the triad in the presence of TEA is presented in Scheme 3.6. In the presence of this sacrificial electron donor, it is still possible to form the same states as in the absence, therefore they are also presented in this scheme. TEA is a common sacrificial electron donor for reductive quenching of $[Ru(bpy)_3]^{2+}$.[86–88] The estimated reaction free energy for electron-transfer from TEA to the excited triad (ΔG_{ET} = +0.11 eV) is just slightly more positive compared to $[Ru(bpy)_3]^{2+}$ (ΔG_{ET} = +0.08 eV). Hence, the excited triad should be reduced by

TEA. After mono-excitation, the triad may be reduced by TEA, but single electron-transfer from the reduced sensitizer to the disulfide is unlikely, due to the endergonic driving force. Considering the less negative disulfide reduction potential in the triad, it may occur. However, due to the slightly endergonic driving force for reductive quenching of the sensitizer, it is also possible that the singly excited triad is excited a second time before it is reduced by TEA. When both sensitizers are reduced, there is, due to the potential inversion, a driving force of at least -0.8 eV to transfer two electrons to the disulfide and to form the charge-separated state Ru^{2+}-[S^- S^-]-Ru^{2+}. The same state can be formed when the oxidized sensitizers in the charge-separated state, Ru^{3+}-[S^- S^-]-Ru^{3+}, are reduced by TEA, which is energetically preferred compared to the former pathway.

Due to the uncertainty regarding the reduction potentials of the disulfide in the triad, the energies of the different states could not be clearly determined. Based on pure thermodynamic estimations and considering the less negative disulfide reduction potential, light-induced electron-accumulation in the triad should take place in the presence of TEA, and is potentially also possible without use of a sacrificial electron donor.

3.2.4 Spectro-Electrochemistry

To identify the twofold charge-separated state, the spectral features of the reduced disulfide needs to be known. In Section 3.1.4, it was already shown that the absorbance of the ligand decreases around 330 nm upon reduction. To determine whether there is a similar bleach in the triad, spectro-electrochemical measurements were performed with ref-Ru-^{t}Bu and the triad.

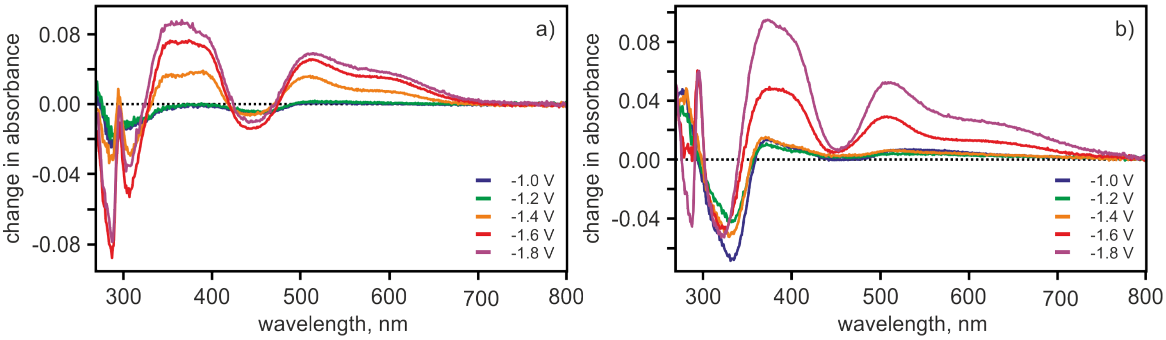

Figure 3.11: Difference spectrum of (a) ref-Ru-^{t}Bu ($1.1 \cdot 10^{-4}$ M) and (b) the triad ($5.0 \cdot 10^{-5}$ M) after reduction at increasingly negative potentials (V vs SCE, see inset) in dry, Ar-purged MeCN, containing 0.1 M $TBAPF_6$ as supporting electrolyte.

The difference spectra of (a) ref-Ru-^{t}Bu and the (b) triad in MeCN after reduction are presented in Figure 3.11. Ref-Ru-^{t}Bu exhibits decreasing absorbance at 287 nm and 308 nm. Starting at a reduction potential of -1.4 V, new broad absorption bands due to

$\pi \rightarrow \pi^*$ transitions centered on the reduced bipyridine ligands around 370 nm and from 510 nm to 610 nm are observed. These changes in absorption are in good agreement with previously performed spectro-electrochemical studies with $[Ru(bpy)_3]^{2+}$.[89]

Applying a potential of -1.0 V, the triad exhibits a bleach at 330 nm and increasing absorbance at 280 nm, which agree with the spectral features of the reduced ligand (see Figure 3.7), and can therefore be assigned to the reduced disulfide moiety. This observation supports the assumption, made in the previous section, that the disulfide reduction potential becomes less negative when it is bound to the positively charged sensitizers. At higher potentials, the bipyridine ligands are reduced too, evidenced by the increasing absorption at 380 nm and 510 nm.

3.2.5 Time-Resolved Emission Spectroscopy

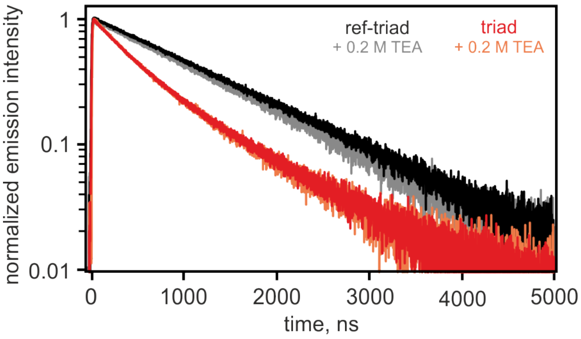

Figure 3.12: Normalized luminescence decays at 625 nm of the triad and ref-Ru-^{t}Bu in the absence (red and black traces, respectively) and presence (orange and grey traces, respectively) of 0.2 M TEA in dry, de-oxygenated MeCN.

In order to get further information about the photochemical processes taking place in the triad, the decay of the emission was measured and lifetimes determined. The emission decays of de-oxygenated, 10^{-5} M solutions of ref-Ru-^{t}Bu and the triad in MeCN, in both the absence and presence of TEA are presented in Figure 3.12. Emission decays were monitored at 625 nm, with laser excitation at 532 nm and a pulse duration of ~10 ns.

The emission of ref-Ru-^{t}Bu decays mono-exponentially, with a lifetime of 1250 ns. The triad exhibits biexponential decay, with lifetimes of 436 and 1215 ns, with contributions of 62% and 38%, respectively. The decay component with the shorter emission lifetime is consistent with luminescence quenching to the same extent as observed in steady-state emission spectra (see Figure 3.9). On the one hand, the biexponential decay may be a result of different conformations of the triad, as briefly discussed in Section 3.2.2. On the other hand, it is suggestive of intramolecular electron-transfer from the photoexcited sensitizer to the disulfide. The estimations made in Section 3.2.3 indicate that the formation of the twofold charge-separated state in the absence of a sacrificial agent is possible. Hence, in the case of double excitation, the shorter observed lifetime may be related to a concerted electron-transfer from the sensitizers to the disulfide upon double excitation. A sequential transfer is unlikely due to an endergonic driving force of at least 0.3 eV for the first electron-transfer step. For the same reason, it is also unlikely that there is single electron transfer to the disulfide upon mono excitation. Consequently, the mono excited triad would decay with the same lifetime as ref-Ru-^{t}Bu.

By adding 0.2 M TEA, the luminescence lifetime of ref-Ru-^{t}Bu is slightly decreased to 1190 ns. The triad also shows just minor lifetime changes in the presence of TEA (1178, 418 ns). This is in agreement with the estimated driving force for reductive quenching of ref-Ru-^{t}Bu and the triad, which showed that TEA is a possible, though weak sacrificial reductant.

3.2.6 Transient Absorption Spectroscopy

Transient absorption spectra of ref-Ru-^{t}Bu (black trace) and the triad (red trace) in MeCN are presented in Figure 3.13. Both ref-Ru-^{t}Bu and the triad exhibit similar transient absorption spectra. There are negative signals around 650 and 465 nm due to stimulated emission and MLCT absorption bleaching, respectively. The absorption bands at 390 and 530 nm are assigned to the formally reduced bipyridine in the ^{3}MLCT excited state of the photosensitizer. In contrast to ref-Ru-^{t}Bu, the spectrum of the triad shows a significant bleach around 330 nm.

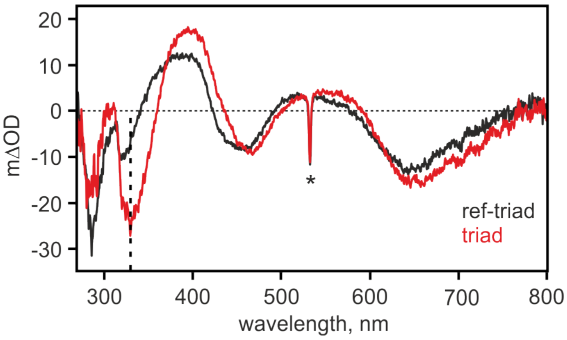

Figure 3.13: Transient absorption spectra of ref-Ru-^{t}Bu ($1.0 \cdot 10^{-5}$ M, black trace) and the triad ($1.0 \cdot 10^{-5}$ M, red trace) in dry, de-oxygenated MeCN. Spectra were recorded directly after excitation with a 10 ns laser pulse at 532 nm, integrated over 200 ns. *Scattered excitation light.

The decay of the transient absorption signal at 390 nm and the bleach recovery at 465 nm are presented in Figure 3.14. As expected, the lifetimes measured at these wavelengths

(~1200 and 400 ns) are consistent with the emission lifetimes, and can therefore be assigned to excited triad. The significant bleach at 330 nm in the transient absorption spectrum of the triad is in the same region as expected for doubly reduced disulfide. Hence, the transient absorption spectrum of the triad may exhibit the superposition of ^{3}MLCT excited state and the charge-separated state Ru^{3+}-[S$^-$ S$^-$]-Ru^{3+}. In this case, it is expected that the bleach at 330 nm recovers with a different lifetime as the bleach at 465 nm and the transient absorption at 390 nm decays. However, the lifetimes determined at 330 nm are the same as measured at 465 and 390 nm (~1200 and 400 ns).

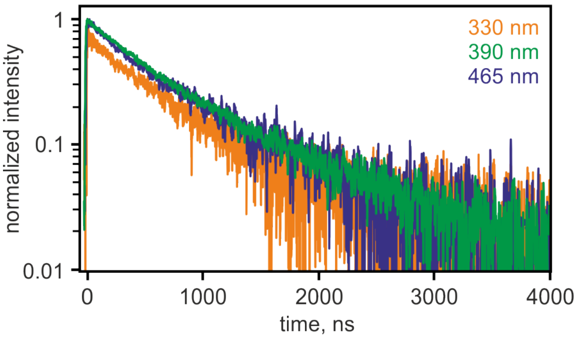

Figure 3.14: Normalized transient absorption decays of the triad in MeCN.

Assuming that this bleach forms due to the twofold disulfide reduction, it might be possible that the formation of the twofold charge-separated species decays faster than it is formed. Then, the decay of this species could not be observed and the lifetime not measured. But in this case a (much) less intense bleach at 330 nm would be expected. On the other hand, it might be possible that the bleach at 330 nm is not a result of the doubly reduced disulfide, but a part of the excited state spectrum. As shown in Figure 3.9, the triad has a stronger ground state absorption around 330 nm compared to ref-Ru-^{t}Bu, that is assigned to the dibenzo[*c*,*e*][1,2]dithiin absorption. Possibly, this band is weakened upon excitation this band is weakened resulting in a bleach in this region. On this assumption the two different decay absorption lifetimes might be attributed to two different triad conformations.

3.2.7 Continuous Irradiation Measurements

In order to form the twofold charge-separated state, the triad was continuously irradiated in the presence of TEA. As shown in Section 3.2.5, TEA is a poor reductive quencher for the triad. However, small amounts of the triad are reduced at excess TEA concentrations upon photoexcitation. It is known that some polypyridyl Ru(II) complexes can be permanently reduced upon irradiation in the presence of TEA.[90] The radical cation of oxidized

TEA can decompose by different pathways, to a final non-radical product. Hence, back electron-transfer from the reduced triad to $TEA^{\bullet +}$ is suppressed and the reduced complex accumulates.

Absorption spectra of the triad in the presence of TEA after several minutes of continuous LED (3.5 W) irradiation at 455 nm are presented in Figure 3.15a. By subtracting the spectrum of the non-irradiated triad from the spectra after irradiation, difference spectra were obtained (Figure 3.15b). There are relatively weak transient absorption bands at 390 and 520 nm and a bleach at 450 nm. Comparison with the spectrum of reduced ref-Ru-^{t}Bu (Figure 3.15c) shows that they can be assigned to spectral features of reduced sensitizer, i.e. reduced bipyridine. Furthermore, the difference spectra shown in Figure 3.15b exhibit a strong bleach at 332 nm, which is in very good agreement with the bleach in the difference spectrum of the reduced ligand (Figure 3.15d), and can therefore be attributed to doubly reduced disulfide.

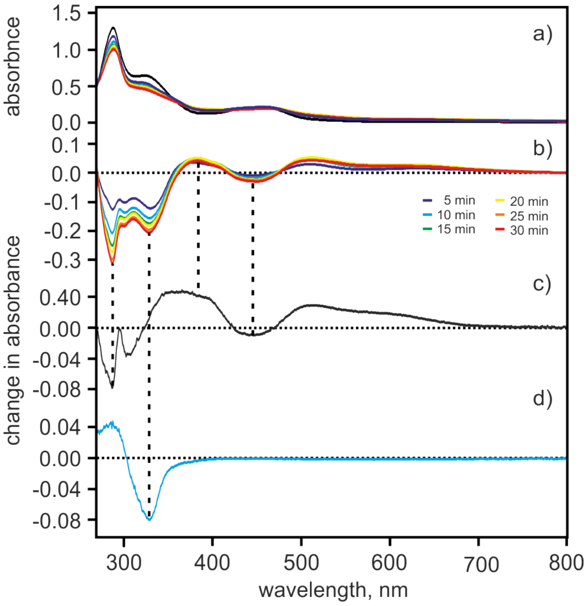

Figure 3.15: (a) UV-vis absorption and (b) UV-vis difference spectra of the triad ($8.7 \cdot 10^{-6}$ M) in dry, de-oxygenated MeCN in the presence of 0.5 M TEA after irradiation at 455 nm for several minutes (see inset); difference spectrum of (c) ref-Ru-^{t}Bu in MeCN and (d) the ligand in DCM after applying potentials of -1.8 and -2.0 V (vs SCE), respectively.

In summary, the formation of the twofold charge-separated state of the triad was shown, accumulating under continuous irradiation in the presence of TEA. Upon irradiation the triad is excited and one of the sensitizers is reduced. A following single electron-transfer to the disulfide is thermodynamically uphill and therefore unlikely (see Section 3.2.3).

Thus, the absorption bands at 390 and 520 nm are assigned to singly reduced triad. In the case that both sensitizers are reduced, there is a strong driving force to transfer the electrons to the disulfide (see Section 3.2.3) such that the disulfide bond breaks and the thiolate groups rotate away from each other, observed as the bleach at 330 nm. With increasing irradiation time, the number of triad molecules where both sensitizers are reduced increases. Consequently, more twofold charge-separated triad is formed and the corresponding bleach becomes more intense.

3.2.8 Summary

In the preceding sections, first insights into the light-induced charge-accumulation of a new molecular triad are given. The triad is a photosensitizer-acceptor-photosensitizer assembly, which was expected to accumulate two electrons in the presence of a sacrificial electron donor. The acceptor is covalently linked to two ruthenium tris(bipyridyl) complexes, which allows the (simultaneous) absorption of two photons. Two of the bipyridine ligands are substituted with *tert*-butyl groups to increase the reducing power of the reduced sensitizer. Dibenzo[*c*,*e*][1,2]dithiin was chosen as an electron acceptor, because it is reduced with potential inversion of more than 1.0 V, resulting in a very strong driving force for the second reduction. Hence, the key feature of the triad is that there is a strong driving force for the second reduction step, which was expected to facilitate electron-accumulation.

Cyclic voltammetric and spectro-electrochemical measurements indicate that the disulfide reduction in the triad is approximately 0.4 V less negative compared to ref-SS. This is assumed to be a result of the close proximity of the disulfide to the two positively charged sensitizers. Accordingly, thermodynamic estimations revealed that two electrons may be transferred to the disulfide if the triad is doubly excited. It was found that the emission of the triad decays biexponentially. Additionally, there is a significant bleach at 330 nm in the transient absorption spectrum of the triad, that is in the same region as expected for the doubly reduced disulfide. Both measurements evidence towards the formation of the twofold charge-separated state upon double excitation. However, the lifetime of this species could not be determined. The bleach at 330 nm recovers with the same lifetime as observed for the excited triad, which is not in accordance with the hypothesis that the twofold charge-separated state was formed.

Alternatively, the triad may be existent in two different conformations explaining the biexponential decay.

Furthermore, the triad was investigated in the presence of TEA and continuous irradiation. Under these conditions the twofold-charge separated state is formed and accumulates.

3.3 Charge-Accumulation in a Molecular Pentad

In the previous sections, light-induced electron-accumulation in a molecular triad was investigated. It was found that in the presence of a sacrificial electron donor the twofold charge-separated state is formed.

In the following, photoinduced charge-accumulation in a molecular pentad was investigated. This pentad also contains dibenzo[*c*,*e*][1,2]dithiin as a two-electron acceptor, which is covalently linked to two ruthenium sensitizers. In contrast to the triad, the ancillary bipyridine ligands are mono-substituted with triarylamine (TAA) moieties, which act as internal electron donors. Previous investigations revealed efficient reductive quenching of excited ruthenium bipyridyl complexes by TAA[52, 91], thus it is also expected for the pentad. The proposed mechanism of light-induced charge-accumulation is presented in Figure 3.16.

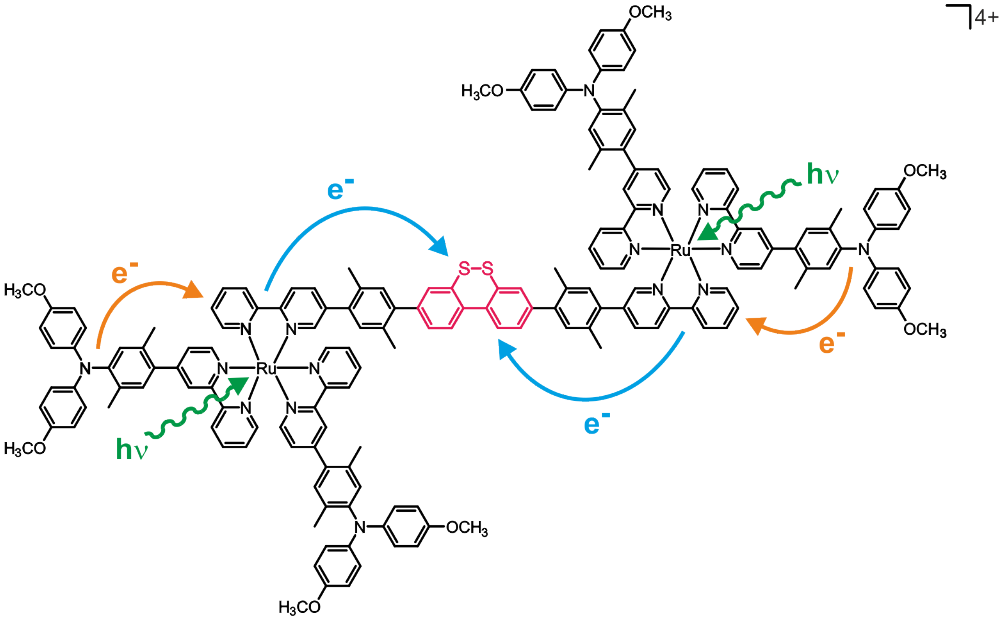

Figure 3.16: Schematic representation of light-induced charge-accumulation in the pentad.

Upon double excitation, the sensitizers of the pentad are reductively quenched by TAA, followed by electron-transfer to the disulfide. In contrast to the triad, the pentad has the advantage that no external reductant is necessary. Furthermore, intramolecular electron-transfer from TAA to the excited sensitizers is much more efficient than reductive quenching of the triad by TEA. For this reason, more efficient formation of the desired photoproduct is expected.

3.3.1 Synthesis of Ref-Ru-TAA and the Pentad

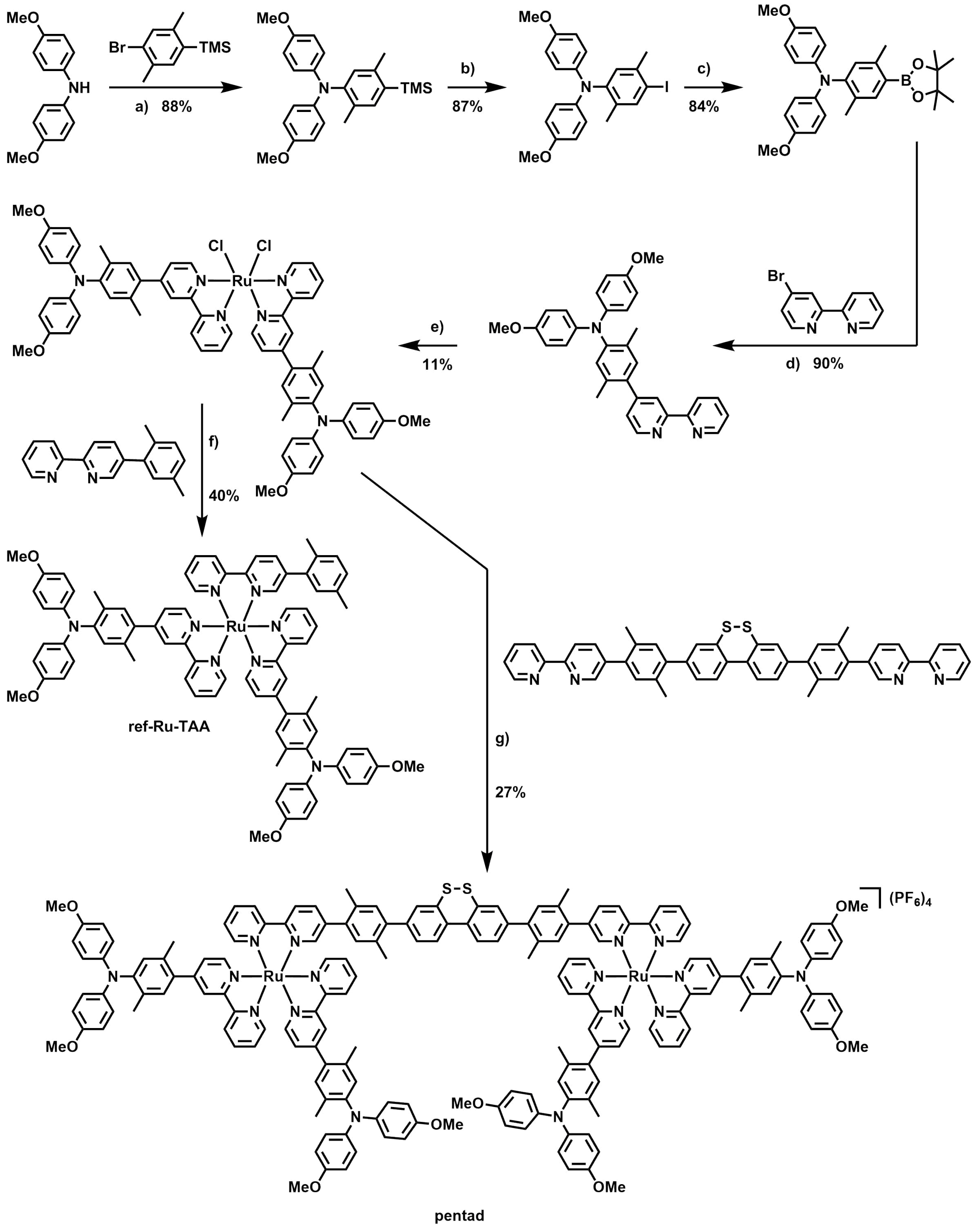
MeO
NH
MeO
Br
TMS
a) 88%
MeO
N
TMS
MeO
b)
87%
MeO
N
I
MeO
c)
84%
MeO
N
B
O
O
MeO
Br
N
N
d) 90%
OMe
MeO
N
N
N
e)
11%
MeO
N
Cl
Cl
N
Ru
N
N
N
MeO
N
OMe
MeO
f)
40%
N
N
MeO
N
N
N
Ru
N
N
N
MeO
ref-Ru-TAA
N
OMe
MeO
S-S
N
N
N
N
g)
27%
MeO
N
S-S
N
N
N
N
Ru
N
N
N
N
Ru
N
N
N
MeO
OMe
(PF6)4
OMe
N
N
OMe
MeO
N
OMe
MeO
OMe
pentad

Scheme 3.7: Synthesis of ref-Ru-TAA and the pentad: a) [Pd(dba)$_2$], KO^{t}Bu, [HP^{t}Bu$_3$]-BF$_4$, toluene, 90 °C, 17 h, b) ICl, DCM, -78 °C, 10 min; c) bis(pinacolato)diboron, [Pd(PPh$_3$)$_4$], KOAc, DMSO, 90 °C, 20.5 h; d) [Pd(PPh$_3$)$_4$], Na$_2$CO$_3$, THF/H$_2$O, 85 °C, 23 h; e) [Ru(DMSO)$_4$Cl$_2$], LiCl, DMF, 170 °C, 90 min; f) EtOH/DCM, reflux, 18 h; g) EtOH/DCM, reflux, 48 h.

The 4-triarylamine-2,2'-bipyridine ligand (4-TAA-bpy) was prepared in four steps, in good yields. Buchwald-Hartwig cross-coupling between 4,4'-dimethoxy-diphenylamine and Br-xy-TMS was first performed, followed by conversion of the TMS group into an iodo group by addition of ICl at -78 °C. The following Miyaura borylation reaction afforded the boronic acid pinacol ester, which was connected to 4-bromo-2,2'-bipyridine through Suzuki coupling to afford 4-TAA-bpy in 90% yield. $[Ru(DMSO)_4Cl_2]$, 4-TAA-bpy and LiCl were then heated to reflux in DMF. Subsequent purification by column chromatography afforded the precursor complex in 11% yield. Bpy-xy-H was coordinated to the precursor by heating to reflux both reactants in a mixture of EtOH and DCM for 18 h. After purification by column chromatography, the nitrate counterion (obtained from the eluent) was exchanged with PF_6^-. Ref-Ru-TAA was isolated in 40% yield. The pentad was prepared and purified the same way, but the reaction mixture was stirred for 48 h, yielding 27%. The different isomers of the pentad were not separated.

3.3.2 Optical Absorption Spectroscopy

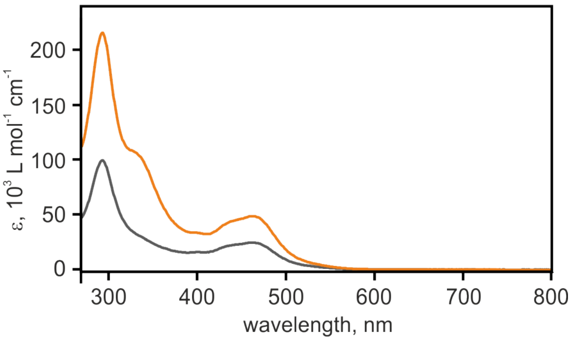

Figure 3.17: UV-vis absorption spectra of the pentad (orange trace) and ref-Ru-TAA (grey trace) in dry MeCN.

The UV-vis absorption spectra of the pentad (orange trace) and ref-Ru-TAA (grey trace) in MeCN are presented in Figure 3.17. Both spectra exhibit $\pi \rightarrow \pi^*$ absorptions centered on the bipyridine ligands at 294 nm, as well as a broad band at 450 nm assigned to the ^{1}MLCT ($d_\pi(Ru) \rightarrow \pi^*(bpy)$) transition. The absorbance of the pentad is twice as intense as the reference, as expected. In contrast to ref-Ru-TAA, the pentad spectrum has an additional shoulder at 330 nm. This band is also observed in the triad spectrum, and can therefore be assigned to the dibenzo[*c*,*e*][1,2]dithiin absorption. Emission of ref-Ru-TAA and the pentad after excitation at 450 nm is completely quenched due to intramolecular electron-transfer from TAA to the sensitizers, and is therefore not presented.

3.3.3 Electrochemistry

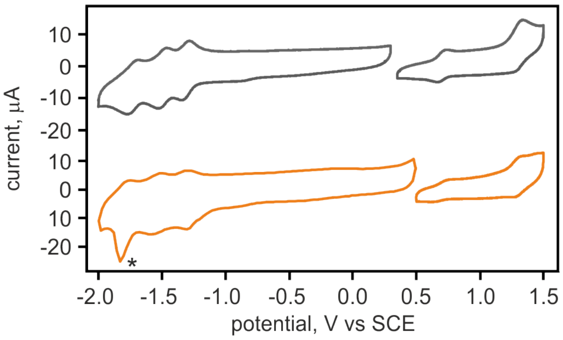

Figure 3.18: Cyclic voltammograms of ref-Ru-TAA ($8.3 \cdot 10^{-5}$ M, grey trace) and the pentad ($3.9 \cdot 10^{-5}$ M, orange trace) in dry, Ar-purged MeCN, containing 0.1 M $TBAPF_6$ as supporting electrolyte, measured at a sweep rate of 0.5 V s^{-1}. The oxidative and reductive sweeps were measured separately to obtain voltammograms of higher quality. *Adsorption on the electrode.

The cyclic voltammograms of ref-Ru-TAA (grey trace) and the pentad (orange trace) in MeCN, are presented in Figure 3.18. Table 3.2 summarizes the redox potentials obtained from the cyclic voltammograms. Additionally, the oxidation and reduction potentials of the excited ruthenium sensitizers ($*[Ru(bpy)_3]^{2+}$) were estimated, on the basis of E^{00} of $[Ru(bpy)_3]^{2+}$ (2.12 eV)[31]. As expected, in both complexes three bipyridine reduction waves between -1.30 and -1.79 V vs SCE are observed. Ruthenium is oxidized at +1.30 and TAA at +0.70 V. The cyclic voltammogram of the triad exhibits a half wave around -1.21 V vs SCE that is assigned to the disulfide reduction (see Section 3.2.3). A reduction peak at the same or similar potential cannot be clearly determined in this cyclic voltammogram.

Table 3.2: Reduction potentials (V vs SCE) of ref-Ru-TAA and the pentad in MeCN extracted from the voltammograms in Figure 3.18, and estimated redox potentials of ^{3}MLCT-excited ref-Ru-TAA and pentad.

	ref-Ru-TAA	pentad
$E(Ru^{3+/2+})$	+1.29	+1.30
$E(TAA^{1+/0})$	+0.70	+0.70
$E(bpy_1{}^{0/-1})$	-1.32	-1.30
$E(bpy_2{}^{0/-1})$	-1.50	-1.54
$E(bpy_3{}^{0/-1})$	-1.73	-1.79
$E(*[Ru(bpy)_3]^{3+/2+})$	-0.83	-0.82
$E(*[Ru(bpy)_3]^{2+/1+})$	+0.80	+0.82

On the basis of these redox potentials, E for the different states of the pentad involved during the charge-accumulation were estimated with Equation 3.2 and ΔG_{ET} with Equation 3.3 (see Section 3.2.3). Investigations with the triad revealed a less negative first reduction potential compared to the estimated value for the disulfide reduction of ref-SS (-1.6 V vs SCE). A potential of -1.21 V vs SCE was extracted from the triad cyclic voltammogram. This value is used for the energy calculations in the pentad. The peak for the return oxidation could not be observed, hence there is no second reduction potential available. For this reason, the second reduction potential of ref-SS (-0.3 V vs SCE) was taken, although it should also be less negative (see Section 3.2.3). The energy level scheme is presented in Scheme 3.8.

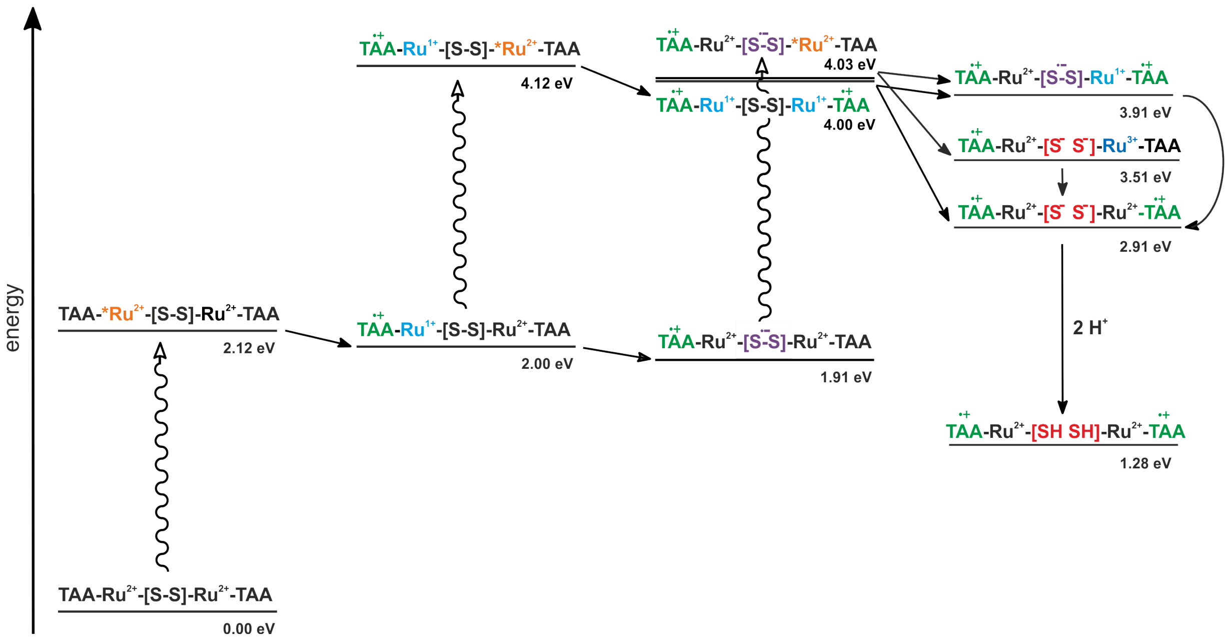
energy
TAA-Ru^{2+}-[S-S]-Ru^{2+}-TAA
0.00 eV
TAA-*Ru^{2+}-[S-S]-Ru^{2+}-TAA
2.12 eV
TAA$^{\bullet+}$-Ru^{1+}-[S-S]-Ru^{2+}-TAA
2.00 eV
TAA$^{\bullet+}$-Ru^{1+}-[S-S]-*Ru^{2+}-TAA
4.12 eV
TAA$^{\bullet+}$-Ru^{2+}-[S$\overset{\bullet-}{}$S]-Ru^{2+}-TAA
1.91 eV
TAA$^{\bullet+}$-Ru^{2+}-[S$\overset{\bullet-}{}$S]-*Ru^{2+}-TAA
4.03 eV
TAA$^{\bullet+}$-Ru^{1+}-[S-S]-Ru^{1+}-TAA$^{\bullet+}$
4.00 eV
TAA$^{\bullet+}$-Ru^{2+}-[S$\overset{\bullet-}{}$S]-Ru^{1+}-TAA$^{\bullet+}$
3.91 eV
TAA$^{\bullet+}$-Ru^{2+}-[S$^-$ S$^-$]-Ru^{3+}-TAA
3.51 eV
TAA$^{\bullet+}$-Ru^{2+}-[S$^-$ S$^-$]-Ru^{2+}-TAA$^{\bullet+}$
2.91 eV
2 H$^+$
TAA$^{\bullet+}$-Ru^{2+}-[SH SH]-Ru^{2+}-TAA$^{\bullet+}$
1.28 eV

Scheme 3.8: Energy scheme for the formation of the charge-separated states in the pentad in MeCN in both the absence and presence of TsOH, based on the redox potentials listed in Table 3.2 and estimated in Section 3.1.3 and 3.2.3 and Appendix.

After excitation of one photosensitizer, it is reductively quenched by electron-transfer from TAA. There are then two possible productive pathways for charge-accumulation. On the one hand, the pentad can be excited again (on the second photosensitizer), followed by reductive quenching. Afterwards, both electrons can be transferred to the disulfide, either sequentially or in a concerted mechanism. In the second pathway, the disulfide is singly reduced prior to the second excitation of the pentad. After absorption of a second photon, the excited sensitizer could be reduced by TAA, but due to the stronger driving force, electron-transfer to the disulfide is more likely. The oxidized ruthenium would then be reduced by TAA in a following step.

On the basis of the thermodynamic estimations, both pathways are possible. If both states, TAA$^{•+}$-Ru^{1+}-[SS]-Ru^{2+}-TAA and TAA$^{•+}$-Ru^{2+}-[SS]$^{•-}$-Ru^{2+}-TAA, would be formed, the latter might have a longer lifetime, due to a less exergonic driving force for charge-recombination and a larger distance between the charges, making a second excitation more probable.

The energies of the charge-separated states are also estimated in the presence of acid. It is assumed that the presence of acid does not affect any other state but the twofold charge-separated state. In Section 3.1.3, it was shown that the reduction of ref-SS is not significantly influenced by TsOH and a protonation of TAA is also not expected.[92] The driving force for dithiolate protonation was estimated with Equation 3.4, on the basis of the pK$_a$ value of TsOH (8.6 in MeCN)[76] and the approximated pK$_a$ value of the dithiol (22.4 in MeCN, see Section 3.1.3), corresponding to thiophenol.

$$\Delta G_{PT} = -\,e \cdot 0.059\ V \cdot (pK_a\,(base) - pK_a\,(acid)) \tag{3.4}$$

The protonation step is strongly exergonic, by approximately 1.6 eV. When the twofold charge-separated and protonated state TAA$^{•+}$-Ru^{2+}-[SH SH]-Ru^{2+}-TAA$^{•+}$ is formed, the only way to recombine to the ground state is through concerted proton-coupled electron-transfer. An initial electron-transfer will not take place, because of the strongly endergonic driving force for electron-transfer from the dithiol to TAA$^{•+}$ of 0.9 eV for the first and 1.1 eV for the second step, based on the oxidation potentials from ref-SHSH (E$_{ox,\,1}$ = 1.56 V, E$_{ox,\,1}$ = 1.82 V, see Section 3.1.3). The same holds true for an initial deprotonation, which is endergonic by 1.6 eV for both protons. Thus, the only mechanism for charge-recombination is a back electron-transfer from the thiol groups to TAA that is concerted with thiol deprotonation by TsO$^-$. For this reason, this state is expected to be relatively stable and long-lived, particularly because TsO$^-$ will be present only at very low (µm) concentrations.

3.3.4 Spectro-Electrochemistry

In the following section, the pentad was investigated spectro-electrochemically. The desired twofold charge-separated state is composed of oxidized TAA and reduced disulfide. The electrochemical reduction of the triad already revealed a bleach around 330 nm, and the same is expected for the pentad.

Difference spectra of ref-Ru-TAA and the pentad in MeCN after reduction are presented in Figure 3.19. The difference spectra of ref-Ru-TAA exhibit broad absorption bands around 355 and 515 nm, due to $\pi \rightarrow \pi^*$ transitions centered on the reduced bipyridine ligands.[89] The former is overlapped with a bleach at 290 nm.The pentad spectra exhibit the same spectral features as ref-Ru-TAA, but there is an additional bleach at 331 nm. As well as for the triad (see Section3.2.4), this bleach is attributed to the two-electron reduction of the disulfide and consequent rotation of the thiolate groups away from each other.

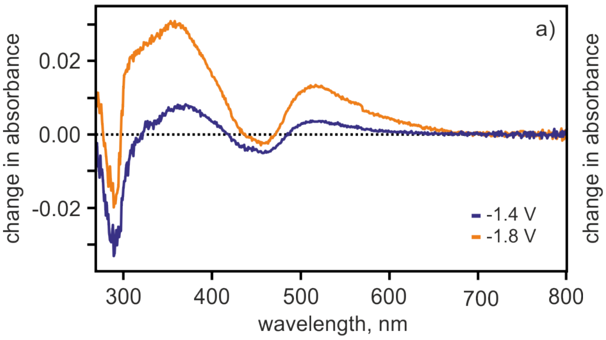

Figure 3.19: Difference spectra of (a) ref-Ru-TAA ($9.0 \cdot 10^{-5}$ M) and (b) the pentad ($3.7 \cdot 10^{-5}$ M) in dry, Ar-purged MeCN, containing 0.1 M $TBAPF_6$ as supporting electrolyte after reduction at increasingly negative potentials (V vs SCE, see inset) in MeCN.

To determine the spectral features of $TAA^{\bullet+}$, both complexes were oxidized and the change in absorbance recorded. Figure 3.20 shows the difference spectra of ref-Ru-TAA (grey trace) and the pentad (orange trace) in MeCN after applying a potential of +1.0 V vs SCE. Both spectra exhibit only signatures of oxidized TAA, since this is the only moiety oxidized at this potential. The spectra exhibit two prominent bands at 370 and 770 nm, and bleaches around 290 and 450 nm. These are in good agreement with previously performed measurements.[52]

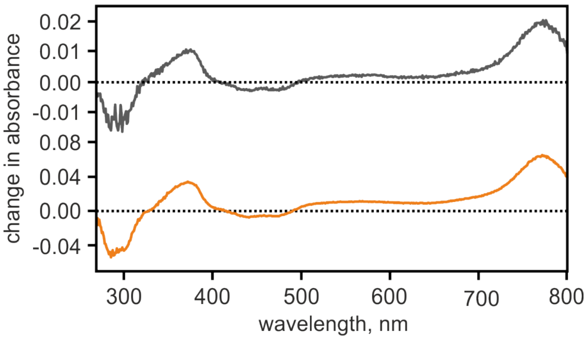

Figure 3.20: Difference spectra of the ref-Ru-TAA ($9.0 \cdot 10^{-5}$ M, grey trace) and the pentad ($3.7 \cdot 10^{-5}$ M, orange trace) in dry, Ar-purged MeCN, containing 0.1 M $TBAPF_6$ as supporting electrolyte obtained after applying a potential of +1.0 V (vs SCE).

3.3.5 Transient and Time Resolved Absorption Measurements

In the Absence of Acid

In order to identify the photoproducts formed upon excitation, the transient absorption spectrum of the pentad in dry, de-oxygenated MeCN was measured, presented in Figure 3.21 (black trace). The sample was excited with 10 ns laser pulses at 532 nm. The spectrum was measured, time integrated over 200 ns, with a time delay of 100 ns after excitation, to exclude the spectral features of short living species (see below). As a result of the strong absorbance around 300 nm, the pentad concentration needed to be relatively low to observe changes in absorption in this spectral region. Due to the low concentration, the optical density (OD) is weak and the spectrum is relatively noisy.

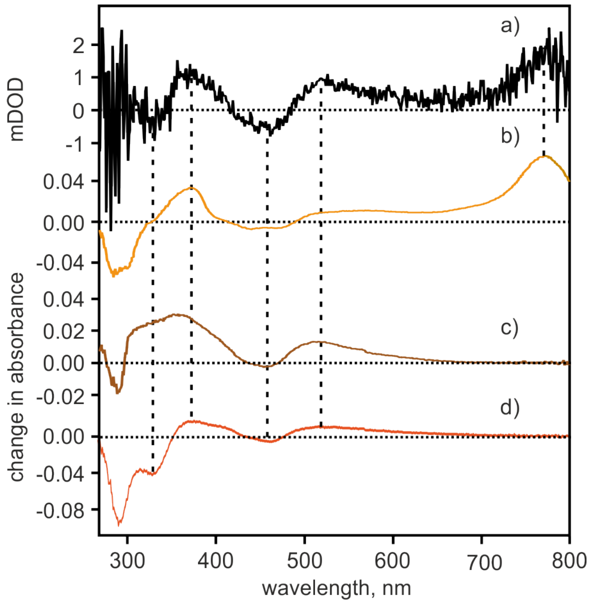

Figure 3.21: (a) Transient absorption spectrum of the pentad ($4.9 \cdot 10^{-6}$ M) in dry, de-oxygenated MeCN, measured 100 ns after excitation at 532 nm with 10 ns laser pulses; (b) difference spectrum of the pentad after applying a potential of +1.0 V (vs SCE); difference spectra of ref-Ru-TAA (c) and the pentad (d) after applying a potential of -1.8 V (vs SCE).

The transient absorption spectrum of the pentad (Figure 3.21a) is compared to its difference spectra after electrochemical oxidation (Figure 3.21b) and reduction (Figure 3.21d), respectively. The absorption band at 778 nm clearly indicates that oxidized TAA is formed. The bands around 370 and 570 nm, and the bleach at 460 nm, are assigned to reduced bipyridine (Figure 3.21c). The bleach at 331 nm indicates that the disulfide is also reduced, and is therefore indicative of the formation of the desired twofold charge-separated state. This bleach is less intense because it overlaps with the absorption of reduced bipyridine (Figure 3.21d).

In order to determine the lifetimes of the photoproducts, time-resolved measurements with the pentad in dry, de-oxygenated MeCN were performed. The absorption decay at 775 nm is presented in Figure 3.22. The absorption of oxidized TAA was chosen because this band is not overlapped with other bands, and $TAA^{\bullet+}$ is expected to be present in all relevant photoproducts. The decay of this band reveals three different species, decaying with lifetimes of <10, 116 and 876 ns. The fastest decay is in the laser limited range, and therefore cannot be determined. It is attributed to the back electron-transfer from the reduced sensitizer to $TAA^{\bullet+}$. This assumption is in agreement with the investigation of ref-Ru-TAA, which decays within 10 ns of photoexcitation. The transient absorption spectrum of the pentad (Figure 3.21a) was measured with a time delay of 100 ns to avoid the spectral feature of this short living state. Hence, the spectrum is a superposition of the spectral features of the remaining two photoproducts. Considering the bleach at 331 nm, one photoproduct is assumed to be the desired twofold charge-separated state, $TAA^{\bullet+}\text{-}Ru^{2+}\text{-}[S^{-}\ S^{-}]\text{-}Ru^{2+}\text{-}TAA^{\bullet+}$. The charge-separated state, $TAA^{\bullet+}\text{-}Ru^{2+}\text{-}[SS]^{\bullet-}\text{-}Ru^{2+}\text{-}TAA$, can be ruled out as the disulfide bond would be still intact after single electron reduction[62], and the absorption at 330 nm therefore not bleached. The spectral features of reduced bipyridine in the transient spectrum indicate that a sensitizer of the third species is reduced. Upon mono excitation, followed by the formation of $TAA^{\bullet+}\text{-}Ru^{1+}\text{-}[SS]\text{-}Ru^{2+}\text{-}TAA$, it is assumed that a second mono charge-separated state, $TAA^{\bullet+}\text{-}Ru^{2+}\text{-}[SS]\text{-}Ru^{1+}\text{-}TAA$, is formed by electron-transfer from the reduced sensitizer to the other non-excited sensitizer or more likely by intramolecular charge-transfer between two TAA moieties. This state where the oxidizing and reducing equivalents are on distant TAA and photosensitizer units, is not shown in Scheme 3.8, since it has essentially the same energy as $TAA^{\bullet+}\text{-}Ru^{1+}\text{-}[SS]\text{-}Ru^{2+}\text{-}TAA$.

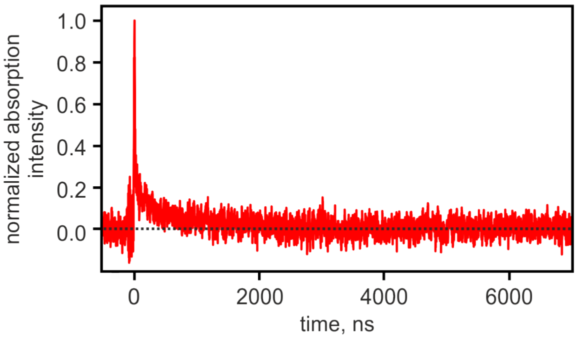

Figure 3.22: Normalized transient absorption decay of the pentad ($1.4 \cdot 10^{-5}$ M) at 775 nm in dry, de-oxygenated MeCN.

On the basis of a triexponential fit, the three species have a contribution of approximately 80%, 10% and 10%, going from the shortest to the longest living photoproduct. As already discussed in the triad section, the formation of the desired twofold charge-separated state relies on double excitation. Regarding this contribution, 90% of the molecules are mono-excited, from which 10% form the singly charge-separated state TAA$^{\bullet+}$-Ru^{2+}-[SS]-Ru^{1+}-TAA. Only 10% are doubly excited, forming TAA$^{\bullet+}$-Ru^{2+}-[S$^-$S$^-$]-Ru^{2+}-TAA$^{\bullet+}$. The transient absorption spectrum in Figure 3.21 is in agreement with this analysis.

In summary, the pentad forms three photoproducts upon excitation by light, including the desired twofold charge-separated state. The lifetime of the latter is either 100 or 870 ns, but could not be unambiguously assigned at this point.

In the Presence of Acid

The absorption decay of the pentad in the presence of 0.1 M TsOH in MeCN at 775 nm is presented in Figure 3.23. It exhibits a triexponential decay, including a long-living species. There is one photoproduct that decays within the duration of the laser pulses (10 ns), and the second has a lifetime of 868 ± 45 ns. The third lifetime could not be determined, because it was too long to be measured with our setup, which is suggestive of accumulation of this photoproduct.

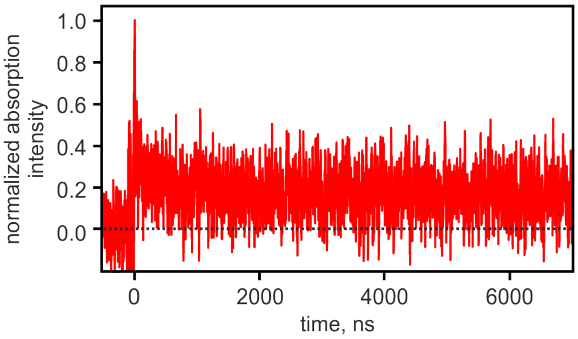

Figure 3.23: Normalized transient absorption decay of the pentad ($1.4 \cdot 10^{-5}$ M) at 775 nm in dry, de-oxygenated MeCN, containing 0.1 M TsOH.

The twofold charge-separated state is the only state that is assumed to be influenced by acid. In Section 3.3.3, a strong driving force for protonation of the thiolate groups was estimated and a long lifetime of the protonated pentad is expected. Hence, the long-living species is assumed to be TAA$^{\bullet+}$-Ru-[SH SH]-Ru-TAA$^{\bullet+}$. This is confirmed by the transient absorption spectrum of the pentad in the presence of ~ 0.1 M TsOH, presented in Figure 3.24 (black trace). It was measured with a time delay of 5 µs after excitation. Furthermore, the spectral signature of oxidized TAA (see Figure 3.2.4) is shown in Figure 3.24a, which was scaled to the intensity of the transient spectrum (red trace). The comparison shows that the spectral features of reduced bipyridine are no longer observed. The absorption bands at 370 nm, around 570 nm and at 770 nm correspond to TAA$^{\bullet+}$. The absorption intensity at 370 nm is decreased, because it is overlapped with the bleach at 330 nm, which is attributed to the doubly reduced disulfide (Figure 3.24b). As demonstrated with ref-SS, protonation does not influence the spectral features of the latter, since the disulfide bond still breaks and the dihedral angle changes (see Section 3.1.4).

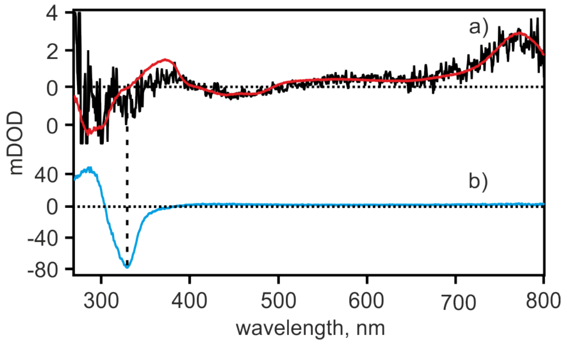

Figure 3.24: (a) Transient absorption spectrum of the pentad ($6.0 \cdot 10^{-6}$ M) in dry, de-oxygenated MeCN measured with a time delay of 5 µs after excitation at 532 nm with 10 ns laser pulse in the presence of ~ 0.1 M TsOH (black trace); difference spectrum of the pentad after oxidation at 1.0 V (vs SCE), scaled to the intensity of the transient spectrum (red trace); (b) difference spectrum of the ligand in dry, de-oxygenated DCM after applying a potential of -2.0 V (vs SCE).

The assignment of the long-living species to the twofold charge-separated state implies that the singly charge-separated states have lifetimes of <10 and 868 ns. This is in very good agreement with the lifetimes determined in the absence of TsOH. These states are not affected by acid and consequently have the same lifetimes in the absence of, as well as in the presence of acid. Therefore, the third lifetime (100 ns) determined in the absence of acid is assigned to the unprotonated twofold charge-separated state.

3.3.6 Continuous Irradiation Measurements

In the previous section, it was shown that the twofold charge-separated state of the pentad is formed, the lifetime of which increases in the presence of TsOH. The lifetime of the protonated species could not be determined because it is too long to be measured with our nanosecond transient absorption setup. The difference spectra of the pentad in dry, de-oxygenated MeCN in the presence of 0.2 M TsOH after continuous LED irradiation at 455 nm are presented in Figure 3.25a. The given times show the overall irradiation time. The difference spectra in 3.25b were obtained from chemically oxidized pentad ($5.6 \cdot 10^{-6}$ M). The oxidant was $Cu(ClO_4)_2 \cdot 6\ H_2O$, which was added in increasing concentrations. The absorption bands at 370 and 773 nm, as well as the bleach at 295 nm and around 455 nm, of the upper spectra are in good agreement with the spectrum of the oxidized pentad, i.e. oxidized TAA. The additional bleach at 331 nm is attributed to the disulfide reduction. Hence, the spectrum of the desired, protonated photoproduct is shown. The spectra were recorded directly after irradiation, and irradiated again directly after the measurement. Thus, the lifetime of the photoproduct is at least in the timescale of minutes. To investigate whether the dithiol-species is even longer living, the sample was irradiated for 75 minutes, and afterwards kept in the absence of light overnight. The next day, the absorption was measured again (dashed black trace). After 14 hours, the absorption bands and bleaches of oxidized TAA decayed and recovered, respectively, by approximately 40%, whereas the bleach at 330 nm changed just slightly, which indicates that TAA decomposed, but the disulfide is still reduced.

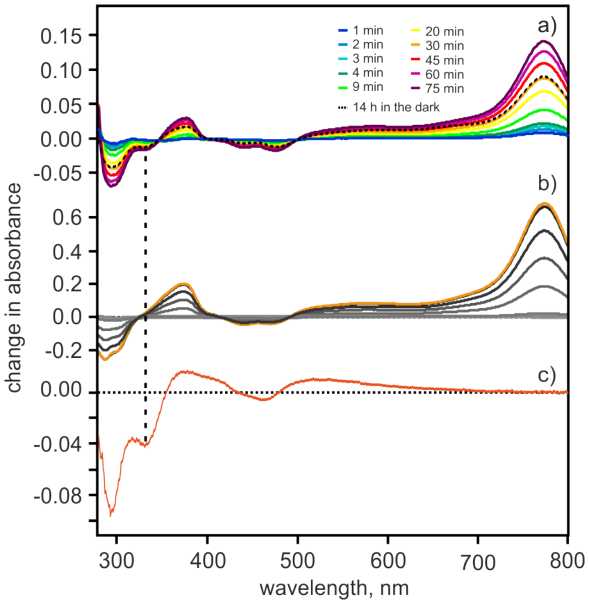

Figure 3.25: (a) Difference spectra of the pentad ($5.3 \cdot 10^{-6}$ M) in MeCN, in the presence of 0.2 M TsOH after continuous irradiation at 455 nm for various times (see inset); difference spectra after (b) chemical oxidation with increasing amounts of $Cu(ClO_4)_2 \cdot 6\ H_2O$ and, (c) after applying a reduction potential of -1.8 V vs SCE.

Although the twofold charge-separated state was assumed to be long-living, the formation of a stable photoproduct was not expected, since the thermodynamic estimations reveal an exergonic driving force of 1.3 eV for charge recombination by concerted proton-coupled electron-transfer (CPET) (see Section 3.3.3). Additionally, the previous investigation of a similar pentad, which contains a central anthraquinone moiety as two-electron acceptor, revealed that, in the presence of TsOH, its protonated twofold charge-separated state has a lifetime of 4.7 µs (see Section 2.4).[52] Hence, charge recombination to the ground state through CPET with TsO^- as base is potentially possible. However, the extremely long lifetime of the pentad investigated in this thesis indicates that the protonated, twofold charge-separated state has an energy close to ground the state, or even below it. The estimation of the higher energy can result from several reasons. For the first disulfide reduction, the potential abstracted from the voltammogram of the triad was used. Because the re-oxidation wave could not be observed, the potential of ref-SS was taken. The difference of the first reduction potential of ref-SS and the disulfide in the triad is 0.4 V, such that the second reduction potential is likely to be shifted to the same extent. In general, the exact determination of the redox potential is difficult due to the potential inversion. It may be even smaller than the -1.21 V vs SCE suggested by the spectroelectrochemical measurements of the triad, where the bleach due to disulfide reduction is already observed at -1.0 V vs SCE (see Section 3.2.4). All of these considerations lead to an energetically lower twofold charge-separated state. Furthermore, there are no $\mathrm{pK_a}$ values for ref-SS available, and were therefore approximated by the $\mathrm{pK_a}$ value of thiophenol. To estimate the driving force for protonation, this value was used twice, although the second thiol group should be less acidic, resulting in a more exergonic driving force.

In summary, it was shown that the twofold charge-separated state can be accumulated in the presence of TsOH. In contrast to the estimations made in Section 3.3.3, the energy of the protonated twofold charge-separated is assumed to be lower than the ground state, resulting in a stable photoproduct.

3.3.7 Summary

In the previous sections, photoinduced charge-accumulation without the use of sacrificial agents was investigated. Based on the triad investigated in section 3.2, a new pentad was designed and synthesized. The triad was extended to a donor-photosensitizer-acceptor-photosensitizer-donor assembly by attaching TAA groups to the bipyridine ligands of the sensitizers, which act as internal electron donors. In contrast to the triad, the pentad was expected to form a twofold charge-separated state without the use of sacrificial reductants. Furthermore, the charge-accumulation was expected to be more efficient due to fast intramolecular reductive quenching of the excited sensitizer by TAA.

Formation of the twofold charge-separated pentad is indicated by a bleach at 331 nm in spectroelectro-chemical measurements. This bleach was also present in the transient absorption spectrum of the pentad, revealing the formation of the desired photoproduct. Hence, it is possible to store two reduction equivalents in the pentad. From the kinetic and transient absorption measurements in the absence and presence of TsOH it could be deduced that the singly charge-separated states $\mathrm{TAA^{\bullet+}}$-$\mathrm{Ru^{1+}}$-[SS]-$\mathrm{Ru^{2+}}$-TAA and $\mathrm{TAA^{\bullet+}}$-$\mathrm{Ru^{2+}}$-[SS]-$\mathrm{Ru^{1+}}$-TAA were formed in 90% yield. The former predominates with 80% and decays within less than 10 ns, the latter has a lifetime of $\sim$ 870 ns. The twofold charge-separated state of the pentad has a lifetime of 100 ns. In the presence of acid, the dithiolate gets irreversibly protonated and the twofold charge-separated state accumulates.

In general, the pentad meets all requirements of a system capable of performing artificial photosynthesis; upon excitation by visible light it forms a relatively long-living charge-separated state without the use of sacrificial agents. Hence, the stored redox equivalents could theoretically be use for solar fuel production. A potentially possible catalytic application is the two-electron reduction via thiol-disulfide interchange.

3.4 Multi-Electron Photoredox Catalysis via Thiolate-Disulfide Interchange

The previous investigations demonstrated that light-induced electron-accumulation can be performed with both the triad and the pentad. In contrast to the triad, charge-accumulation in the pentad takes place without the use of a sacrificial electron source. However, both complexes provide two electrons, which can potentially be used to reduce other molecules.

Thiol-disulfide interchange is a fundamental mechanism to reduce disulfides and to oxidize thiols in nature (see Section 2.6).[64] This reaction occurs via an S_N2 mechanism, which is shown in Scheme 3.10 (top).[70] Thiolate is an active nucleophile that attacks the disulfide from the backside, forming a "trisulfide-like" transition state.[64] A common reducing agent used for enzyme activation is dithiothreitol (DTT^{red}).[69] Usually added in excess amounts, it reduces the disulfides via two sequential thiol-disulfide exchange reactions. The twofold charge-separated triad and pentad also contain two thiolate groups, thus a sequential thiolate-disulfide interchange reaction should also be possible. The advantage of the triad and pentad, compared to DTT^{red} or other common reducing agents, is that the exchange reaction can be performed catalytically. The proposed mechanism with the pentad as the catalyst is shown in Scheme 3.9.

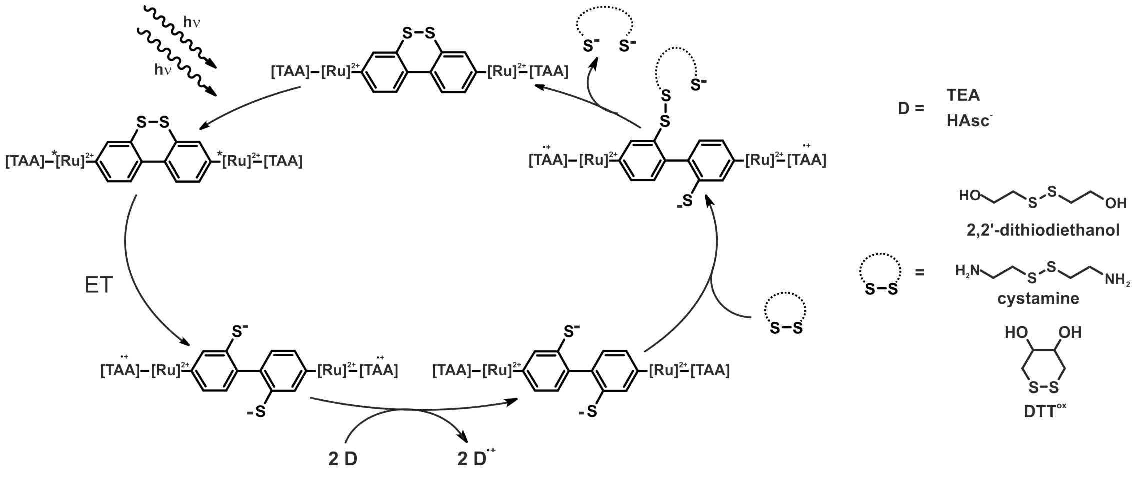

Scheme 3.9: Proposed mechanism for the catalytic reduction of disulfides in the presence of the pentad.

At first, formation of the twofold charge-separated state of the pentad is induced by visible light, followed by reduction of the oxidized TAA groups by a sacrificial electron donor. Two subsequent thiol-disulfide exchange reactions with an other disulfide can then occur, reducing it to a dithiolate and oxidizing the catalyst to the disulfide, i.e. to the ground state, which closes the catalytic cycle.

Disulfides are known to have large one-electron reduction potentials. A few experimentally determined potentials of aliphatic acyclic and cyclic disulfides can be found in the literature, varying from -2.72 V vs SCE for di-*tert*-butyl disulfide, to -1.65 V vs SCE for diphenyldisulfide (both in DMF)[93]; 1,2-dithiolane is reduced at -1.77 V[94] vs SCE in MeCN. On the basis of thermodynamic considerations, ruthenium complexes in their reduced form ($E(Ru)^{2+/1+}$ = -1.3 V vs SCE in MeCN) should not be able to reduce such disulfides via two subsequent single electron-transfers. However, it was shown that it is possible to reduce disulfides using reductants with less negative reduction potentials. DAASBJERG et al. and MARAN et al. investigated the reduction of acyclic aliphatic and aromatic disulfides.[93, 95, 96] They used the radical anions of several molecules as electron donors, which were electrochemically generated. Although most of the reductants had significantly less negative reduction potentials compared to those of the disulfides, the latter was reduced in all cases. They found that the disulfides dissociate after single electron-transfer via a so-called “loose radical-ion dissociative electron-transfer mechanism”.[96] After electron uptake, the disulfide bond elongates and a loose radical anion is formed, in which the SOMO is localized at the disulfide bond. Hence, the energy of the S-S bond decreases and it cleaves (see Scheme 3.10 bottom).[96] The formed thiyl radical can then be reduced in a second step.

Although disulfides can be reduced via single electron-transfer, it may be more efficient via thiol-disulfide interchange, as this mechanism does not depend on reducing power at all, and should therefore take place in any case.

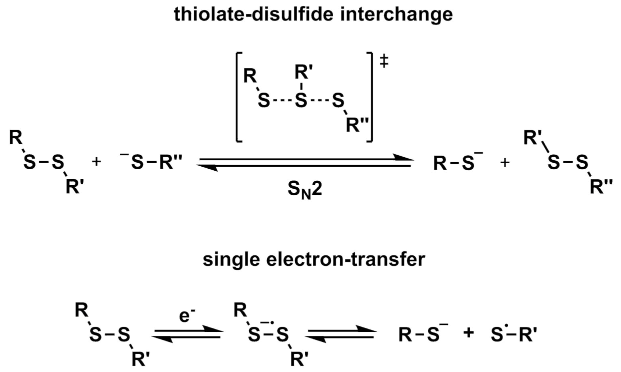

Scheme 3.10: Thiolate-disulfide interchange and dissociative single electron-transfer mechanisms.

3.4.1 Results and Discussion

In the following, the results of the reduction of various disulfides, catalyzed by the triad and pentad, are presented. To test whether the disulfides are reduced via single electron-transfer, the reactions were also performed with ref-Ru-^{t}Bu and ref-Ru-TAA. Two different sacrificial electron donors were tested. Reactions were performed in de-oxygenated, deuterated solvents in flame-sealed NMR-tubes under an Ar atmosphere and continuous LED (3.5 W) irradiation at 455 nm. Product formation was monitored by ^{1}H-NMR spectroscopy (400 MHz). NMR spectra for all measurements are presented in the Appendix. Conversions were calculated by integrating one substrate peak and the corresponding product peak. The product yield was determined with an error of approximately ±0.2%. The turnover number (TON) was calculated by dividing the product concentration by the catalyst concentration.

Table 3.3: Product yields and TONs for the reduction of cystamine catalyzed by ref-Ru-^{t}Bu ($(4.6 \pm 0.7) \cdot 10^{-5}$ M) and the triad ($(2.2 \pm 0.3) \cdot 10^{-5}$ M) in the presence of TEA or HAsc$^-$ reductant.

entry	catalyst	substrate	e$^-$-donor	MeCN:H_2O v:v	time	yield	TON
1	ref-Ru-^{t}Bu	cystamine	TEA	1:4	49 h	0.2%	1
2	triad	cystamine	TEA	1:4	61 h	1.3%	12
3	ref-Ru-^{t}Bu	cystamine	HAsc$^-$	1:4	56 h	7.1%	41
4	triad	cystamine	HAsc$^-$	1:4	56 h	4.6%	50
5	ref-Ru-^{t}Bu	2,2'-dithio-diethanol	TEA	1:0	66 h	5.6%	25
6	ref-Ru-^{t}Bu	DTT^{ox}	TEA	1:0	44 h	0.6%	4
7	triad	DTT^{ox}	TEA	1:0	22 h	3.5%	36

Test reactions were performed using the triad and ref-Ru-^{t}Bu as catalysts, with cystamine as the substrate. The concentration of the electron source was 100 mM, and the substrate 23 ± 3 mM. The triad concentration corresponds to approximately 0.1 mol% amount of disulfide. The concentration of ref-Ru-^{t}Bu was approximately twice as high as the triad, to ensure an equimolar effective photosensitizer concentration. The results are summarized in Table 3.3. It was already shown that in the presence of TEA, the twofold charge-separated state of the triad can be accumulated under continuous irradiation (see Section

3.2.7), hence, it was also used as a sacrificial electron donor in this approach. Since cystamine is not soluble in neat MeCN, a 1:4 (v:v) solvent mixture of MeCN and water was used. The irradiation time was 49 h with ref-Ru-^{t}Bu, and 61 h with the triad. Despite the very long irradiation time, only a low conversion of cystamine to cysteamine of 1.2% was achieved in the presence of the triad (entry 2), with a TON of 12. Ref-Ru-^{t}Bu reduced only 0.2% of the substrate (entry 1). That there was low conversion in the presence of ref-Ru-^{t}Bu indicates that cystamine is reduced by single electron-transfer from the reduced catalyst. The low yield is a result of the inefficiency of TEA to reductively quench ref-Ru-^{t}Bu. Consequently, only small amounts of reduced Ref-Ru-^{t}Bu are present, that are able to reduce cystamine by single-electron-transfer. The higher yield in the presence of the triad indicates that, in this case, cystamine was reduced via thiol-disulfide interchange. It was shown that the charge-separated state of the triad is formed by electron-transfer from the excited sensitizer, probably even if TEA is present. It can be concluded that the formation of the twofold charge-separated state is more efficient than the reduction of ref-Ru-^{t}Bu, resulting in a higher conversion with the triad via thiol-disulfide interchange.

Sodium ascorbate (HAsc$^-$) was also tested as a sacrificial electron donor in the same solvent mixture. It is a stronger reductant than TEA, by 0.2 V[97]. In the presence of ref-Ru-^{t}Bu, a higher conversion was achieved than in the presence of the triad, although both reaction mixtures were irradiated the same time (see entries 3 and 4). Due to the higher reducing power of HAsc$^-$, ref-Ru-^{t}Bu is reduced more efficiently, and consequently more cystamine could be reduced by single electron-transfer, compared to entry 1. It is possible that the triad also reduces the disulfide via single electron-transfer from the reduced sensitizer. When this would be exclusively the case, the yield should be same with both catalysts, due to the same effective concentration of photosensitizer. Hence, it is likely that thiol-disulfide interchange also takes place, but it seems to be less efficient than the single electron-transfer, indicated by the lower yield in entry 4 compared to entry 3. Due to stronger reducing power of HAsc$^-$compared to TEA, it is also possible that the doubly excited triad may be reduced prior to electron-transfer to the disulfide. For this reason, a higher amount of twofold charge-separated triad may be generated, which would explain the higher yield in entry 4 compared to entry 2. However, charge-accumulation was not investigated in protic solvents, and can therefore not be evaluated properly. For this reason, the following reactions were performed in neat acetonitrile. Because cystamine is not soluble in MeCN, it was exchanged for 2,2'-dithio-diethanol.

TEA was again used as the reductant and ref-Ru-^{t}Bu as the catalyst, yielding 5.6% conversion (entry 5). Compared to entry 1, the yield is significantly increased, which might be due to the change from protic to polar aprotic solvents. Because of hydrogen-bonding, the oxidation potential of TEA is shifted to more positive values. Hence, it is a weaker reductant for ref-Ru-^{t}Bu, resulting in a lower conversion in the presence of water. By using TEA as a sacrificial agent, it also needs to be considered that after its oxidation a proton can be cleaved, generating the TEA radical.[98] It is assumed to be highly reducing, thus it may also be involved in the reduction of the disulfide by single electron-transfer.

To counteract dissociative single electron reduction, the substrate was replaced with trans-4,5-dihydroxy-1,2-dithiane (DTT^{ox}), which has a cyclic structure. Due to this, the disulfide bond cleavage upon single electron reduction is entropically less favored compared to acyclic disulfides, such that it may stay intact, or not even be reduced. Additionally, the calculations of 4,4´-bipyridyl-3,3´-disulfide (see Section 2.5.1), which has also a cyclic structure, showed that the disulfide bond did not cleave upon mono-reduction.[62] In the presence of TEA and ref-Ru-^{t}Bu, only low amounts of DTT^{ox} were reduced after 44 h (entry 6). Comparison with entry 5 shows that the cyclic structure indeed influenced the reaction. Hence, the reaction was repeated with the triad as catalyst (entry 7). Compared to entry 6, the conversion and TON increased significantly, even though the irradiation time was only one third as long. Accordingly, DTT^{ox} is reduced much more efficiently via thiol-disulfide interchange with the triad, compared to single electron-transfer from ref-Ru-^{t}Bu.

Table 3.4: Product yields and TONs of the reduction of DTT^{ox} catalyzed by various ruthenium complexes in dry, de-oxygenated MeCN in the presence of TEA as reductant.

entry	catalyst	TEA	hυ (455 nm)	yield	TON
8	✗	✓	✓	0%	0
9	$[Ru(bpy)_3]^{2+}$	✓	✗	0%	0
10	$[Ru(bpy)_3]^{2+}$	✗	✓	0%	0
11	$[Ru(bpy)_3]^{2+}$	✓	✓	**1.5%**	**9**
12	ref-Ru-^{t}Bu	✓	✓	0.7%	4
13	triad	✓	✗	0%	0
14	triad	✗	✓	0%	0
15	triad	✓	✓	**3.9%**	**42**
16	ref-Ru-TAA	✓	✓	1.6%	9
17	pentad	✓	✗	0%	0
18	pentad	✗	✓	0%	0
19	pentad	✓	✓	**3.6%**	**41**

With these results in hand, the catalytic two-electron reduction of DTT^{ox} (22 mM) to DTT^{red} was repeated with all catalysts including ref-Ru-TAA and the pentad, under the same reaction conditions. Neat acetonitrile was used as the solvent and dry TEA (100 mM) as the electron source. The reaction time was 20 h in all cases. The catalyst concentration was $2 \cdot 10^{-5}$ M for both the triad and the pentad, and $4 \cdot 10^{-5}$ M for ref-Ru-^{t}Bu and ref-Ru-TAA. To have a more general reference complex, without any substituents on the bipyridine unit that might influence the reaction, the catalysis was also performed with $[Ru(bpy)_3]^{2+}$. The yields and TONs printed in bold type have been measured with a 600 MHz NMR spectrometer. Hence, these results are more precise in comparison to the other values. The obtained results are summarized in Table 3.4. Additionally, control experiments were performed either in the absence of TEA, light or catalyst. There was no conversion in all cases, showing that each component plays a crucial role. The reactions catalyzed by the reference complexes resulted in relatively low yields and TONs varying from four to nine. Within the error tolerance, the triad and pentad afforded the same results, with yields around 3.7% and TONs around 40.

The overall low conversion of DTT^{ox} to DTT^{red}, catalyzed by the triad and pentad, can be explained by considering the thermodynamics. The reaction free energy (ΔG) of the thiol-disulfide interchange between the reduced dibenzo[*c*,*e*][1,2]dithiin of the catalyst and DTT^{ox} can be approximated using a thermodynamic cycle, with the help of bond dissociation energies (BDE) and pK$_a$ values (see Scheme 3.11 and Equations 3.5 - 3.8). Since the BDEs of dibenzo[*c*,*e*][1,2]dithiin and DTT^{ox}, and the pK$_a$ value of the former are not reported, the corresponding values of thiophenol[99, 100] and methanethiol[101, 102] were taken. Assuming $\Delta H \approx \Delta G$ (ΔH = reaction enthalpy) the reaction free energy can be estimated using Equations 3.5 - 3.8. The BDEs are those of the broken and formed bonds, R is the ideal gas constant, and T the temperature. The exact calculation of ΔG is given in the Appendix.

$$\Delta G_1 = -2.303 \cdot RT \cdot pK_a(PhSh) \tag{3.5}$$

$$\Delta G_2 = \mathit{\Sigma}\ \mathrm{BDE}_{broken}\ \text{-}\ \mathit{\Sigma}\ \mathrm{BDE}_{formed} \tag{3.6}$$

$$\Delta G_3 = 2.303 \cdot RT \cdot pK_a(DTT) \tag{3.7}$$

$$\Delta G_4 = \Delta G_1 + \Delta G_2 + \Delta G_3 \tag{3.8}$$

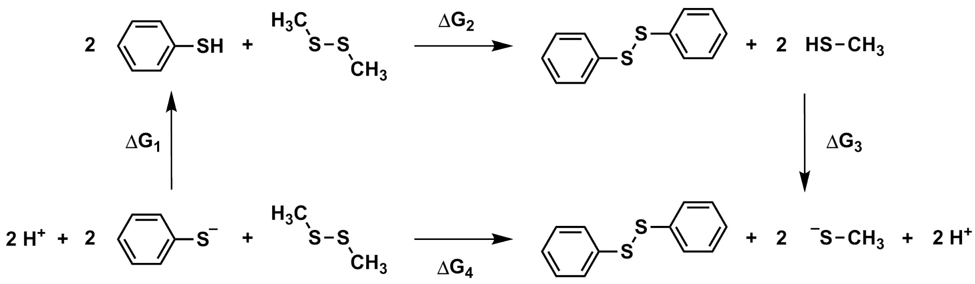

Scheme 3.11: Thermodynamic cycle for the reaction of thiophenol and methanethiol.

The estimated ΔG_4 is +6.8 kcal mol^{-1}. Although this is only a rough approximation, the positive value clearly indicates that the reaction equilibrium is strongly on the reactant side. For this reason, the conversion of DTT^{ox} to DTT^{red} by thiol-disulfide interchange with the triad or pentad cannot be significantly increased. By increasing the irradiation time to 48 h or more, the yield only increases slightly, indicating that the equilibrium is almost reached.

3.4.2 Summary

In summary, the two-electron reduction of small disulfides catalyzed by the triad and pentad was investigated. Both the pentad and triad form the twofold charge-separated state upon excitation with visible light, the former in the absence and the latter in the presence of an external reductant. The formed thiolate groups can then perform two subsequent thiol-disulfide interchange reactions with the substrate, a disulfide, which is thereby reduced to the dithiolate. By using a sacrificial electron donor, the catalyst can be re-reduced, such that reaction can be performed catalytically. It was found that the acyclic disulfides cystamine and 2,2'-dithio-diethanol are already reduced by dissociative single electron-transfer from ref-Ru-^{t}Bu, which was initially reduced by TEA or HAs$^-$. By replacing the acyclic substrate with cyclic DTT^{ox}, reduction via single electron-transfer could be significantly decreased, as the disulfide bond dissociation is entropically less favored, due to the cyclic structure. Hence, in the presence of the triad and pentad, the conversion to DTT^{red} by thiol-disulfide interchange was significantly higher. The TONs of the conversion of DTT^{ox} catalyzed by triad or pentad are four times higher than catalyzed by $[Ru(bpy)_3]^{2+}$. However, the relatively low yield of ~4% cannot be significantly increased, as the equilibrium of the reaction is almost reached at this point.

3.4.3 Outlook

A potential application of the catalytic reduction of DTT^{ox} by the triad or pentad is catalytic enzyme activation. As mentioned above, DTT^{red} is a common agent to activate enzymes that contain thiol groups in their active centers. It is normally added in excess amounts, i.e. >10 equivalents.[103, 104] As the pentad or triad are themselves probably too large to reach the active site, DTT would act as an electron carrier. The proposed mechanism is presented in Scheme 3.12. Cycle 1 was already explained above; it summarizes the light-induced electron-accumulation, followed by the conversion of DTT^{ox} to DTT^{red}. Photocatalytically generated DTT^{red} is able to activate the enzyme by additional thiol-disulfide interchange reactions (see cycle 2).

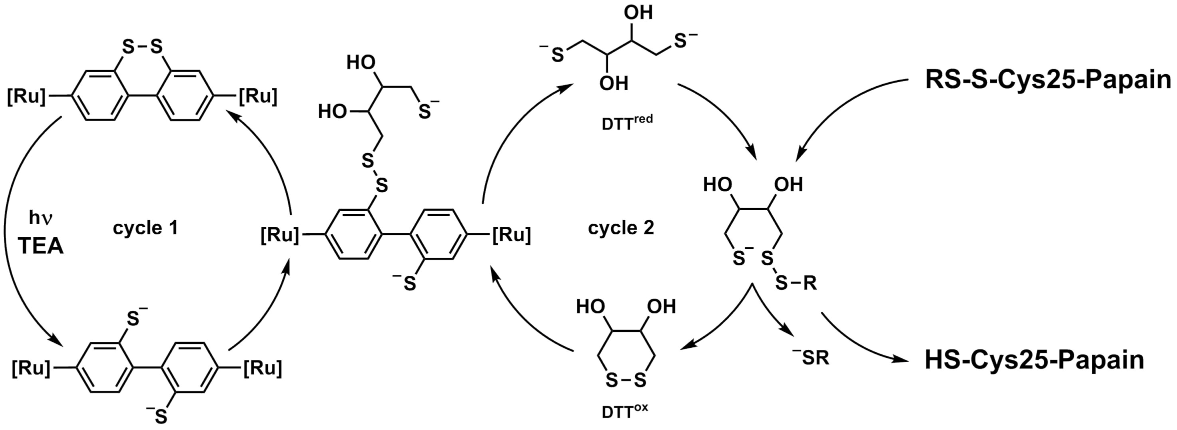

Scheme 3.12: Proposed mechanism for the catalytic papain activation.

A potential protein to test this reaction is papain. It is a cysteine protease, cleaving peptide bonds, and therefore plays an important role in many biological processes. Furthermore, it has medicinal and industrial uses; used, for example, as a tenderizer for meat.[105] An additional feature is its stability in some organic solvents. The proteolytic activity of papain in a mixture of 99% MeCN and 1% aqueous buffer has been previously investigated. It was found that after 24 h the activity did not significantly decrease.[106] This is important because the PF_6-salts of triad and pentad are not soluble in water. However, it was shown that a 4:1 (v:v) mixture of water and MeCN can potentially be used (see Table 3.3, entry 2). Suitable reaction conditions need to be investigated in the future.

4 General Summary

The main aim of this thesis was to develop a purely molecular system capable of accumulating multiple redox equivalents without the use of sacrificial agents, by exploiting potential inversion of an electron acceptor.

It was demonstrated previously by other researchers that the extent of potential inversion in dibenzo[*c*,*e*][1,2]dithiin is very large; this two-electron acceptor was therefore chosen. Cyclic voltammetric measurements revealed the second reduction potential to be more than 1.0 V less negative than the first. Consequently, there is a very strong driving force for the second electron-transfer, making this step more favorable in comparison to other unproductive pathways occurring in accumulative electron-transfer, thereby facilitating formation of the twofold charge-separated state.

The triad, composed of two ruthenium trisbipyridyl photosensitizers and the central disulfide acceptor moiety, was synthesized to get first insights into electron-accumulation in the presence of a sacrificial reductant. In contrast to ref-SS, the reduction of the dibenzo[*c*,*e*][1,2]dithiin moiety bound to the two positively charged sensitizers is assumed to be approximately 0.4 V less negative. Accordingly, electron-accumulation in the triad might be possible without the use of an external electron donor. There is evidence that two electrons may be transferred to the disulfide from the sensitizers if both are excited, but it could not clearly be confirmed. However, in the presence of TEA and continuous irradiation with visible light the twofold charge-separated state is formed and accumulates.

Furthermore, the triad was extended to a pentad by linking TAA groups to the bipyridine ligands of the sensitizers, which act as internal electron donors. The formation of the twofold charge-separated pentad was confirmed by transient absorption spectroscopy. It is assigned as having a lifetime of approximately 100 ns, which was shown to increase in the presence of acid. Cyclic voltammetric measurements of ref-SS demonstrated that the formation of doubly reduced disulfide is not influenced by TsOH, but the formed thiolate groups are protonated, making them significantly more difficult to re-oxidize. Although the charge-separated and protonated pentad, $\mathrm{TAA}^{\bullet+}$-Ru^{2+}-[SH SH]-Ru^{2+}-$\mathrm{TAA}^{\bullet+}$, can potentially recombine to the ground state by concerted proton-coupled electron-transfer, it accumulates. Consequently, the energy of this state is close to, or even below, that of the ground state.

By forming a relatively long-living twofold charge-separated state upon irradiation with visible light, and without the use of sacrificial agents, the pentad, in general, meets the requirements for artificial photosynthesis. Hence, it could potentially be used for solar fuel production, not least because a catalytic application was also demonstrated in this work.

It was shown that both the triad and pentad can be used as two-electron photoredox catalysts. Since the electrons are stored in the thiolate groups, thiol-disulfide interchange reactions with other disulfides can be performed. Whereas acyclic disulfides can be reduced via subsequent single electron-transfer with ruthenium trisbipyridyl complexes, the reduction is more difficult to achieve with cyclic disulfides, as the bond cleavage is entropically less favored. However, via thiol-disulfide interchange, significant amounts of $\mathrm{DTT}^{\mathrm{ox}}$ were reduced to $\mathrm{DTT}^{\mathrm{red}}$, catalyzed by the pentad and triad in the presence of TEA. The TON for the two-electron reduction was four times higher when catalyzed by these complexes than by $[\mathrm{Ru(bpy)_3}]^{2+}$, indicating that thiol-disulfide interchange is significantly more efficient than single electron-transfer. In conclusion, this approach showed that the stored redox equivalents can be used for catalytic application.

In summary, these results demonstrated that the exploitation of potential inversion is a very promising concept for successful photoinduced charge-accumulation in molecular systems.

5 Experimental Section

5.1 Analytical Methods

General Methods

All commercially available reagents were purchased from commercial sources and used as received. Dry DCM, THF and Et_2O were obtained from a solvent purification system from Innovative Technology. All other dry solvents used for synthesis or spectroscopic measurements were purchased from Sigma Aldrich and used as received. Deuterated solvents for NMR spectroscopy were purchased from Cambridge Isotope Laboratories or Sigma Aldrich. Thin layer chromatography was performed on silica plates from Merck (60 F254). Column chromatography was performed on silica gel (40-63 µm, Silicycle).

NMR Spectroscopy

^{1}H-NMR spectra were recorded on a Bruker Avance III NMR spectrometer operating at 250 MHz, 400 MHz, 500 MHz or 600 MHz proton frequency, and ^{13}C spectra spectra at 101 MHz on a Bruker Advance III spectrometer. All chemical shifts (δ) are given in ppm and referenced to residual solvent peaks.[107] Coupling constants are listed in Hz and the multiplicity is abbreviated as follows: singlet (s), doublet (d), doublet of doublets (dd), doublet of doublet of doublets (ddd), triplet (t), doublet of triplets (dt), triplet of doublets (td), quartet (q), and multiplet (m).

Mass Spectrometry

ESI mass spectra were recorded on a Bruker Esquire 3000plus Ion-trap ESI-MS operating in positive mode. The high resolution mass spectra were measured on a Bruker maXis 4G QTOF ESI spectrometer operating in positive mode by Dr. Heinz Nadig (Department of Chemistry at the University of Basel).

Elemental Analysis

Elemental analyses were performed on a Vario Micro Cube from Elementar by Ms. Sylvie Mittelheisser (Department of Chemistry at the University of Basel).

Cyclic Voltammetry

Cyclic voltammetric measurements were performed with a Versa Stat3-200 potentiostat from Princeton Applied Research. Measurements were performed in dry, Ar-purged MeCN or DCM with tetra-*n*-butylammonium hexafluorophosphate (0.1 M) as supporting electrolyte. A three-electrode setup was used to measure cyclic voltammograms, containing a glassy carbon disc serving as working electrode, a silver wire as counter electrode and an SCE reference electrode. Spectro-electrochemical measurements were performed in a quartz cuvette with a platinum gauze as working electrode, a platinum wire as counter electrode and an SCE reference electrode.

UV-Vis Spectroscopy

UV-Vis absorption spectra were measured on a Cary 5000 UV-Vis-NIR spectrophotometer from Varian.

Steady-State Luminescence

Steady-state luminescence measurements were performed with a Fluorolog-322 from Horiba Jobin-Yvon.

Transient Absorption Spectroscopy

Transient absorption spectra were measured with an LP920-KS spectrometer from Edinburgh Instruments equipped with an iCCD camera from Andor. Single-wavelength kinetics were recorded using a R928 photomultiplier tube. A frequency-doubled Quantel Brilliant b laser served as excitation source. The duration of the laser excitation pulse was approximately 10 ns with a repetition frequency of 10 Hz. The pulse energy used for transient absorption measurements were in the range of 12 mJ to 15 mJ. Transient absorption spectra were time-averaged over a detection period of 200 ns directly after excitation, unless otherwise stated. Quartz cuvettes from Starna were used for all optical measurements. To perform measurements under inert conditions, Schlenk cuvettes were used, and the solvent was degassed by four cycles of freeze pump thaw.

Photoredox Catalysis

Photoredox catalysis experiments were performed in flame-sealed NMR tubes. All disulfides are commercially available and were used as received. DTT$^{\mathrm{ox}}$ used for entries 11, 15 and 19 was deuterated prior to use, by stirring it for 1 h in D_2O, followed by removal of the solvents under reduced pressure, to minimize the amount of OH-signals in the NMR spectrum. The samples were prepared as follows: the substrates were dissolved in deuterated solvents, and the solutions were degassed by four cycles of freeze pump thaw. The solution was then filled into an NMR tube, frozen in a liquid nitrogen bath and the NMR tube sealed under vacuum using a hand-held gas burner. The samples were irradiated at 455 nm with an M455L2 LED from Thorlabs (1020 mW) at room temperature. ^{1}H-NMR spectra were recorded with a 400 MHz instrument, except for the spectra of entries 11,15 and 19, which were measured with a 600 MHz spectrometer.

5.2 Synthesis of Ref-SS

2,2'-Bis-O-(N,N-dimethylthiocarbamato)biphenyl[108]

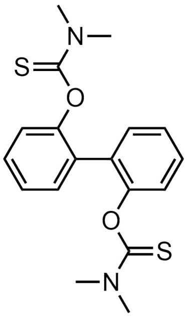

NaH (60% in oil, 520 mg, 13.0 mmol) was added in small portions to a solution of biphenyl-2,2'-diol (1.01 g, 5.42 mmol) in DMF (11 mL), and the mixture stirred at room temperature (rt) for 10 min under a nitrogen atmosphere. After addition of dimethylthiocarbamoyl chloride (2.10 g, 17.0 mmol), the solution was stirred for 3 h at 85 °C. After cooling to rt, aqueous $NaHCO_3$ solution was added. The white precipitate was filtered, washed with water, and dissolved in DCM. The organic solution was washed with water, dried over Na_2SO_4, and the solvent removed under reduced pressure. Purification by column chromatography (SiO_2, pentane : EtOAc (7:3)), followed by recrystallization from acetone afforded the product as a white solid (684 mg, 35%). ^{1}H-NMR (400 MHz, $CDCl_3$): δ 7.45 - 7.34 (m, 4H), 7.26 (td, J = 7.5, 1.3 Hz, 2H), 7.23 - 7.15 (m, 2H), 3.26 (s, 6H), 3.03 (s, 6H) ppm.

2,2'-Bis-S-(N,N-dimethylthiocarbamato)biphenyl[109]

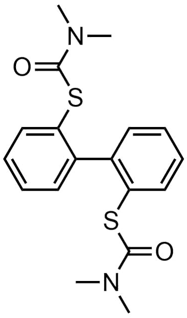

2,2'-Bis-O-(N,N-dimethylthiocarbamato)biphenyl (370 mg, 1.03 mmol) was dissolved in tetradecane (2 mL) and heated at 270 °C for 2.3 h under a nitrogen atmosphere. Purification by column chromatography (SiO_2, pentane : EtOAc (1:1)) afforded the product as a white solid (192 mg, 52%). ^{1}H-NMR (400 MHz, $CDCl_3$): δ 7.66 - 7.56 (m, 2H), 7.45 - 7.33 (m, 4H), 7.34 - 7.24 (m, 2H), 2.88 (s, 12H) ppm.

2,2'-Dimercaptobiphenyl[110]

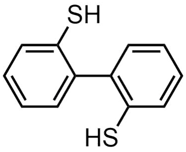

A solution of 2,2‘-bis-S-(N,N-dimethylthiocarbamato)biphenyl (184 mg, 0.51 mmol) in dry THF (8 mL) was added to a mixture of $LiAlH_4$ (194 mg, 5.11 mmol) in dry THF (1.6 mL) at 0 °C. After complete addition, the mixture was heated at 65 °C for 6.5 h under a nitrogen atmosphere, followed by addition of aqueous HCl-solution (5-10 V%). The product was then extracted into Et_2O, the organic phase was dried over Na_2SO_4, and the solvent removed under reduced pressure. Purification by column chromatography (SiO_2, pentane : EtOAc (1:1)) afforded the product as a beige solid (80.0 mg, 72%). ^{1}H-NMR (400 MHz, $CDCl_3$): δ 7.44 - 7.39 (m, 2H), 7.31 - 7.21 (m, 4H), 7.20 - 7.16 (m, 2H), 3.29 (s, 2H) ppm. ^{13}C-NMR (100 MHz, $CDCl_3$): δ 139.1, 131.9, 130.4, 129.5, 128.8, 125.9 ppm.

Dibenzo[c,e][1,2]dithiin

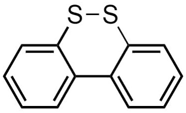

2,2'-Dimercaptobiphenyl (40 mg, 0.18 mmol) and sodium ascorbate (390 mg, 1.97 mmol) were dissolved in MeCN (14 mL) and water (9 mL), and stirred for 6 h at rt. The product was then extracted into Et_2O, the organic phase was dried over Na_2SO_4 and the solvent removed under reduced pressure. Purification by column chromatography (SiO_2, pentane : EtOAc (1:1)) afforded the product as a beige solid (30.0 mg, 76%).^{1}H-NMR (400 MHz, $CDCl_3$): δ 7.70 (dd, J = 7.9, 1.4 Hz, 2H), 7.52 (dd, J = 7.6, 1.4 Hz, 2H), 7.38 (td, J = 7.6, 1.4 Hz, 2H), 7.28 (td, J = 7.5, 1.4 Hz, 2H) ppm. ^{13}C-NMR (100 MHz, $CDCl_3$): δ 138.1, 136.3, 129.1, 128.7, 128.0 ppm.

5.3 Synthesis of the Ligand

2,2‘-Dimethoxy-4,4‘-dinitrobiphenyl[111]

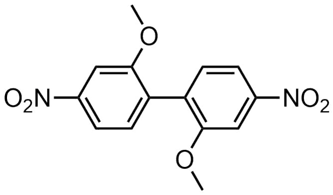

A mixture of 4-iodo-3-methoxynitrobenzene (10.1 g, 36.3 mmol) and activated copper powder (9.80 g, 0.15 mol) in dry DMF (40 mL) was stirred at 180 °C for 18 h under a nitrogen atmosphere. The hot suspension was filtered over celite, and the residue was washed with hot DMF. One third of the solvent was removed under reduced pressure, and the remaining filtrate was stored overnight at 4 °C. The precipitate was collected and washed with MeOH. This afforded the product as a pale brown solid (4.23 g, 76%). ^{1}H-NMR (400 MHz, $CDCl_3$): δ 7.92 (dd, J = 8.3, 2.2 Hz, 2H), 7.84 (d, J = 2.2 Hz, 2H), 7.38 (d, J = 8.3 Hz, 2H), 3.88 (s, 6H) ppm. ^{13}C-NMR (100 MHz, $CDCl_3$): δ 158.2, 146.8, 132.5, 118.34, 107.4 ppm.

2,2‘-Dimethoxy-4,4‘diaminobiphenyl[112]

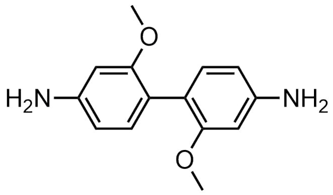

2,2‘-Dimethoxy-4,4‘-dinitrobiphenyl (4.13 g, 13.6 mmol), tetra-n-butylammonium bromide (8.75 g, 27.1 mmol) and sodium sulfide nonahydrate (65.2 g, 0.27 mol) were dissolved in toluene (50 mL) and water (7.0 mL), and the suspension stirred at 95 °C for 16 h. After cooling to rt, the mixture was decanted, the product extracted into toluene, and the combined organic phases washed with water and brine. The organic phase and the separated orange solid were combined and the solvent removed under reduced pressure. Purification by column chromatography (SiO_2, EtOAc) afforded the product as a yellow solid (2.71 g, 82%). ^{1}H-NMR (400 MHz, $CDCl_3$): δ 7.01 (d, J = 8.2 Hz, 2H), 6.32 (dd, J = 8.2, 2.2 Hz, 2H), 6.31 (d, J = 2.2 Hz, 2H), 3.72 (s, 6H), 3.67 (s, 4H) ppm. ^{13}C-NMR (100 MHz, $CDCl_3$): δ 158.2, 146.8, 132.5, 118.4, 107.2, 99.1 ppm.

2,2‘-Dimethoxy-4,4‘diiodobiphenyl[113]

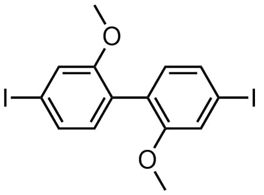

2,2‘-Dimethoxy-4,4‘-aminobiphenyl (1.13 g, 4.62 mmol) was suspended in MeCN (60 mL), and water (60 mL) and concentrated HCl (20.0 mL, 0.24 mol) were added. The mixture was cooled down to -10 °C, and a 0 °C cold solution of $NaNO_2$ (1.60 g, 23.2 mmol) in water (8.5 mL) added dropwise. After stirring at rt for 15 min, a 0 °C cold solution of KI (7.68 g, 46.3 mmol) in water (18 mL) was added at -10 °C. After complete addition, the solution was stirred at 80 °C overnight. A saturated aqueous $NaHCO_3$ solution was then added until pH = 9 was reached. After addition of saturated aqueous $Na_2S_2O_3$ solution, the product was extracted into DCM. The combined organic phases were washed with brine and dried over Na_2SO_4, and the solvent removed under reduced pressure. Purification by column chromatography (SiO_2, pentane : EtOAc (10:1)) afforded the product as a white solid (1.87 g, 87%). ^{1}H-NMR (400 MHz, $CDCl_3$): δ 7.36 (dd, J = 7.9, 1.6 Hz, 2H), 7.29 (d, J = 1.6 Hz, 2H), 6.94 (d, J = 7.9 Hz, 2H), 3.77 (s, 6H) ppm. ^{13}C-NMR (100 MHz, $CDCl_3$): δ 157.5, 132.7, 129.8, 126.6, 120.56, 93.7, 56.0 ppm.

4,4-Diiodo-2,2-biphenol[114]

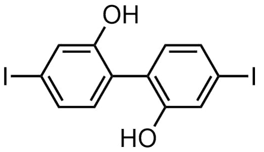

2,2‘-Dimethoxy-4,4‘diiodobiphenyl (2.76 g, 5.91 mmol) was dissolved in dry DCM (45 mL). After slow addition of a solution of BBr_3 in DCM (1.0 M, 9.5 mL) at -78 °C, the solution was stirred at rt overnight under a nitrogen atmosphere. The mixture was then quenched carefully with aqueous HCl solution (10%) at 0 °C. The product was extracted into Et_2O, the combined organic phases washed with water and dried over Na_2SO_4. Removal of the solvent under reduced pressure afforded the product as a pale brown solid (2.51 g, 97%). ^{1}H-NMR ($CDCl_3$, 400 MHz): δ 7.41 (d, J = 1.7 Hz, 2H) 7.39 (dd, J = 7.9, 1.7 Hz, 2H), 6.94 (d, J = 7.9 Hz, 2H), 5.43 (s, 2H) ppm.

Dimethylthiocarbamic acid O-(2'dimethylthiocarbamoyloxy-4,4'-diiodobiphenyl-2-yl) ester[61, 110]

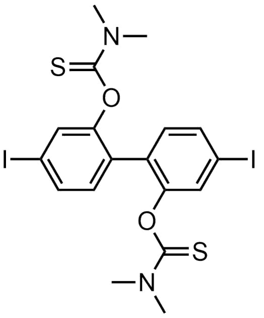

4,4-Diiodo-2,2-biphenol (2.97 g, 6.77 mmol) was dissolved in dry DMF (28 mL). NaH (60% in oil, 0.83 mg, 20.8 mmol) was added in small portions at 0 °C, and the mixture stirred for 45 min at rt under a nitrogen atmosphere. Dimethylthiocarbamoyl chloride (3.80 g, 30.7 mmol) was then added, and the solution stirred at 95 °C overnight. After cooling to rt, the mixture was poured into aqueous KOH solution (2%, 50 mL). The white precipitate was filtered off and washed with water. The solid was dissolved in DCM, washed with water, and the solvent removed under reduced pressure. Recrystallization from acetone afforded the product as a pale yellow solid (2.45 g, 53%). ^{1}H-NMR ($CDCl_3$, 400 MHz): δ 7.57 (dd, J = 8.1, 1.7 Hz, 2H) 7.52 (d, J = 1.7 Hz, 2H), 7.11 (d, J = 8.1 Hz, 2H), 3.29 (s, 6H), 3.07 (s, 6H) ppm.

Dimethylthiocarbamic acid S-(2'-dimethylcarbamoylsulfanyl-4,4'-diiodobiphenyl-2-yl) ester[61]

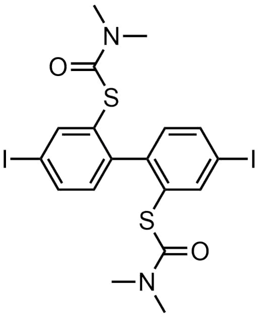

Neat dimethylthiocarbamic acid O-(2'dimethylthiocarbamoyloxy-4,4'-diiodobiphenyl-2-yl)-ester (1.00 g, 1.63 mmol) was heated at 265 °C for 1.5 h under a nitrogen atmosphere. Purification by column chromatography (SiO_2, pentane : EtOAc (2:1)) afforded the product as a pale yellow solid (0.44 g, 44%). ^{1}H-NMR ($CDCl_3$, 400 MHz): δ 7.93 (d, J = 1.8 Hz, 2H), 7.70 (dd, J = 8.1, 1.8 Hz, 2H), 7.00 (d, J = 8.1 Hz, 2H), 2.89 (s, 12H) ppm. ^{13}C-NMR ($CDCl_3$, 100 MHz): δ 165.7, 145.1, 144.5, 138.1, 132.2, 130.5, 93.3, 37.1 ppm.

5-Bromo-2,2'-bipyridine[115]

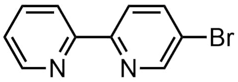

2-Iodo-5-bromopyridine (3.28 g, 11.5 mmol) and Pd(PPh_3)$_4$ (332 mg, 0.29 mmol) were dissolved in dry THF (20 mL), and 2-pyridylzinc bromide in THF (0.5 M, 30 mL) added. After stirring at 75 °C for 18 h under a nitrogen atmosphere, the mixture was treated with an aqueous solution of EDTA and Na_2CO_3 (0.1 M, 1:1).The product was extracted into DCM and washed with water. The combined organic phases were dried over Na_2SO_4 and the solvent removed under reduced pressure. Purification by column chromatography (SiO_2, pentane : Et_2O (4:1)) afforded the product as a white solid (2.09 g, 77%). ^{1}H-NMR (400 MHz, $CDCl_3$): δ 8.72 (dd, J = 2.4, 0.7 Hz, 1H), 8.67 (ddd, J = 4.8, 1.8, 0.9 Hz, 1H), 8.37 (dt, J = 8.0, 1.1 Hz, 1H), 8.32 (dd, J = 8.6, 0.7 Hz, 1H), 7.94 (dd, J = 8.5, 2.4 Hz, 1H), 7.82 (ddd, J = 8.0, 7.5, 1.8 Hz, 1H), 7.33 (ddd, J = 7.5, 4.8, 1.2 Hz, 1H) ppm.

Bpy-xy-TMS[116]

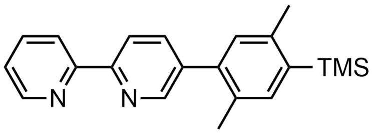

5-Bromo-2,2'-bipyridine (1.49 g, 6.34 mmol), 2,5-dimethyl-4-trimethylsilylphenylboronic acid (1.62 g, 7.29 mmol) and Na_2CO_3 (2.02 g, 19.0 mmol) were dissolved in degassed THF (50 mL) and water (50 mL). Pd(PPh_3)$_4$ (366 mg, 0.32 mmol) was then added, and the mixture stirred for 24 h at 90 °C under a nitrogen atmosphere. After cooling to rt, the product was extracted into DCM, and the organic phase washed with water and brine. The solution was dried over Na_2SO_4 and the solvent removed under reduced pressure. Purification by column chromatography (SiO_2, 1. pentane : EtOAc (4:1), 2. pentane : EtOAc (2:1)) afforded the product as a white solid (1.96 g, 93%). ^{1}H NMR (400 MHz, $CDCl_3$): δ 8.72 (ddd, J = 4.9, 1.8, 0.9 Hz, 1H), 8.69 (dd, J = 2.3, 0.8 Hz, 1H), 8.49 (dd, J = 8.2, 6.5 Hz, 2H), 7.88 (td, J = 7.7, 1.8 Hz, 1H), 7.83 (dd, J = 8.2, 2.3 Hz, 1H), 7.40 (s, 1H), 7.36 (ddd, J = 7.5, 4.8, 1.2 Hz, 1H), 7.09 (d, J = 0.9 Hz, 1H), 2.49 (s, 3H), 2.31 (s, 3H), 0.37 (s, 9H) ppm.

Bpy-xy-Br[117]

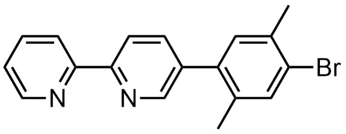

Bpy-xy-TMS (350 mg, 1.05 mmol) and KOAc (206 mg, 2.10 mmol) were dissolved in THF (4.5 mL) and cooled to 0 °C. Br_2 (0.22 mL, 4.29 mmol) was added in the absence of light, and the solution stirred at rt for 2.5 h. After addition of TEA (1.20 mL, 8.65 mmol) and saturated aqueous $Na_2S_2O_3$ solution, the product was extracted into DCM.The combined organic phases were washed with water and brine, dried over Na_2SO_4, and the solvent removed under reduced pressure. Purification by column chromatography (SiO_2, pentane : Et_2O (6:1)) afforded the product as a colorless viscous oil (314 mg, 88%) ^{1}H-NMR (400 MHz, $CDCl_3$): δ 8.71 (ddd, J = 4.8, 1.8, 0.9 Hz, 1H), 8.63 (dd, J = 2.3, 0.8 Hz, 1H), 8.44 (tt, J = 8.0, 1.0 Hz, 2H), 7.84 (td, J = 7.8, 1.8 Hz, 1H), 7.76 (dd, J = 8.2, 2.3 Hz, 1H), 7.50 (s, 1H), 7.33 (ddd, J = 7.5, 4.8, 1.2 Hz, 1H), 7.14 (s, 1H), 2.41 (s, 3H), 2.26 (s, 3H) ppm.

Bpy-xy-bpin

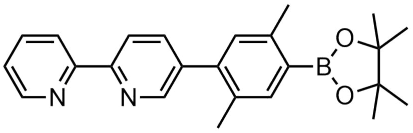

Bpy-xy-Br (314 mg, 0.93 mmol), bis(pinacolato)diboron (361 mg, 1.42 mmol) and KOAc (412 mg, 4.20 mmol) were dissolved in dry and degassed DMF (7 mL), and $Pd(PPh_3)_4$ (65 mg, 0.09 mmol) added. The mixture was stirred at 120 °C for 17 h under a nitrogen atmosphere, and after cooling to rt, saturated aqueous NH_4Cl solution was added. The resulting suspension was extracted with DCM. The combined organic phases were washed with water and brine, dried over Na_2SO_4, and the solvent removed under reduced pressure. Purification by column chromatography (SiO_2, pentane : Et_2O (3:1)) afforded the product as a colorless, strongly viscous oil (317 mg, 88%). ^{1}H NMR (400 MHz, $CDCl_3$): δ 8.60 (ddd, J = 4.9, 1.8, 0.9 Hz, 1H), 8.57 (dd, J = 2.3, 0.9 Hz, 1H), 8.35 (tt, J = 7.0, 1.0 Hz, 2H), 7.77 - 7.66 (m, 2H), 7.64 (s, 1H), 7.21 (ddd, J = 7.5, 4.8, 1.2 Hz, 1H), 7.01 (s, 1H), 2.47 (s, 3H), 2.20 (s, 3H), 1.26 (s, 12H) ppm.

Protected Ligand

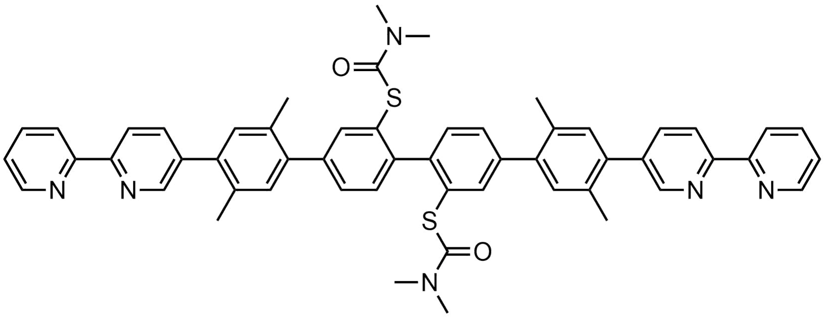

Bpy-xy-bpin (154 mg, 0.39 mmol), dimethylthiocarbamic acid S-(2'-dimethyl-carbamoylsulfanyl-4,4'-diiodobiphenyl-2-yl) ester (100 mg, 0.17 mmol) and Na_2CO_3 (408 mg, 3.85 mmol) were dissolved in degassed THF (7 mL) and water (2.4 mL). $Pd(PPh_3)_4$ (18.8 mg, 0.02 mmol) was added, and the mixture was stirred at 85 °C for 22 h under a nitrogen atmosphere. After cooling to rt, the product was extracted into DCM, and the combined organic phases washed with water and brine. The organic phase was dried over Na_2SO_4, and the solvent was removed under reduced pressure. Purification by column chromatography (SiO_2, Et_2O : TEA (100:1)) afforded the product as a slightly yellow solid (34.9 mg, 24%). ^{1}H-NMR (400 MHz, $CDCl_3$): δ 8.75 - 8.69 (m, 4H), 8.47 (ddd, J = 9.8, 8.1, 1.0 Hz, 4H), 7.87 (ddd, J = 7.7, 5.7, 2.0 Hz, 4H), 7.68 (t, J = 1.2 Hz, 2H), 7.47 - 7.42 (m, 4H), 7.36 - 7.31 (m, 4H), 7.22 (s, 2H), 2.93 (s, 12H), 2.41 (s, 6H), 2.35 (s, 6H) ppm.

Ligand

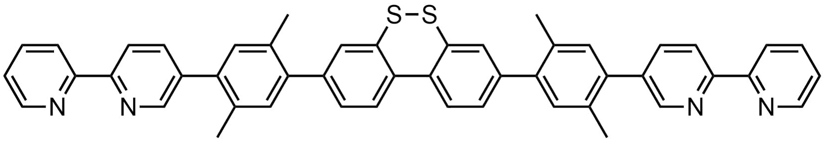

The protected ligand (34.9 mg, 0.04 mmol) was dissolved in degassed THF (3 mL) and MeOH (3 mL), and NaOH (40 mg, 1.0 mmol) added. After stirring for 2 h at 80 °C under a nitrogen atmosphere, the mixture was cooled to rt. Water was added and the solution neutralized with diluted HCl solution. Afterwards, the product was extracted into DCM, and the combined organic phases washed with water and brine. The organic phase was dried over Na_2SO_4, and the solvent removed under reduced pressure. The crude product was purified by column chromatography (SiO_2, Et_2O : TEA (100:1)), affording a mixture of the disulfide and dithiol species. Stirring of the mixture in DCM under air, followed by removal of the solvent, afforded the product as a slightly yellow solid (10 mg, 34%). ^{1}H-NMR (400 MHz, $CDCl_3$): δ 8.76 - 8.70 (m, 4H), 8.53 - 8.42 (m, 4H), 7.90 - 7.80 (m, 6H), 7.57 (d, J = 1.8 Hz, 2H), 7.43 (dd, J = 8.0, 1.8 Hz, 2H), 7.34 (ddd, J = 7.6, 4.8, 1.2 Hz, 2H), 7.27 (s, 2H), 7.24 (s, 2H) 2.38 (s, 6H), 2.36 (s, 6H) ppm. MS (ESI) calcd for $H_{37}C_{48}N_4S_2$ ($[M+H^+]^+$): *m/z* 733.25. Found: *m/z* 733.20.

5.4 Synthesis of Ref-Ru-^{t}Bu and the Triad

Xy-B(OH)$_2$[118]

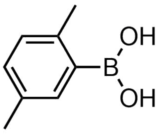

Magnesium turnings (77.0 mg, 3.17 mmol) were suspended in dry THF (1 mL), and a solution of 2,5-dimethylbromobenzene (536 mg, 0.4 mL, 2.90 mmol) in dry THF (4 mL) added dropwise. The mixture was heated to reflux for 3.5 h under a nitrogen atmosphere. After cooling to -78 °C, boric acid (366 mg, 0.40 mL, 3.52 mmol) was added, and the reaction mixture stirred at rt for 2.5 d. Aqueous HCl solution (2 M, 5 mL) was then added slowly, and the solution stirred for 20 min. The product was extracted into Et_2O, and the combined organic phases washed with water and brine. The organic phase was dried over Na_2SO_4, and the solvent removed under reduced pressure. Purification by column chromatography (SiO_2, DCM : pentane (2:1) → EtOAc → EtOAc : MeOH (90:10)) afforded the product as a white solid (300 mg, 69%). ^{1}H-NMR (400 MHz, $CDCl_3$): δ 8.00 (dd, *J* = 2.0, 0.9 Hz, 1H), 7.26 (s, 1H), 7.17 (d, *J* = 7.7 Hz, 1H), 2.77 (s, 3H), 2.39 (d, *J* = 1.0 Hz, 3H) ppm. ^{13}C-NMR (100 MHz, $CDCl_3$): δ 164.8, 156.8, 151.1, 150.0, 125.0, 124.4, 37.0 ppm.

Bpy-xy-H[116]

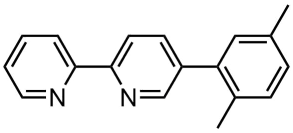

5-Bromo-2,2'-bipyridine (251 mg, 1.07 mmol), xy-B(OH)$_2$ (184 mg, 1.15 mmol) and Na_2CO_3(380 mg, 3.58 mmol) were dissolved in degassed THF (8 mL) and water (8 mL). $Pd(PPh_3)_4$ (62.0 mg, 0.05 mmol) was then added, and the mixture was stirred at 90 °C for 20 h under a nitrogen atmosphere. After cooling to rt, the product was extracted into DCM, the combined organic phases washed with water and brine. The organic phase was dried over Na_2SO_4, and the solvent removed under reduced pressure. Purification by column chromatography (SiO_2, pentane : Et_2O (4:1)) afforded the product as a yellow oil (238 mg, 86%). ^{1}H-NMR (400 MHz, $CDCl_3$): δ 8.73 (ddd, *J* = 4.8, 1.8, 0.9 Hz, 1H),

8.69 (dd, J = 2.3, 0.9 Hz, 1H), 8.50 - 8.45 (m, 2H), 7.86 (td, J = 7.8, 1.8 Hz, 1H), 7.82 (dd, J = 8.1, 2.3 Hz, 1H), 7.35 (ddd, J = 7.5, 4.8, 1.2 Hz, 1H), 7.24 (d, J = 7.7 Hz, 1H), 7.19 - 7.14 (m, 1H), 7.13 (d, J = 1.7 Hz, 1H), 2.40 (d, J = 0.9 Hz, 3H), 2.31 (s, 3H) ppm. ^{13}C-NMR (100 MHz, $CDCl_3$): δ 156.2, 154.7, 149.5, 149.4, 138.0, 137.8, 137.6, 137.1, 135.8, 132.7, 130.7, 130.7, 129.0, 123.8, 121.2, 120.6, 21.1, 20.1 ppm.

Ru((dbbpy)$_2$Cl$_2$[119]

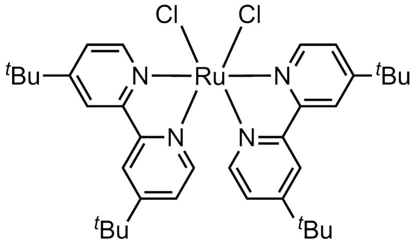

$RuCl_3 \cdot 0.5\, H_2O$ (83 mg, 0.40 mmol), 4,4'-di-*tert*-butyl-2,2'-bipyridine (215 mg, 0.80 mmol) and LiCl (11 mg, 0.26 mmol) were dissolved in DMF (2 mL), and heated to reflux for 6 h under a nitrogen atmosphere. Purification by column chromatography (SiO_2, acetone) afforded the product as a dark violet solid (67 mg, 23%). ^{1}H-NMR (400 MHz, acetone-d$_6$): δ 10.07 (d, J = 6.0 Hz, 2H), 8.54 (d, J = 2.1 Hz, 2H), 8.42 (d, J = 2.1 Hz, 2H), 7.68 (dd, J = 5.7, 2.1 Hz, 2H), 7.49 (s, 2H), 7.09 (dd, J = 5.9, 2.1 Hz, 2H), 1.53 (s, 18H), 1.32 (s, 18H) ppm.

Ref-Ru-^{t}Bu

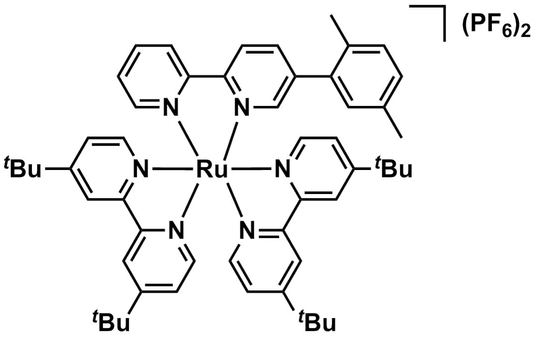

Ru(dbbpy)$_2$Cl$_2$ (15.0 mg, 0.02 mmol) and bpy-xy-H (5.5 mg, 0.02 mmol) were dissolved in EtOH (1.2 mL) and DCM (0.4 mL), and heated to reflux for 17 h under a nitrogen atmosphere, before the solvent was removed under reduced pressure. The crude product was purified by column chromatography (SiO_2, acetone → acetone : water (85:15) → acetone : water : sat. aqueous KNO_3 (85:14:1)). After removal of the organic solvent under reduced pressure, the complex was precipitated by adding saturated aqueous KPF_6 solution. Filtration, followed by washing with water and Et_2O, afforded the product as a

red solid (22 mg, 87%). ^{1}H-NMR (400 MHz, acetone-d$_6$): δ 8.90 - 8.81 (m, 6H), 8.24 - 8.16 (m, 2H), 8.06 (d, J = 6.0 Hz, 1H), 8.03 - 7.99 (m, 1H), 7.98 (d, J = 6.0 Hz, 1H), 7.96 (d, J = 6.0 Hz, 1H), 7.86 (d, J = 6.0 Hz, 1H), 7.72 (d, J = 2.0 Hz, 1H), 7.52 - 7.52 (m, 5H), 7.14 (d, J = 1.2 Hz, 2H), 7.00 (s, 1H), 2.28 (s, 3H), 1.95 (s, 3H), 1.40 (s, 9H), 1.40 (s, 9H), 1.39 (s, 9H), 1.36 (s, 9H) ppm. HRMS (ESI) calcd for $C_{54}H_{64}N_6Ru$ ([M-2(PF$_6^-$)]$^{2+}$): *m/z* 449.2119. Found: *m/z* 449.2124. Elemental analysis calcd for $C_{54}H_{64}F_{12}N_6P_2Ru \cdot 1.0\ H_2O$: C, 53.77; H, 5.52; N, 6.97. Found: C, 53.82; H, 5.54; N, 7.09.

Triad

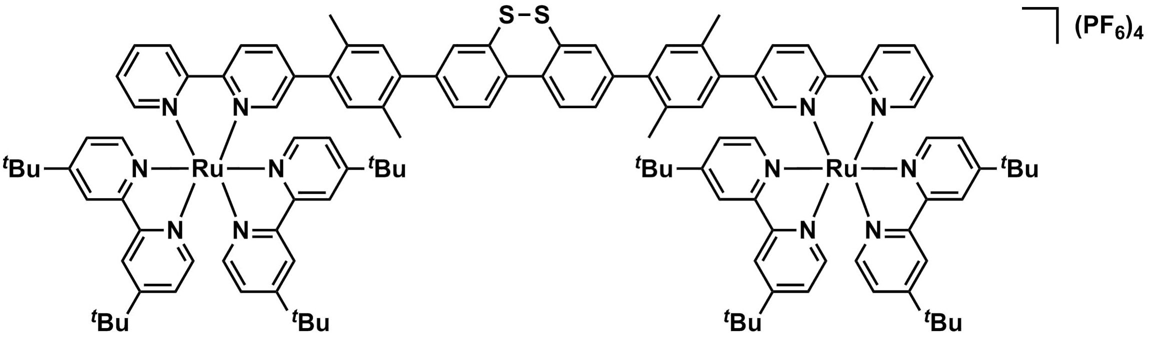

The ligand (10.0 mg, 13.6 mmol) and Ru((^{t}Bu)$_2$bpy)$_2$Cl$_2$ (19.4 mg, 27.4 mmol) were dissolved in EtOH (1.5 mL) and DCM (0.5 mL), and heated to reflux for 46 h under a nitrogen atmosphere. The crude product was purified by column chromatography (SiO$_2$, acetone → acetone : water (85:15) → acetone : water : sat. aqueous KNO$_3$ (85:15:1)). After removal of the organic solvent under reduced pressure, the complex was precipitated by adding saturated aqueous KPF$_6$ solution. The solid was filtered off and washed with water affording the product as a red solid (15 mg, 43%). ^{1}H-NMR (500 MHz, acetone-d$_6$): δ 8.95 - 8.76 (m, 12H), 8.28 (dd, J = 8.4, 2.0 Hz, 2H), 8.25 - 8.19 (m, 2H), 8.09 (d, J = 6.0 Hz, 2H), 8.06 - 7.92 (m, 8H), 7.89 (d, J = 6.0 Hz, 2H), 7.84 (d, J = 1.9 Hz, 2H), 7.66 - 7.56 (m, 10H), 7.53 (d, J = 1.8 Hz, 2H), 7.46 (dd, J = 8.0, 1.9 Hz, 2H), 7.24 (s, 2H), 7.20 (s, 2H), 2.31 (s, 6H), 2.06 (s, 6H), 1.41 (s, 18H), 1.41 (s, 36H), 1.38 (s, 18H) ppm. HRMS (ESI) calcd for $C_{120}H_{132}N_{12}Ru_2S_2$ ([M-2(PF$_6^-$)]$^{2+}$): *m/z* 502.2061. Found: *m/z* 502.2071. Elemental analysis calcd for $C_{120}H_{132}F_{24}N_{12}P_4Ru_2S_2 \cdot 2.0\ H_2O$: C, 54.92; H, 5.22; N, 6.40. Found: C, 54.68; H, 5.28; N, 6.62.

5.5 Synthesis of Ref-Ru-TAA and the Pentad

TAA-TMS[120]

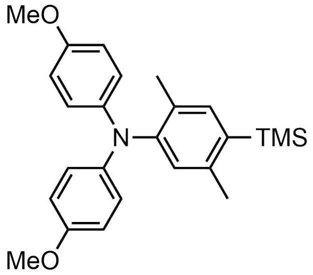

4,4'-Dimethoxydiphenylamine (1.16 g, 5.06 mmol), Br-xy-TMS (1.43 g, 5.56 mmol), potassium *tert*-butoxide (1.69 g, 15.1 mmol), tri-*tert*-butyl-phosphonium tetrafluoroborate (79.0 mg, 0.25 mmol) and Pd(dba)$_2$ (160 mg, 0.28 mmol) were dissolved in dry and degassed toluene (25 mL), and stirred for 17 h at 90 °C under a nitrogen atmosphere. After cooling to rt, the mixture was diluted with water (100 mL) and the product extracted into DCM. The organic solution was dried over Na_2SO_4, and the solvent removed under reduced pressure. Purification by column chromatography (SiO_2, pentane : EtOAC (10:1)) afforded the product as a white solid (1.81 g, 88%). ^{1}H-NMR (250 MHz, $CDCl_3$): δ 7.25 (s, 1H), 6.91 - 6.82 (m, 5H), 6.80 - 6.68 (m, 4H), 3.76 (s, 6H), 2.33 (s, 3H), 1.97 (s, 3H), 0.33 (s, 9H) ppm.

TAA-I[120]

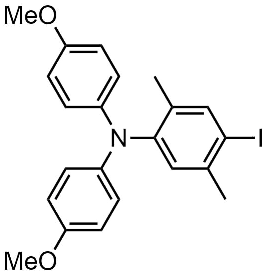

TAA-TMS (1.81 g, 4.46 mmol) was dissolved in dry DCM (30 mL). After cooling to -78 °C, iodine monochloride (1.45 g, 0.46 mL, 9.01 mmol) in dry DCM (10 mL) was added dropwise. The mixture was stirred at -78 °C for 10 min under a nitrogen atmosphere, then aqueous $Na_2S_2O_3$ solution was added. After warming to rt, the product was extracted into DCM. The combined organic phases were then dried over Na_2SO_4, and the solvent removed under reduced pressure. Purification by column chromatography (SiO_2, pentane : DCM (1:1)) afforded the product as a white solid (1.78 g, 87%). ^{1}H-NMR (400 MHz, $CDCl_3$): δ 7.63 (s, 1H), 7.14 - 6.37 (m, 9H), 3.78 (s, 6H), 2.29 (s, 3H), 1.91 (s, 3H) ppm.

TAA-bpin[120]

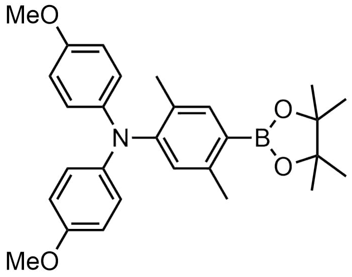

TAA-I (1.59 g, 3.46 mmol), bis(pinacolato)diboron (1.53 g, 6.03 mmol) and KOAc (1.53 g, 15.5 mmol) were dissolved in dry and degassed DMSO (20 mL), before $Pd(PPh_3)_2Cl_2$ (140 mg, 0.12 mmol) was added. The mixture was stirred for 20.5 h at 90 °C under a nitrogen atmosphere. After cooling to rt, saturated, aqueous NH_4Cl solution and water were added. The product was extracted into Et_2O, the combined organic phases dried over Na_2SO_4, and the solvent removed under reduced pressure. Purification by column chromatography (SiO_2, pentane : EtOAC (10:1)) afforded the product as a slightly yellow solid (1.47 g, 84%). ^{1}H-NMR (400 MHz, $CDCl_3$): δ 7.58 (s, 1H), 7.85 - 7.82 (m, 5H), 6.78 - 6.70 (m, 4H), 3.77 (s, 6H), 2.40 (s, 3H), 1.93 (s, 3H), 1.34 (s, 12H) ppm.

4-TAA-bpy

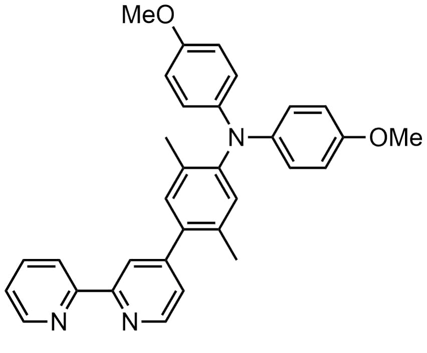

4-Bromo-2,2'-bipyridine (410 mg, 1.74 mmol), TAA-bpin (800 mg, 1.74 mmol) and Na_2CO_3 (1.87 g, 17.7 mmol) were dissolved in degassed water (8 mL) and THF (32 mL). After addition of $Pd(PPh_3)_4$ (190 mg, 0.16 mmol), the solution was stirred at 85 °C for 23 h under a nitrogen atmosphere. After cooling to rt, the product was extracted into DCM, and the organic phase washed with water and brine. The organic phase was dried over Na_2SO_4, and the solvent removed under reduced pressure. Purification by column chromatography (SiO_2, pentane : EtOAc (4:1) → EtOAc) afforded the product as a yellow solid (771 mg, 90%). ^{1}H-NMR (400 MHz, $CDCl_3$): δ 8.80 - 8.70 (m, 3H), 8.57 (s, 1H), 7.94 (t, J = 7.9 Hz, 1H), 7.49 (s, 1H), 7.41 (t, J = 6.2 Hz, 1H), 7.17 (s, 1H), 6.97 (s, 1H), 6.95 - 6.86 (m, 4H), 6.85 - 6.75 (m, 4H), 3.79 (s, 6H), 2.25 (s, 3H), 1.99 (s, 3H) ppm.

Ru(4-TAA-bpy)$_2$Cl$_2$

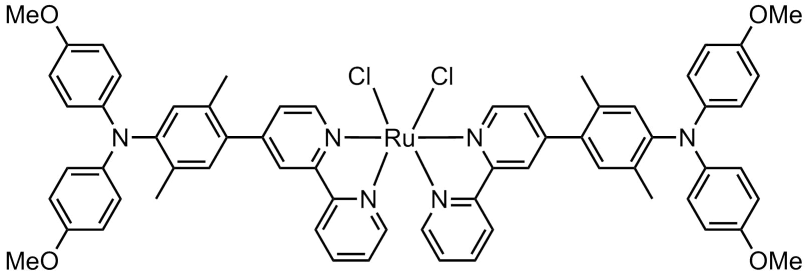

Ru(DMSO)$_4$Cl$_2$ (114 mg, 0.23 mmol), 4-TAA-bpy (227 mg, 0.47 mmol) and LiCl (40 mg, 0.94 mmol) were dissolved in dry DMF (14 mL), and the solution stirred for 90 min at 170 °C under a nitrogen atmosphere, before the solvent was removed under reduced pressure. Purification by column chromatography (SiO$_2$, 1. acetone, 2. DCM : MeOH (50:3, v:v), 3. DCM : MeOH (9:1, v:v)) afforded the product as a dark violet solid (30 mg, 11%). MS (ESI) calcd for $H_{58}C_{64}ClN_6O_4Ru$ ([M-Cl$^-$]$^+$): *m/z* 1111.33. Found: *m/z* 1111.41.

Ref-Ru-TAA

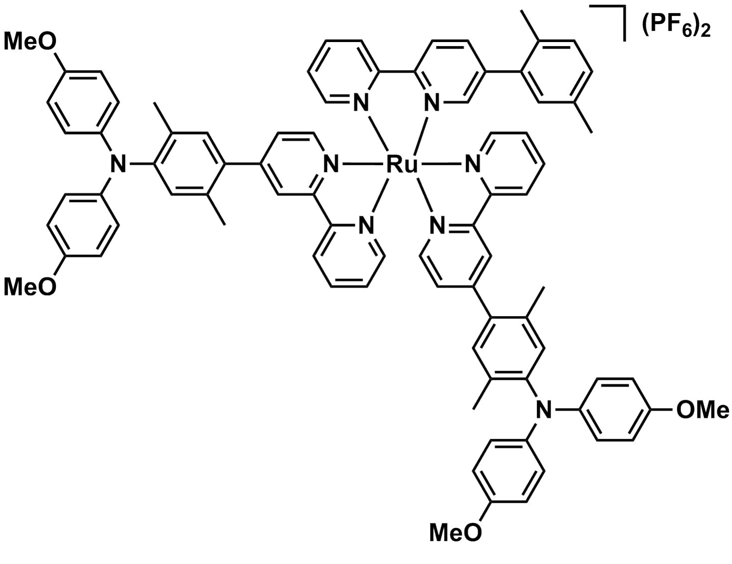

Ru(4-TAA-bpy)$_2$Cl$_2$(23.0 mg, 0.02 mmol) and bpy-xy-H (5.5 mg, 0.02 mmol) were dissolved in EtOH (0.5 mL) and DCM (1.5 mL), and heated to reflux for 18 h under a nitrogen atmosphere, before the solvent was removed under reduced pressure. The crude product was purified by column chromatography (SiO$_2$, acetone → acetone : water (90:10) → acetone : water : sat. aqueous KNO$_3$ (95:4:1)). After removal of the organic solvent under reduced pressure, the complex was precipitated by adding saturated aqueous KPF$_6$ solution. The solid was filtered off, and washed with water and Et$_2$O, affording the product as a red solid (13 mg, 40%). ^{1}H-NMR (400 MHz, acetonitrile-d$_3$): δ 8.64 - 8.52 (m, 4H), 8.50

(dd, $J = 6.4$, 1.9 Hz, 2H), 8.13 - 8.05 (m, 3H), 8.01 (td, $J = 7.9$, 1.5 Hz, 1H), 7.93 - 7.86 (m, 1H), 7.88 - 7.77 (m, 3H), 7.76 (d, $J = 5.9$ Hz, 1H) 7.65 (dd, $J = 2.0$, 0.7 Hz, 1H), 7.50 - 7.35 (m, 5H), 7.27 (d, $J = 8.1$ Hz, 2H), 7.13 (d, $J = 1.2$ Hz, 2H), 6.99 (d, $J = 2.2$ Hz, 3H), 6.84 (d, $J = 1.0$ Hz, 16H), 3.75 (s, 12H), 2.25 (s, 3H), 2.23 (s, 3H), 2.15 (s, 6H), 2.01 (s, 6H) ppm. HRMS (ESI) calcd for $C_{82}H_{74}N_8O_4Ru$ ([M-2(PF_6^-)]$^{2+}$): *m/z* 669.2444. Found *m/z* 668.2442. Elemental analysis calcd for $C_{82}H_{74}F_{12}N_8O_4P_2Ru \cdot 1.5\ H_2O$: C, 59.56; H, 4.69; N, 6.78. Found: C, 59.39; H, 4.80; N, 7.03.

Pentad

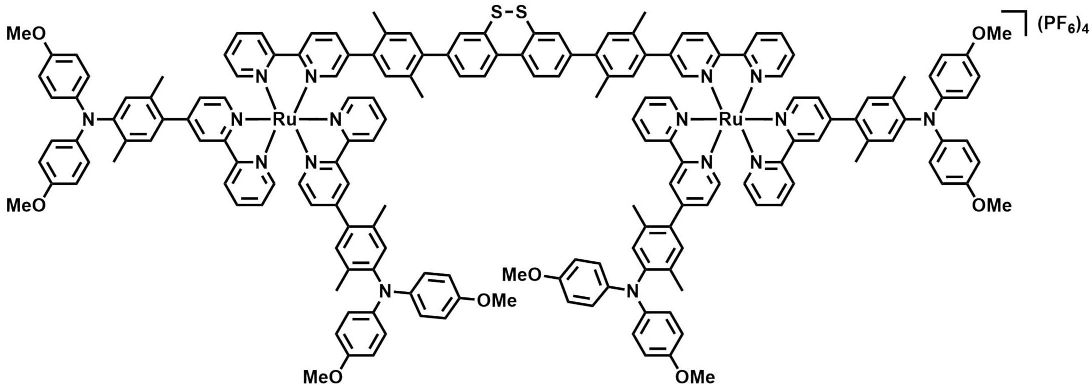

Ru(4-TAA-bpy)$_2$Cl$_2$ (28.2 mg, 0.02 mmol) and the ligand (9.00 mg, 0.01 mmol) were dissolved in EtOH (0.8 mL) and DCM (2.4 mL), and heated to reflux for 48 h under a nitrogen atmosphere, before the solvent was removed under reduced pressure. The crude product was purified by column chromatography (SiO_2, acetone → acetone : water (90:10) → acetone : water : sat. aqueous KNO_3 (95:4:1)). After removal of the organic solvent under reduced pressure, the complex was precipitated by adding saturated aqueous KPF_6 solution. Filtration, followed by washing with water and Et_2O afforded the product as a red solid (11.4 mg, 27%). ^{1}H-NMR (400 MHz, acetone-d$_6$): δ 9.05 (dt, $J = 8.1$, 1.6 Hz, 4H), 8.99 - 8.90 (m, 4H), 8.89 (dt, $J = 3.8$, 1.6 Hz, 4H), 8.35 - 8.12 (m, 18H), 8.10 (d, $J = 1.8$ Hz, 2H), 7.97 (d, $J = 8.1$ Hz, 2H), 7.72 - 7.55 (m, 10H), 7.54 (d, $J = 1.8$ Hz, 2H), 7.47 (dd, $J = 8.1$, 1.9 Hz, 2H), 7.30 (d, $J = 5.5$ Hz, 4H), 7.22 (d, $J = 3.8$ Hz, 4H), 7.00 (s, 4H), 6.86 (d, $J = 1.6$ Hz, 32H), 3.77 (s, 12H), 3.77 (s, 12H), 2.27 (s, 12H), 2.14 (s, 6H), 2.09 (s, 6H), 2.00 (s, 12H) ppm. HRMS (ESI) calcd $C_{176}H_{152}N_{16}O_8Ru_2S_2$ for ([M-4(PF_6^-)]$^{4+}$): *m/z* 721.4887. Found: *m/z* 721.4899. Elemental analysis calcd for $C_{176}H_{152}F_{24}N_{16}O_8P_4Ru_2S_2 \cdot 8\ H_2O$: C, 58.57; H, 4.69; N, 6.21. Found: C, 58.57; H, 4.77; N, 6.07.

6 Appendix

Estimated Energies of the Different Species Involved during the Charge-Accumulation in the Triad in MeCN from Section 3.2.3.

In the Absence of TEA

- Ru^{2+}-[S S]-Ru^{2+}

  This state is the ground state and its energy is set to **0.00 eV**

- $^*Ru^{2+}$-[S S]-Ru^{2+}

  This state corresponds to the ^{3}MLCT state of $[Ru((^tBu)bpy)_2(bpy)]^{2+}$ with an energy of **2.10 eV**

- Ru^{3+}-$[S\ S]^{\bullet -}$-Ru^{2+}

  E = -e · [E(S $S^{0/1}$) - E($Ru^{3+/2+}$)] = -e · (-1.6 V - 1.19 V) = **2.79 eV**

  (E = -e · [E(S $S^{0/1}$) - E($Ru^{3+/2+}$)] = -e · (-1.21 V - 1.19 V) = **2.40 eV**)

- $^*Ru^{2+}$-[S S]-$^*Ru^{2+}$

  E = E^{00} + E^{00} = **4.20 eV**

- Ru^{3+}-$[S\ S]^{\bullet -}$-$^*Ru^{2+}$

  E = -e · [E(S $S^{0/1}$) - E($Ru^{3+/2+}$)] + E^{00} = -e · (-1.6 V - 1.19 V) + 2.10 eV = **4.89 eV**

  (E = -e · [E(S $S^{0/1}$) - E($Ru^{3+/2+}$)] + E^{00} = -e · (-1.21 V - 1.19 V) + 2.10 eV = **4.50 eV**)

- Ru^{3+}-[S^- S^-]-Ru^{3+}

  E = -e · [E(S $S^{0/1}$) - E($Ru^{3+/2+}$)] = -e · ((-1.6 V - 0.3 V) - (1.19 V + 1.19 V)) = **4.28 eV**

  (E = -e · [E(S $S^{0/1-}$) + E(S $S^{1-/2-}$) - 2 · E($Ru^{3+/2+}$)] = -e · (-1.21 V - 0.3 V - 2 · 1.19 V) = **3.89 eV**)

In the Presence of TEA

- TEA Ru^{2+}-[S S]-Ru^{2+} TEA

  This state is the ground state and its energy is set to **0.00 eV**

- TEA *Ru^{2+}-[S S]-Ru^{2+} TEA

  This state corresponds to the ^{3}MLCT state of [Ru((^{t}Bu)bpy)$_2$(bpy)]$^{2+}$ with an energy of **2.10 eV**

- TEA Ru^{3+}-[S S]$^{\bullet-}$-Ru^{2+} TEA

  E = -e $\cdot$ [E(S S$^{0/1}$) - E(Ru$^{3+/2+}$)] = -e $\cdot$ (-1.6 V - 1.19 V) = **2.79 eV**

  (E = -e $\cdot$ [E(S S$^{0/1}$) - E(Ru$^{3+/2+}$)] = -e $\cdot$ (-1.21 V - 1.19 V) = **2.40 eV**)

- TEA$^{\bullet+}$ Ru^{1+}-[S S]-Ru^{2+} TEA

  E = -e $\cdot$ [E(Ru$^{2+/1+}$) - E(TEA$^{1+/0}$)] = -e $\cdot$ (-1.36 V - 0.85 V) = **2.21 eV**

- TEA$^{\bullet+}$ Ru^{2+}-[S S]$^{\bullet-}$-Ru^{2+} TEA

  E = -e $\cdot$ [E(S S$^{0/1-}$) - E(TEA$^{1+/0}$)] = -e $\cdot$ (-1.6 V - 0.85 V) = **2.45 eV**

  (E = -e $\cdot$ [E(S S$^{0/1-}$) - E(TEA$^{1+/0}$)] = -e $\cdot$ (-1.21 V - 0.85 V) = **2.06 eV**)

- TEA *Ru^{2+}-[S S]-*Ru^{2+} TEA

  E = E^{00} + E^{00} = **4.20 eV**

- TEA Ru^{3+}-[S S]$^{\bullet-}$-*Ru^{2+} TEA

  E = -e $\cdot$ [E(S S$^{0/1}$) - E(Ru$^{3+/2+}$)] + E^{00} = -e $\cdot$ (-1.6 V - 1.19 V) + 2.10 eV = **4.89 eV**

  (E = -e $\cdot$ [E(S S$^{0/1}$) - E(Ru$^{3+/2+}$)] + E^{00} = -e $\cdot$ (-1.21 V - 1.19 V) + 2.10 eV = **4.50 eV**)

- TEA$^{\bullet+}$ Ru^{1+}-[S S]-*Ru^{2+} TEA

  E = -e $\cdot$ [E(Ru$^{2+/1+}$) - E(TEA$^{1+/0}$)] + E^{00} = -e $\cdot$ (-1.36 V - 0.85 V) + 2.10 eV = **4.31 eV**

- TEA Ru^{3+}-[S^{-} S^{-}]-Ru^{3+} TEA

  E = -e $\cdot$ [E(S S$^{0/1}$) - E(Ru$^{3+/2+}$)] = -e $\cdot$ ((-1.6 V - 0.3 V) - (1.19 V + 1.19 V)) = **4.28 eV**

  (E = -e $\cdot$ [E(S S$^{0/1-}$) + E(S S$^{1-/2-}$) - 2 $\cdot$ E(Ru$^{3+/2+}$)] = -e $\cdot$ (-1.21 V - 0.3 V - 2 $\cdot$ 1.19 V) = **3.89 eV**)

- TEA$^{\bullet+}$ Ru^{1+}-[S S]-Ru^{1+} TEA$^{\bullet+}$

  E = -e $\cdot$ [2 $\cdot$ E(Ru$^{2+/1+}$) - 2 $\cdot$ E(TEA$^{1+/0}$)] = -e $\cdot$ (2 $\cdot$ (-1.36 V) - 2 $\cdot$ 0.85 V) = **4.42 eV**

- TEA$^{\bullet+}$ Ru^{1+}-[S S]$^{\bullet-}$-Ru^{2+} TEA$^{\bullet+}$

  E = -e $\cdot$ [E(S S$^{0/1}$) - E(Ru$^{2+/1+}$) - 2 $\cdot$ E(TEA$^{1+/0}$)] = -e $\cdot$ (-1.6 V -1.36 V - 2 $\cdot$ 0.85 V) = **4.66 eV**

$(E = -e \cdot [E(S\ S^{0/1}) - E(Ru^{2+/1+}) - 2 \cdot E(TEA^{1+/0})] = -e \cdot (-1.21\ V - 1.36\ V - 2 \cdot 0.85\ V) = \mathbf{4.27\ eV})$

- $TEA^{\bullet+}$ Ru^{2+}-[S^{-} S^{-}]-Ru^{2+} $TEA^{\bullet+}$

  $E = -e \cdot [E(S\ S^{0/1}) - E(S\ S^{1-/2-}) - 2 \cdot E(TEA^{1+/0})] = -e \cdot (-1.6\ V - 0.3\ V - 2 \cdot 0.85\ V) = \mathbf{3.60\ eV}$

  $(E = -e \cdot [E(S\ S^{0/1}) - E(S\ S^{1-/2-}) - 2 \cdot E(TEA^{1+/0})] = -e \cdot (-1.21\ V - 0.3\ V - 2 \cdot 0.85\ V) = \mathbf{3.21\ eV})$

Estimated Energies of the Different Species Involved during the Charge-Accumulation in the Pentad in MeCN from Section 3.3.3.

- TAA-Ru^{2+}-[S S]-Ru^{2+}-TAA

  This state is the ground state and its energy is set to **0.00 eV**

- TAA-$*Ru^{2+}$-[S S]-Ru^{2+}-TAA.

  This state corresponds to the ^{3}MLCT state of $[Ru(bpy)_3]^{2+}$ with an energy of **2.12 eV**

- $TAA^{\bullet+}$-Ru^{1+}-[S S]-Ru^{2+}-TAA

  $E = -e \cdot [E(Ru^{2+/1+}) - E(TAA^{1+/0})] = -e \cdot (-1.30\ V - 0.70\ V) = \mathbf{2.00\ eV}$

- $TAA^{\bullet+}$-Ru^{2+}-$[S\ S]^{\bullet-}$-Ru^{2+}-TAA

  $E = -e \cdot [E(S\ S^{0/1-}) - E(TAA^{1+/0})] = -e \cdot (-1.21\ V - 0.70\ V) = \mathbf{1.91\ eV}$

- $TAA^{\bullet+}$-Ru^{1+}-[S S]-$*Ru^{2+}$-TAA

  $E = -e \cdot [E(Ru^{2+/1+}) - E(TAA^{1+/0})] + E^{00} = -e \cdot (-1.30\ V - 0.70\ V) + 2.12\ eV = \mathbf{4.12\ eV}$

- $TAA^{\bullet+}$-Ru^{2+}-$[S\ S]^{\bullet-}$-$*Ru^{2+}$-TAA

  $E = -e \cdot [E(S\ S^{0/1-}) - E(TAA^{1+/0})] + E^{00} = -e \cdot (-1.21\ V - 0.70\ V) + 2.12\ eV = \mathbf{4.03\ eV}$

- $TAA^{\bullet+}$-Ru^{1+}-[S S]-Ru^{1+}-$TAA^{\bullet+}$

  $E = -e \cdot [2 \cdot E(Ru^{2+/1+}) - 2 \cdot E(TAA^{1+/0})] = -e \cdot (2 \cdot (-1.30\ V) - 2 \cdot (0.70\ V)) = \mathbf{4.00\ eV}$

- $TAA^{\bullet+}$-Ru^{2+}-$[S\ S]^{\bullet-}$-Ru^{1+}-$TAA^{\bullet+}$

  $E = -e \cdot [E(S\ S^{0/1-}) - E(Ru^{2+/1+}) - 2 \cdot E(TAA^{1+/0})] = -e \cdot (-1.21\ V - 1.30\ V - 0.70\ V) = \mathbf{3.91\ eV}$

- $TAA^{\bullet+}$-Ru^{2+}-[S^{-} S^{-}]-Ru^{3+}-TAA

  $E = -e \cdot [E(S\ S^{0/1-}) - E(S\ S^{1-/2-}) - E(Ru^{3+/2+}) - E(TAA^{1+/0})] = -e \cdot (-1.21\ V - 0.30\ V - 1.3\ V - 0.70\ V) = \mathbf{3.51\ eV}$

- TAA$^{\bullet+}$-Ru^{2+}-[S^{-} S^{-}]-Ru^{2+}-TAA$^{\bullet+}$

  E = -e · [E(S S$^{0/1-}$) - E(S S$^{1-/2-}$) - 2 · E(TAA$^{1+/0}$)] = -e · (-1.21 V - 0.30 V - 2 · 0.70 V) = **2.91 eV**

- TAA$^{\bullet+}$-Ru^{2+}-[SH SH]-Ru^{2+}-TAA$^{\bullet+}$

  E = -e · [E(S S$^{0/1-}$) - E(S S$^{1-/2-}$) - 2 · E(TAA$^{1+/0}$)] -e · 0.056 V · [2 · (pK$_{a}$(PhSH) - pK$_{a}$(TsOH))] = -e · (-1.21 V - 0.30 V - 2 · 0.70 V) -e · 0.059 V · (2 · (22.4-8.6)) = **1.28 eV**

NMR Spectra

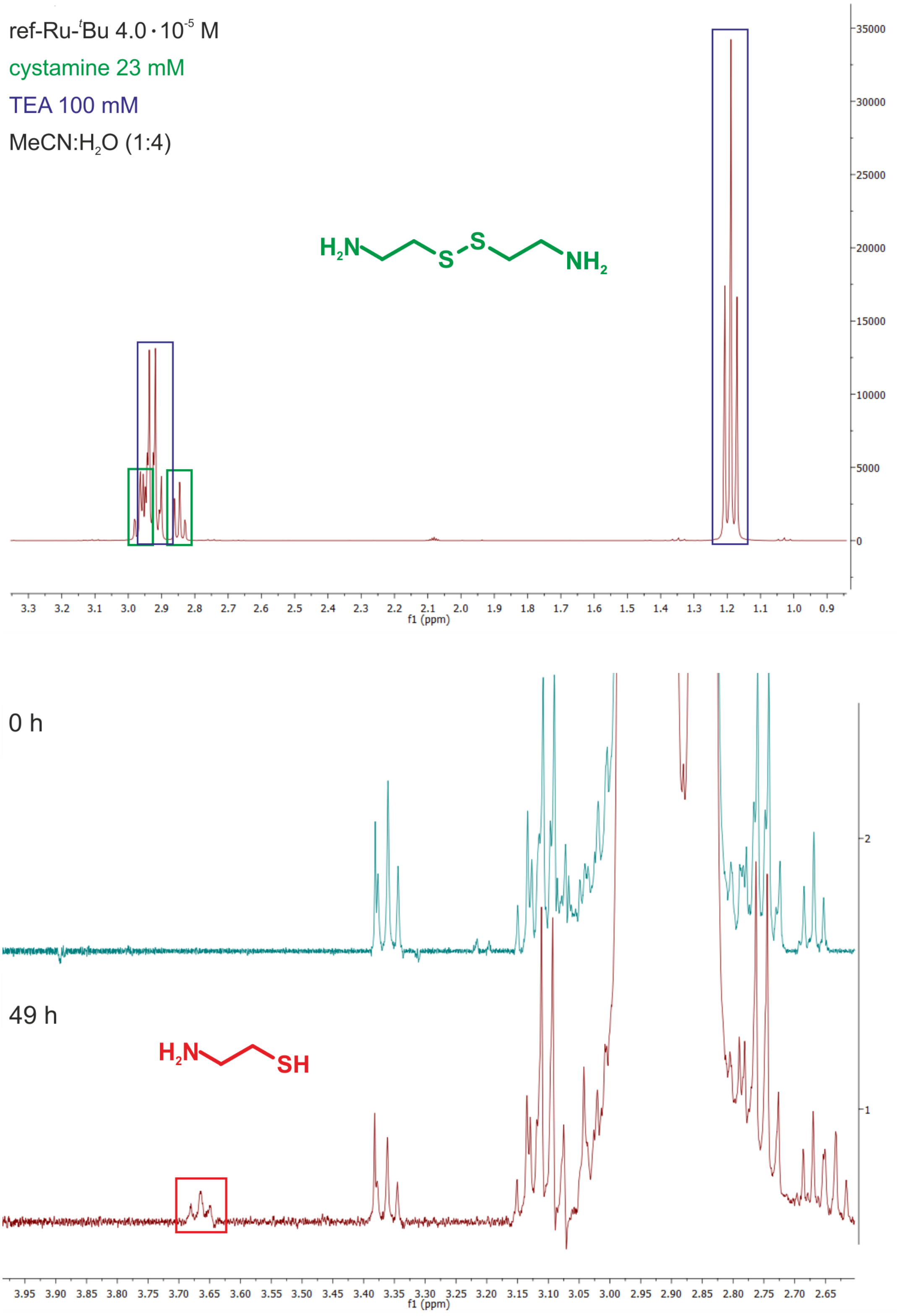

Figure 6.1: NMR spectra corresponding to entry 1 in Table 3.3.

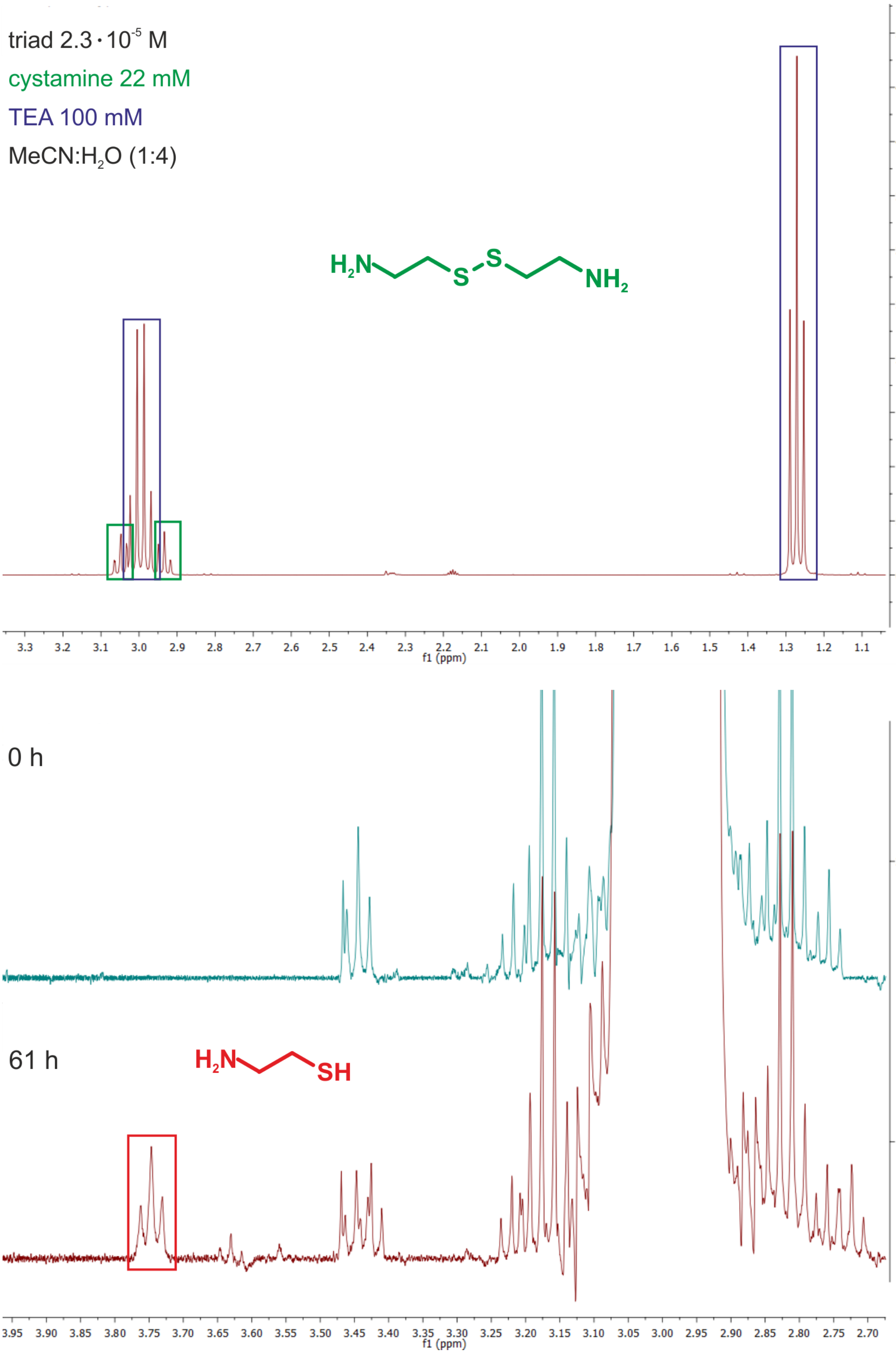

Figure 6.2: NMR spectra corresponding to entry 2 in Table 3.3.

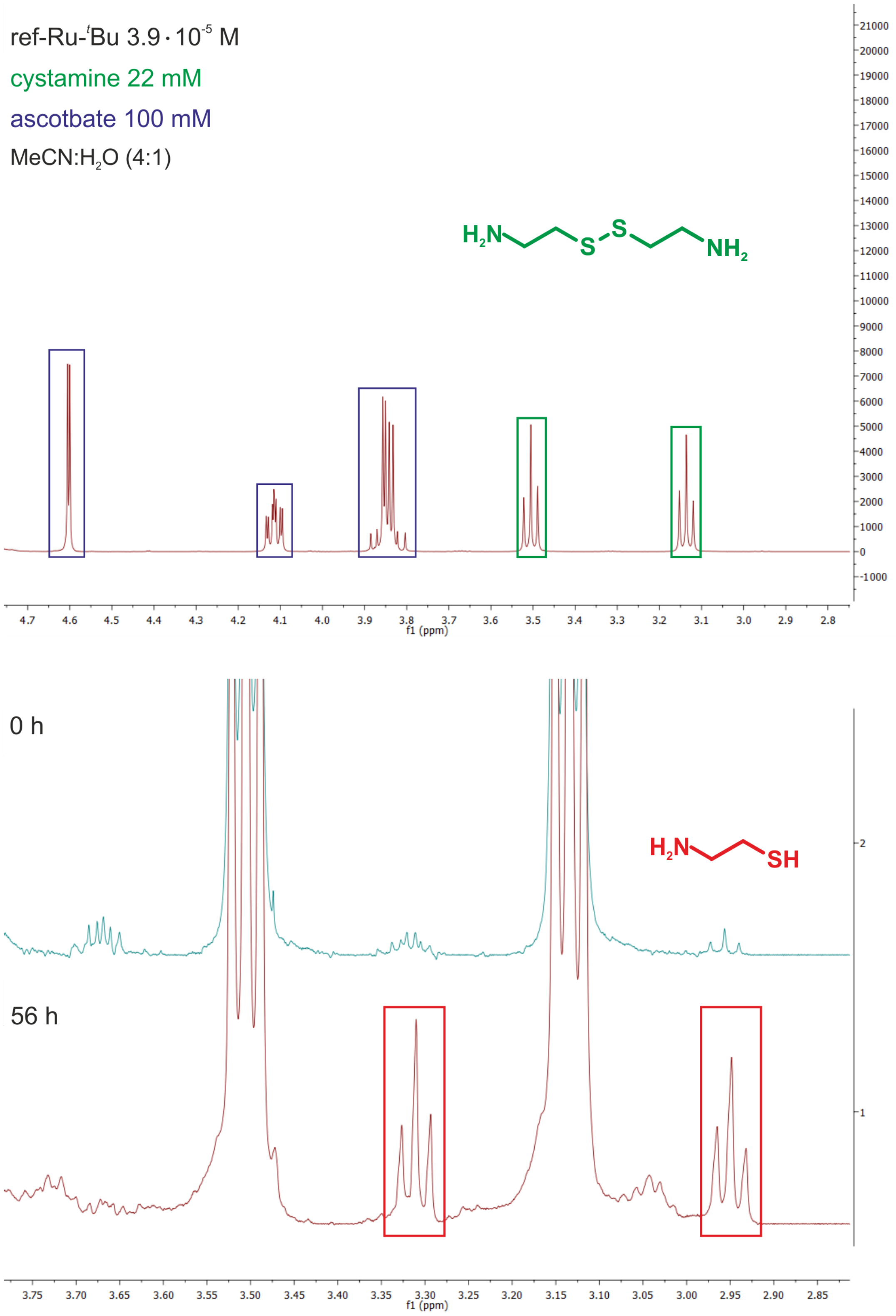

Figure 6.3: NMR spectra corresponding to entry 3 in Table 3.3.

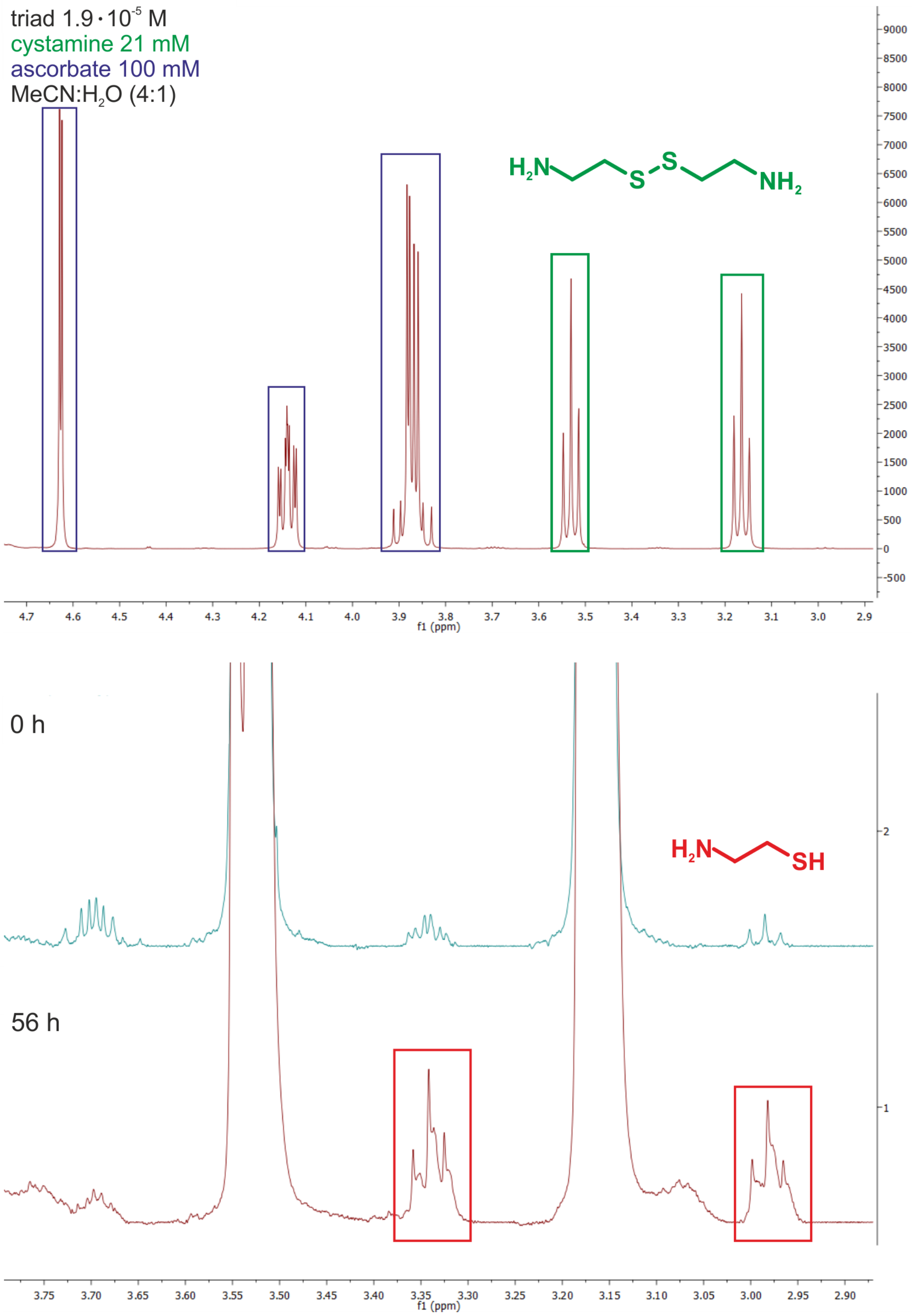

Figure 6.4: NMR spectra corresponding to entry 4 in Table 3.3.

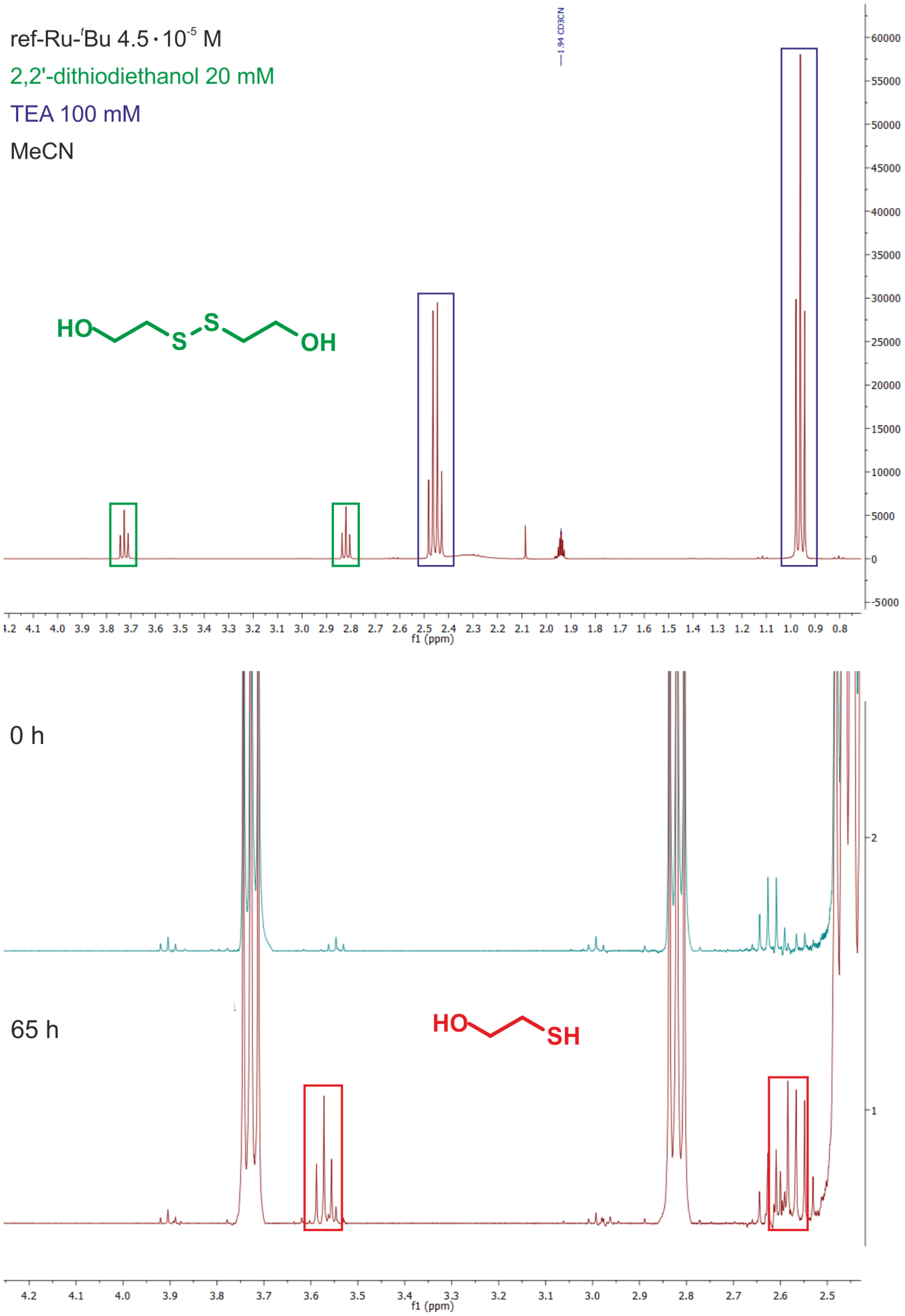

Figure 6.5: NMR spectra corresponding to entry 5 in Table 3.3.

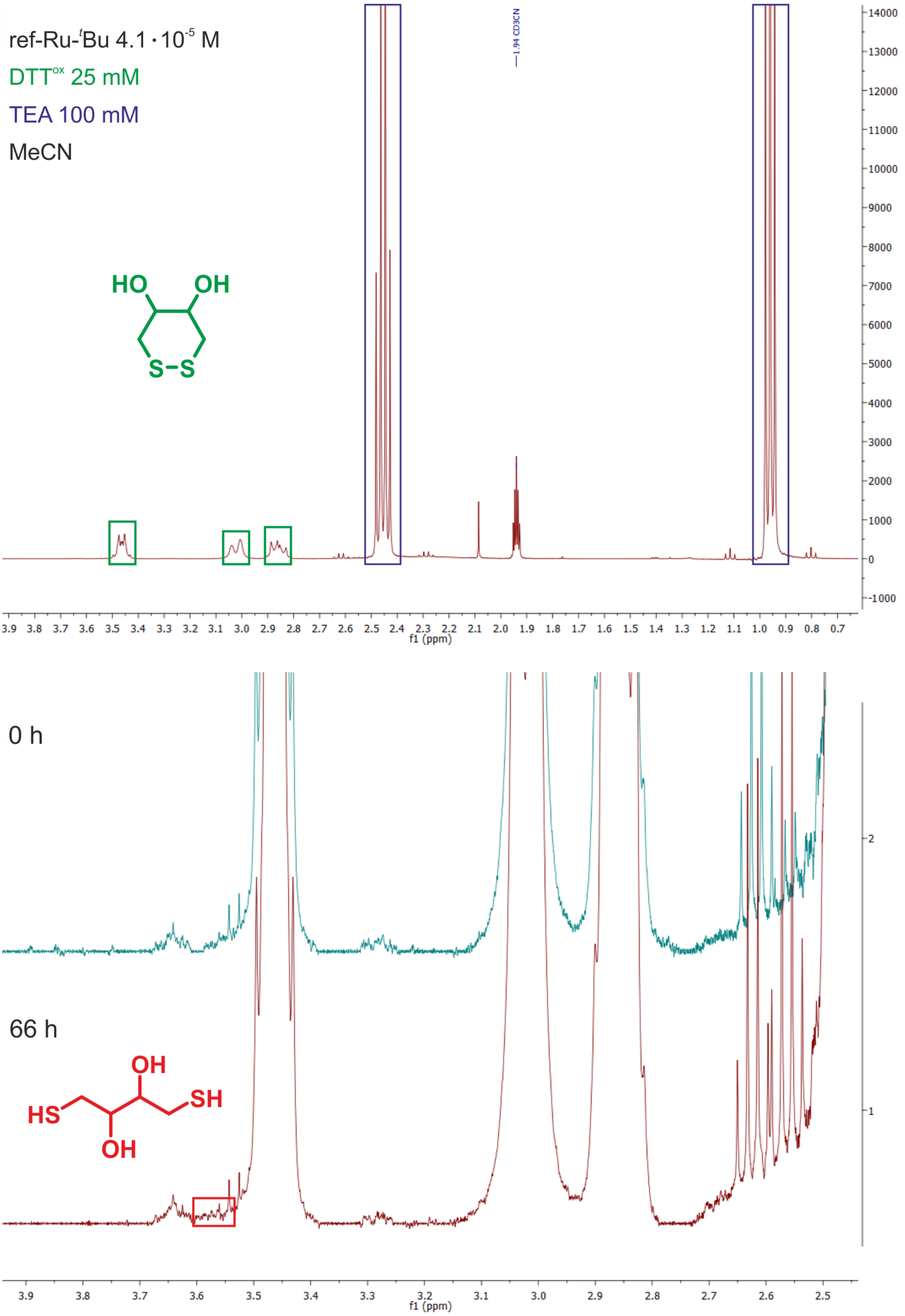

Figure 6.6: NMR spectra corresponding to entry 6 in Table 3.3.

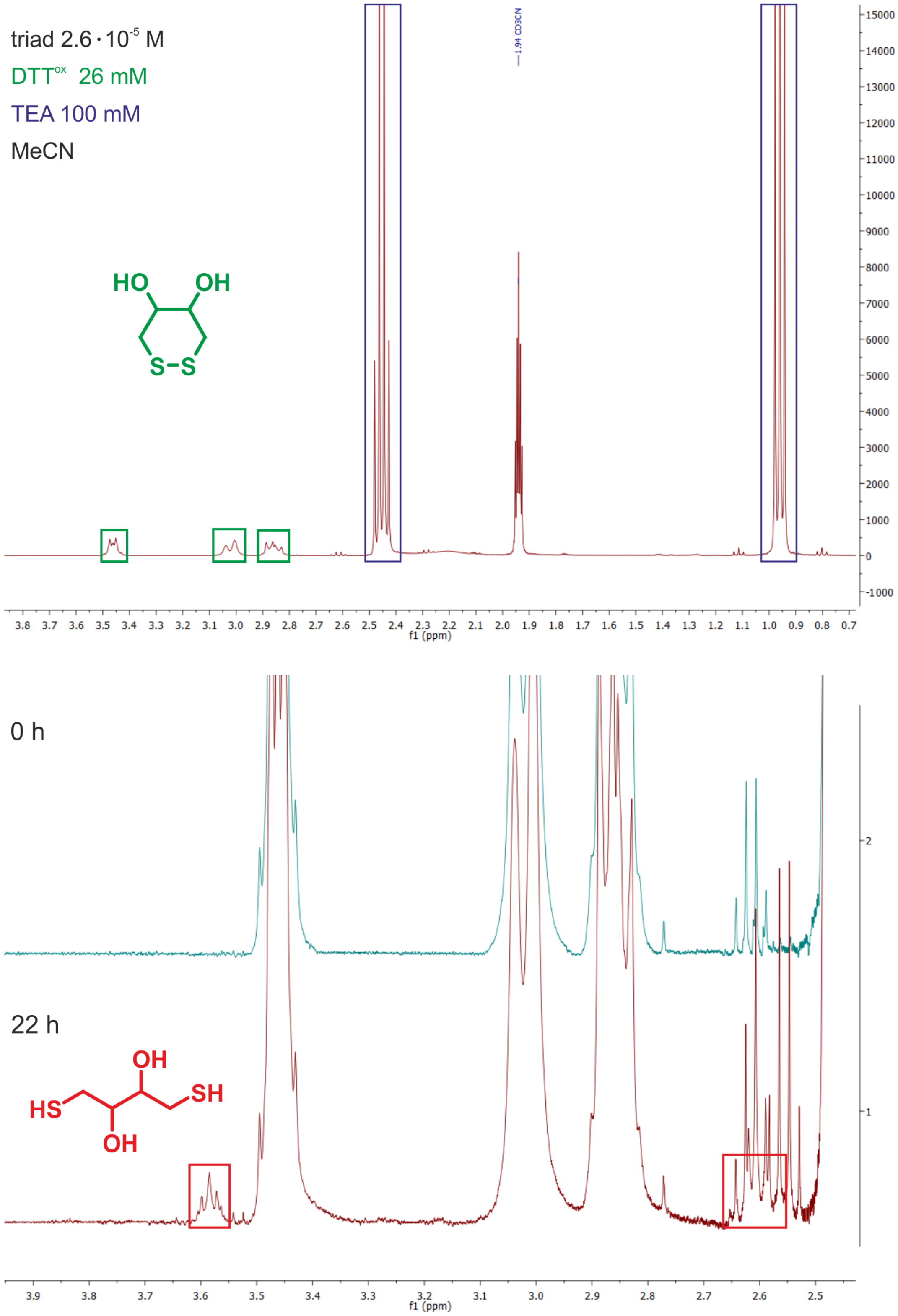

Figure 6.7: NMR spectra corresponding to entry 7 in Table 3.3.

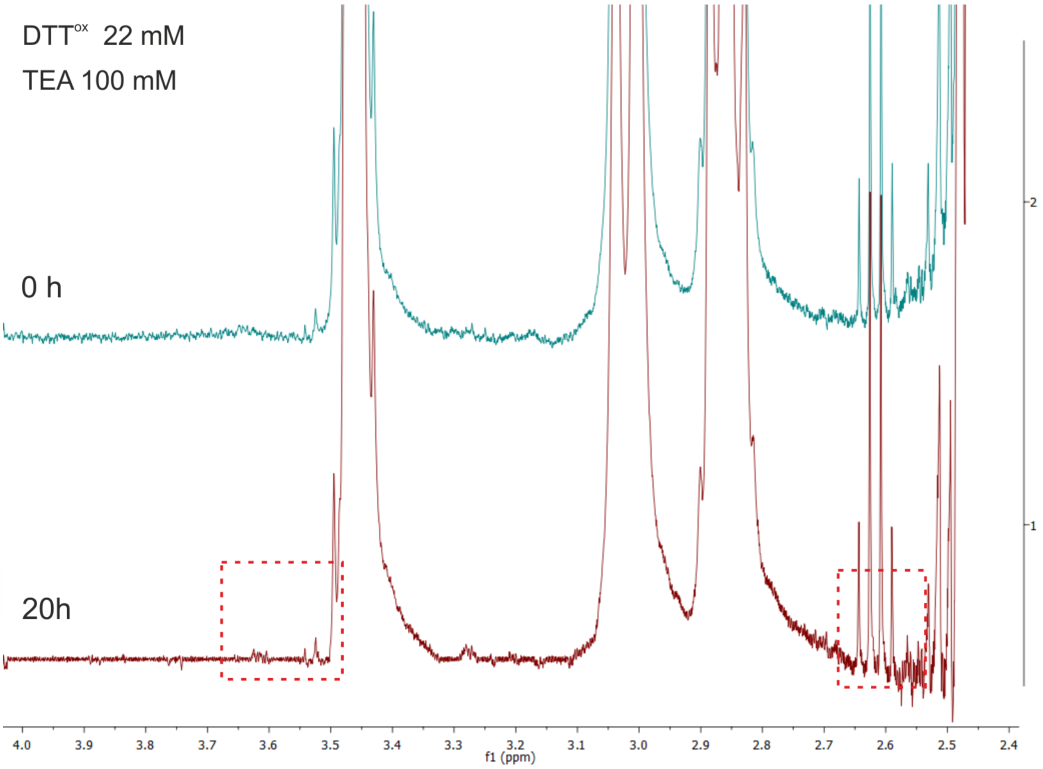

Figure 6.8: NMR spectra corresponding to entry 8 in Table 3.4.

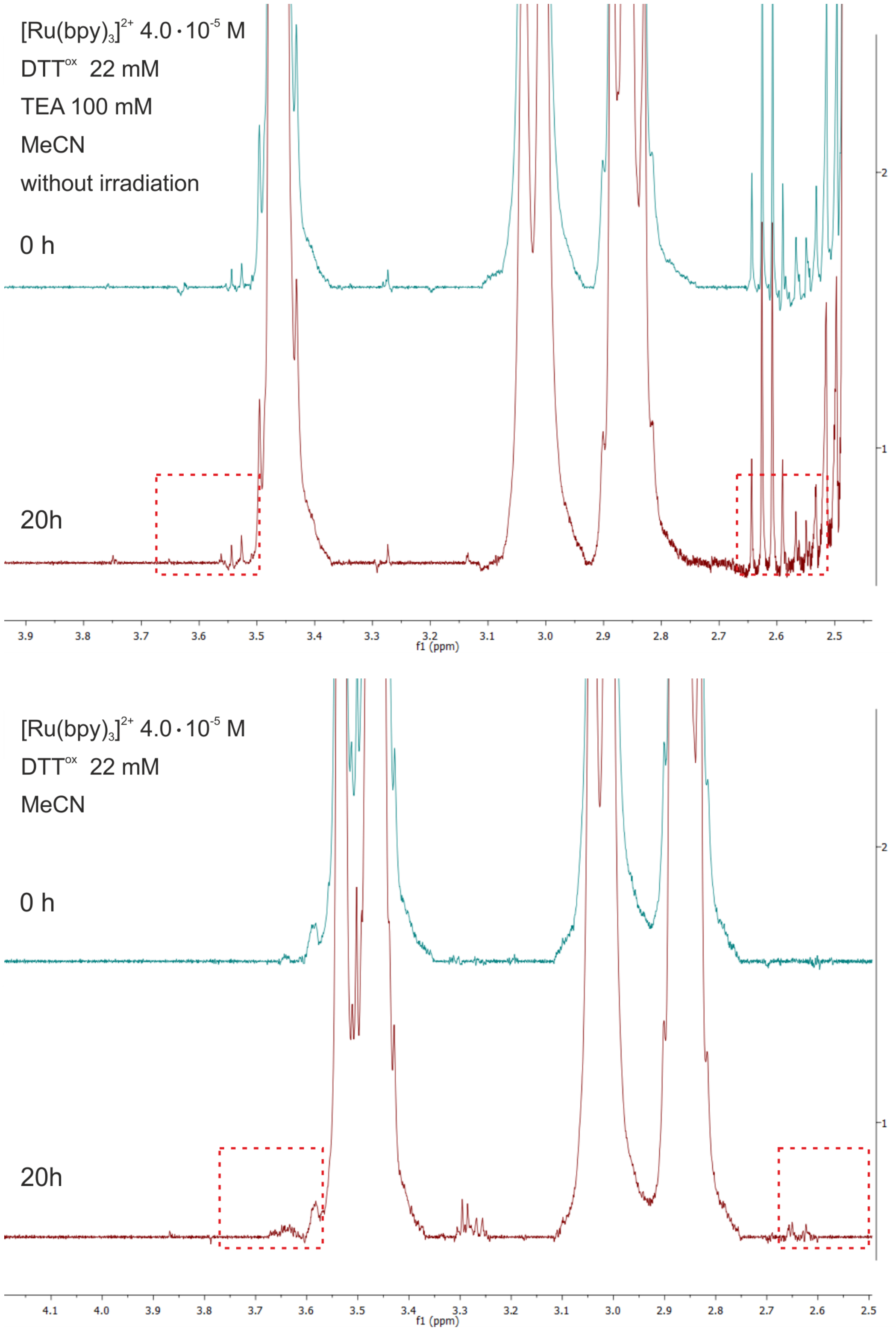

Figure 6.9: NMR spectra corresponding to entries 9 and 10 in Table 3.4.

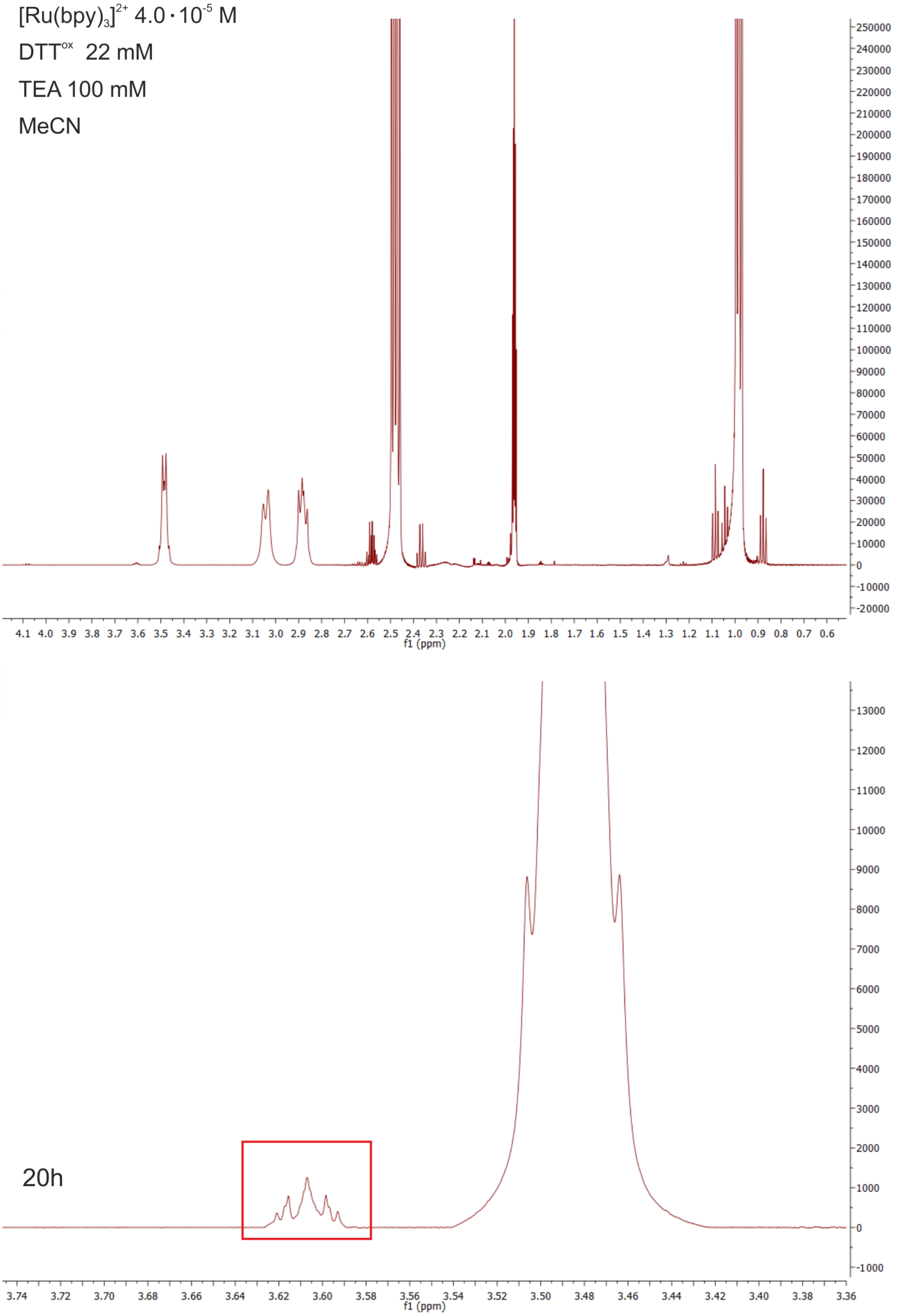

Figure 6.10: NMR spectra corresponding to entry 11 in Table 3.4.

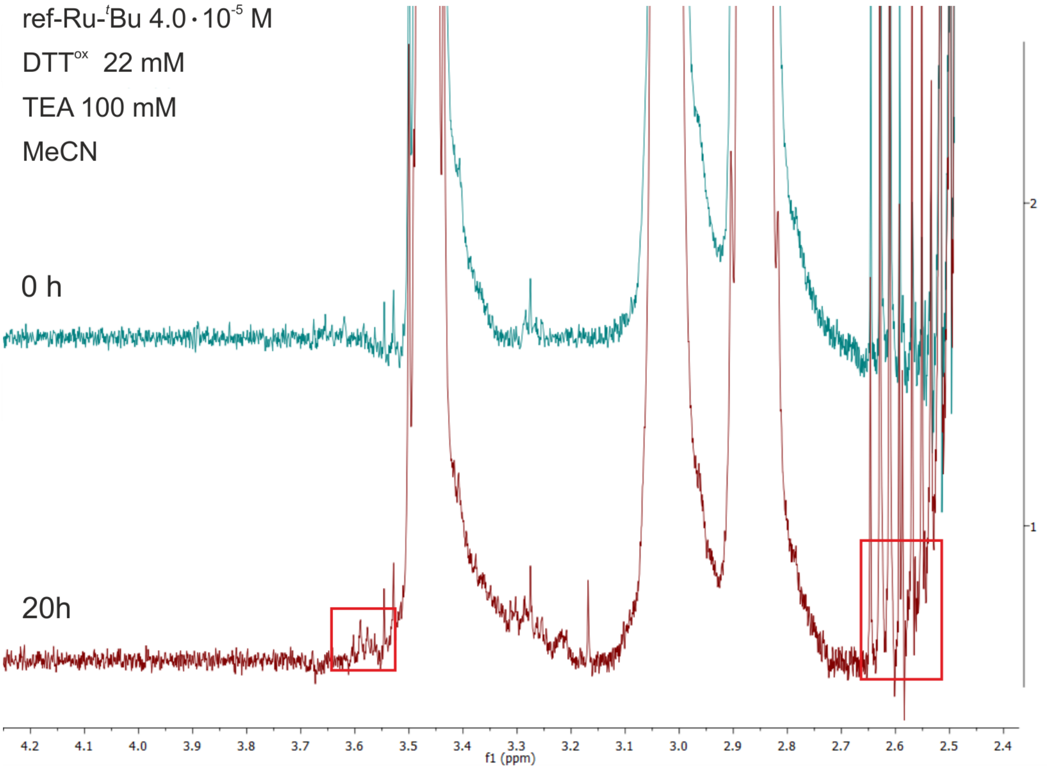

Figure 6.11: NMR spectra corresponding to entry 12 in Table 3.4.

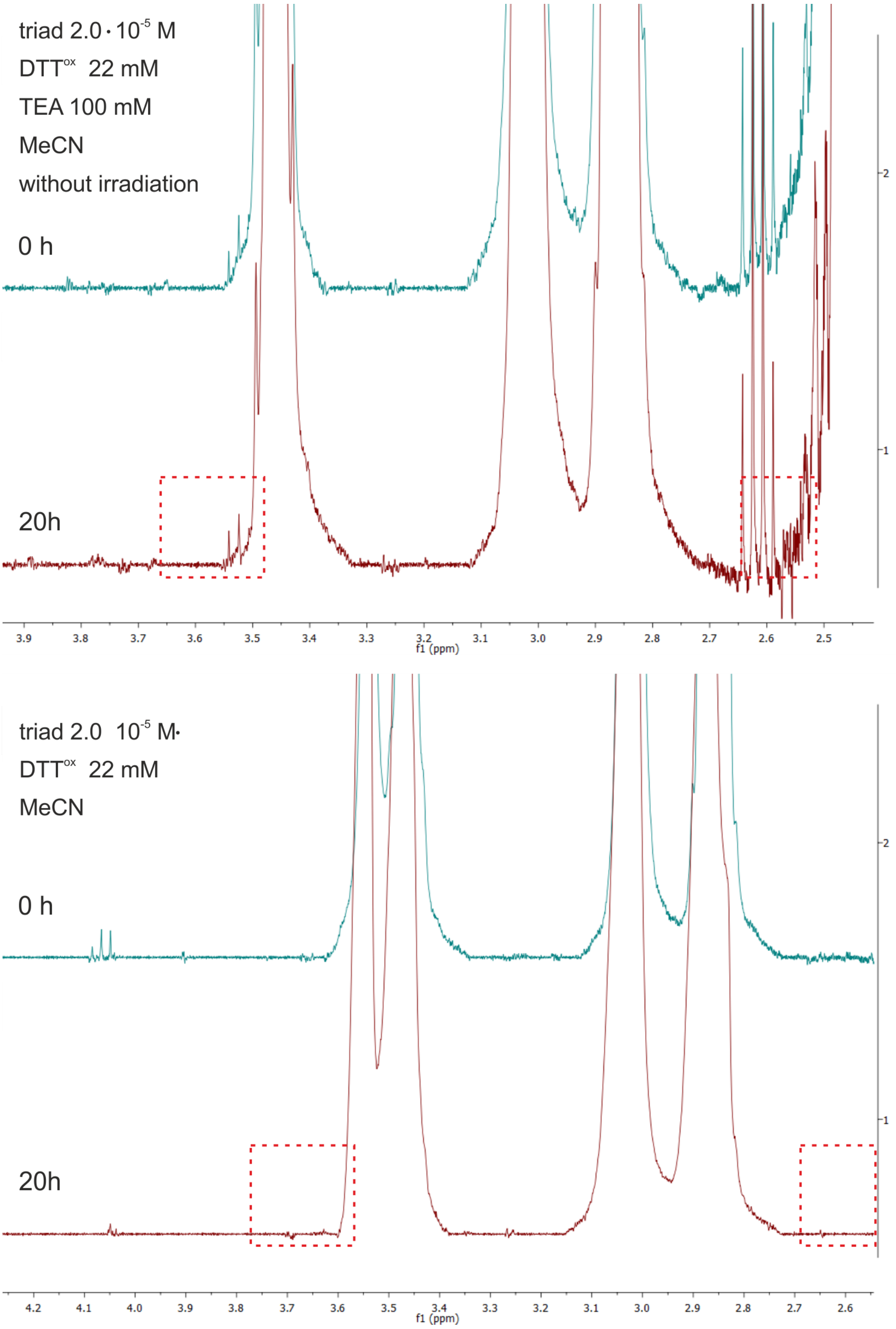

Figure 6.12: NMR spectra corresponding to entries 13 and 14 in Table 3.4.

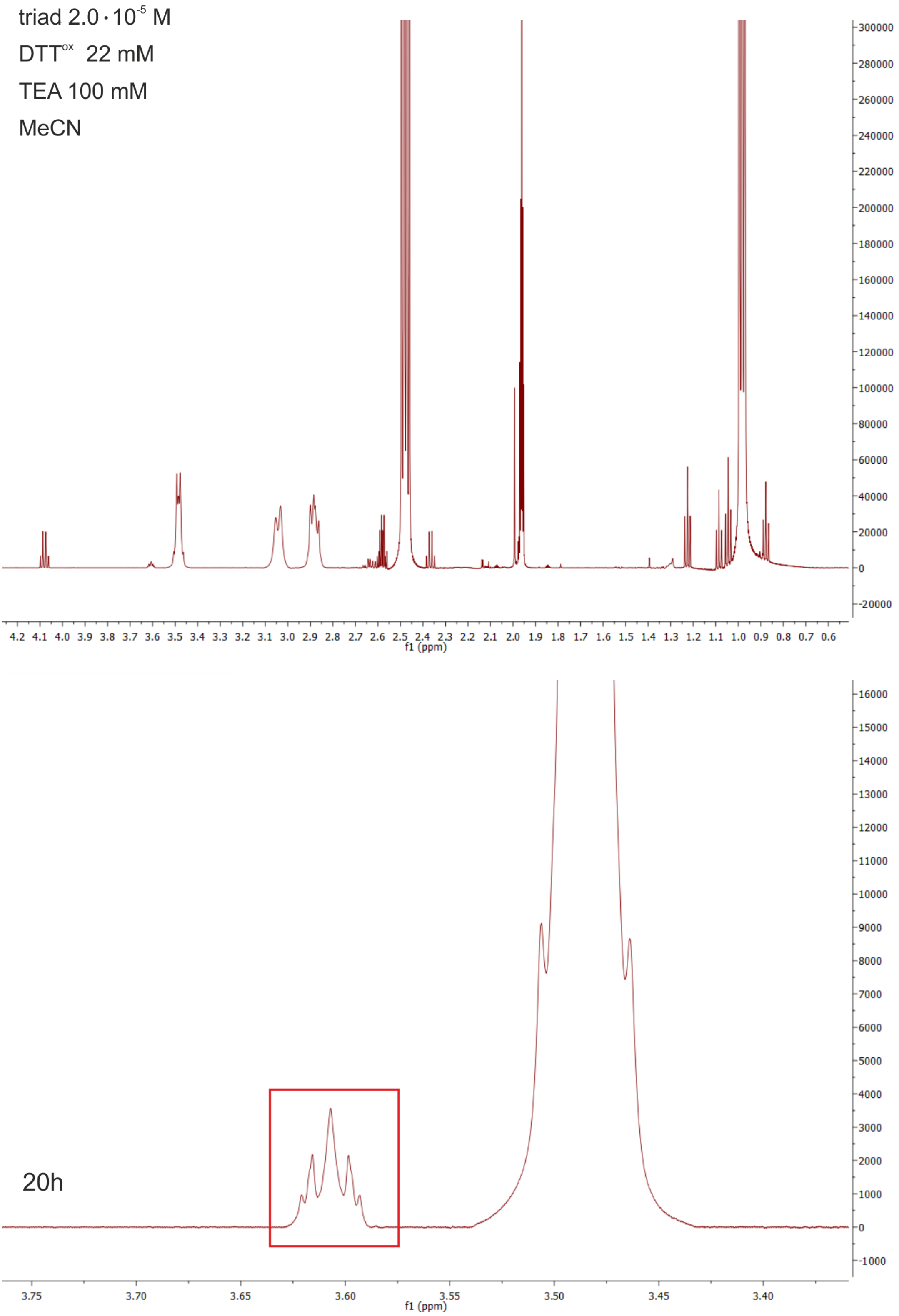

Figure 6.13: NMR spectra corresponding to entry 15 in Table 3.4.

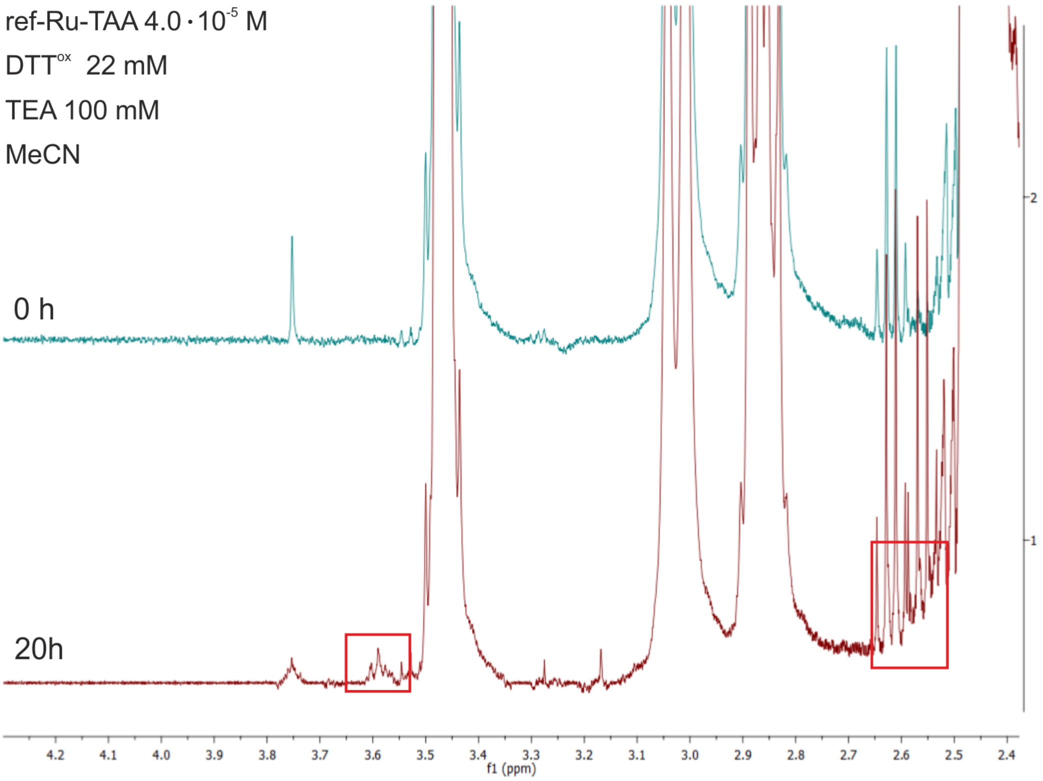

Figure 6.14: NMR spectra corresponding to entry 16 in Table 3.4.

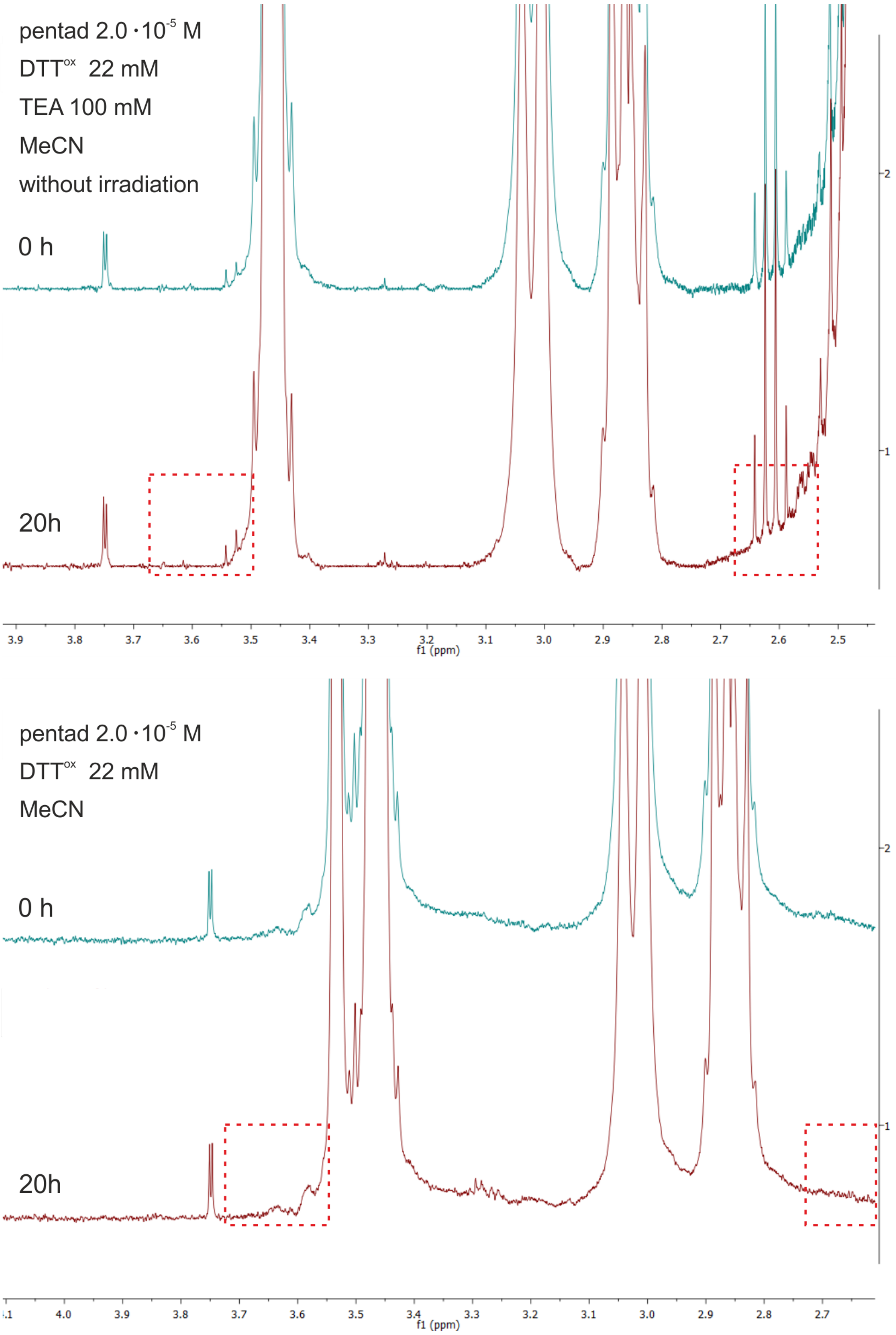

Figure 6.15: NMR spectra corresponding to entries 17 and 18 in Table 3.4.

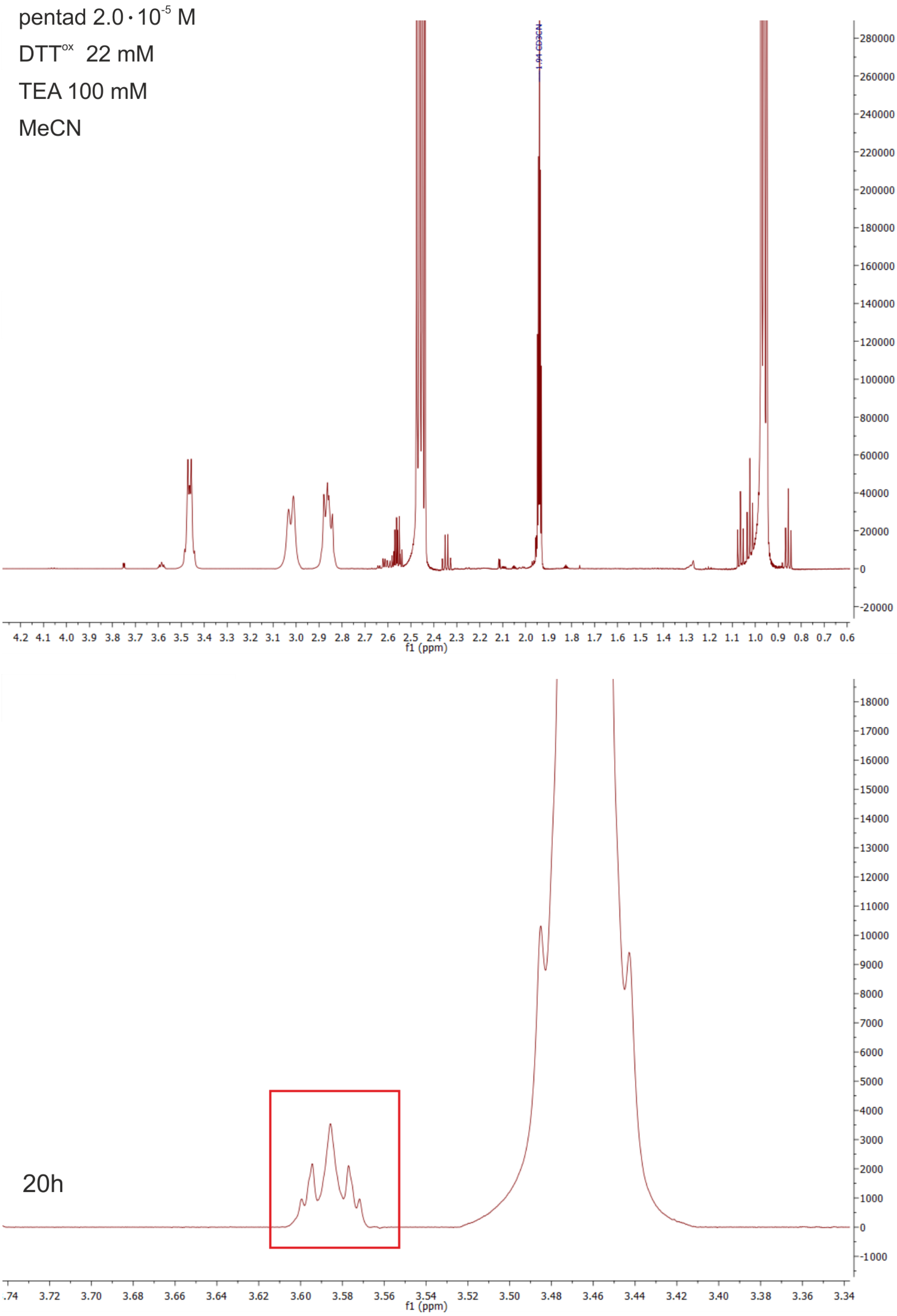

Figure 6.16: NMR spectra corresponding to entry 19 in Table 3.4.

Reaction Free Energy Estimation of the Thiol-Disulfide Interchange between Thiophenol and Methanethiol

Gas-Phase Bond Dissociation Energies:

- BDE(Ph**SS**PH)[99] = 55 kcal mol^{-1}
- BDE(Ph**SH**)[100] = 83 kcal mol^{-1}
- BDE(CH_3**SS**CH_3)[101] = 65 kcal mol^{-1}
- BDE(CH_3**SH**)[102] = 87 kcal mol^{-1}

pK$_a$-Values:

The pK$_a$ values were given in DMSO and converted into the value in MeCN with Equation 3.1.

- pK$_a$(PhSH)[77] = 22.4
- pK$_a$(DTT^{red})[77] = 25.9

Estimation of the Reaction Free Energy:

- $\Delta G_1 = -2.303 \cdot RT \cdot pK_a(PhSh)$ = - 2.303 · 8.314 J mol^{-1} K^{-1} · 298 K · 22.4

  = -128 kJ mol^{-1} = **-30.6 kcal mol^{-1}**

- ΔG_2 = Σ BDE$_{broken}$ - Σ BDE$_{formed}$= 2 · 83 kcal mol^{-1} + 65 kcal mol^{-1}

  - 2 · 87 kcal mol^{-1} - 55 kcal mol^{-1} = **2.0 kcal mol^{-1}**

- $\Delta G_3 = 2.303 \cdot RT \cdot pK_a(DTT)$ = 2.303 · 8.314 J mol^{-1} K^{-1} · 298 K · 25.9

  = -148 kJ mol^{-1} = **35.4 kcal mol^{-1}**

- $\Delta G_4 = \Delta G_1 + \Delta G_2 + \Delta G_3$ = -30.6 kcal mol^{-1} + 2.0 kcal mol^{-1}

  + 35.4 kcal mol^{-1} = **6.8 kcal mol^{-1}**

Bibliography

[1] Lewis, N. S.; Nocera, D. G. *Proceedings of the National Academy of Sciences* **2006**, *103*, 15729–15735.

[2] Key World Energy Statistics. International Energy Agency, 2017; `www.iea.org`.

[3] Balzani, V.; Credi, A.; Venturi, M. *ChemSusChem* **2008**, *1*, 26–58.

[4] Gust, D.; Moore, T. A.; Moore, A. L. *Accounts of Chemical Research* **2009**, *42*, 1890–1898.

[5] Tuller, H. L. *Materials for Renewable and Sustainable Energy* **2017**, *6*, 1–16.

[6] Wöhrle, D.; Tausch, M. W.; Stohrer, W.-D. *Photochemie*; Wiley VCH, 1998.

[7] Tachibana, Y.; Vayssieres, L.; Durrant, J. R. *Nature Photonics* **2012**, *6*, 511–518.

[8] Barber, J. *Inorganic Chemistry* **2008**, *47*, 1700–1710.

[9] Tommos, C.; Babcock, G. T. *Accounts of Chemical Research* **1998**, *31*, 18–25.

[10] Umena, Y.; Kawakami, K.; Shen, J.-R.; Kamiya, N. *Nature* **2011**, *473*, 55–60.

[11] Barber, J.; Tran, P. D. *Journal of The Royal Society Interface* **2013**, *10*, 1–16.

[12] Kok, B.; Forbush, B.; McGloin, M. *Photochemistry and Photobiology* **1970**, *11*, 457–475.

[13] Haumann, M. *Science* **2005**, *310*, 1019–1021.

[14] Dau, H.; Haumann, M. *Biochimica et Biophysica Acta - Bioenergetics* **2007**, *1767*, 472–483.

[15] Messinger, J.; Badger, M.; Wydrzynski, T. *Proceedings of the National Academy of Sciences* **1995**, *92*, 3209–3213.

[16] McEvoy, J. P.; Brudvig, G. W. *Physical Chemistry Chemical Physics* **2004**, *6*, 4754–4763.

[17] Sproviero, E.; GasconA, J.; McEvoy, J.; Brudvig, G.; Batista, V. *Coordination Chemistry Reviews* **2008**, *252*, 395–415.

[18] Siegbahn, P. E. M. *Chemistry - A European Journal* **2006**, *12*, 9217–9227.

[19] Siegbahn, P. E. M. *Accounts of Chemical Research* **2009**, *42*, 1871–1880.

[20] Siegbahn, P. E. M. *Physical Chemistry Chemical Physics* **2012**, *14*, 4849–4856.

[21] Gade, L. H. *Koordinationschemie*; Wiley VCH, 1998.

[22] Atkins, P. W.; de Paula, J. *Physikalische Chemie*; Wiley VCH, 2006.

[23] Koziar, J. C.; Cowan, D. O. *Accounts of Chemical Research* **1978**, *11*, 334–341.

[24] Ahmed, F. *Journal of Chemical Education* **1987**, *64*, 427–428.

[25] Minkin, V. I. *Pure and Applied Chemistry* **1999**, *71*, 1919–1981.

[26] Verhoeven, J. W. *Pure and Applied Chemistry* **1996**, *68*, 2223–2286.

[27] Juris, A.; Balzani, V.; Barigelletti, F.; Campagna, S.; Belser, P.; von Zelewsky, A. *Coordination Chemistry Reviews* **1988**, *84*, 85–277.

[28] Bensasson, R.; Salet, C.; Balzani, V. *Journal of the American Chemical Society* **1976**, *98*, 3722–3724.

[29] Demas, J. N.; Taylor, D. G. *Inorganic Chemistry* **1979**, *18*, 3177–3179.

[30] Prier, C. K.; Rankic, D. A.; MacMillan, D. W. C. *Chemical Reviews* **2013**, *113*, 5322–5363.

[31] Vlcek, A. A.; Dodsworth, E. S.; Pietro, W. J.; Lever, A. B. P. *Inorganic Chemistry* **1995**, *34*, 1906–1913.

[32] Marcus, R. A. *The Journal of Chemical Physics* **1956**, *24*, 966–978.

[33] Marcus, R. A. *The Journal of Chemical Physics* **1957**, *26*, 867–871.

[34] Marcus, R. A. *The Journal of Chemical Physics* **1957**, *26*, 872–877.

[35] Marcus, R. A. *Discuss. Faraday Soc.* **1960**, *29*, 21–31.

[36] Marcus, R. A. *The Journal of Physical Chemistry* **1963**, *67*, 853–857.

[37] Hush, N. S. *Transactions of the Faraday Society* **1961**, *57*, 557–580.

[38] Marcus, R.; Sutin, N. *Biochimica et Biophysica Acta - Reviews on Bioenergetics* **1985**, *811*, 265–322.

[39] Bartlett, P. N. *Bioelectrochemistry: Fundamentals, Experimental Techniques and Applications*; John Wiley & Sons, 2008.

[40] Kuss-Petermann, M.; Wenger, O. S. *Phys. Chem. Chem. Phys.* **2016**, *18*, 18657–18664.

[41] Hammarström, L. *Accounts of Chemical Research* **2015**, *48*, 840–850.

[42] Bonn, A. G. Towards photoinduced charge accumulation in purely molecular d6 metal complexes with oligo-triarylamine donors. Ph.D. thesis, University of Basel, 2015.

[43] Bonn, A. G.; Neuburger, M.; Wenger, O. S. *Inorganic Chemistry* **2014**, *53*, 11075–11085.

[44] Bonn, A. G.; Wenger, O. S. *Chimia International Journal for Chemistry* **2015**, *69*, 17–21.

[45] Konduri, R.; Ye, H.; MacDonnell, F. M.; Serroni, S.; Campagna, S.; Rajeshwar, K. *Angewandte Chemie International Edition* **2002**, *41*, 3185–3187.

[46] Wouters, K. L.; de Tacconi, N. R.; Konduri, R.; Lezna, R. O.; MacDonnell, F. M. *Photosynthesis Research* **2006**, *87*, 41–55.

[47] Karlsson, S.; Boixel, J.; Pellegrin, Y.; Blart, E.; Becker, H.-C.; Odobel, F.; Hammarström, L. *Journal of the American Chemical Society* **2010**, *132*, 17977–17979.

[48] Karlsson, S.; Boixel, J.; Pellegrin, Y.; Blart, E.; Becker, H.-C.; Odobel, F.; Hammarström, L. *Faraday Discuss.* **2012**, *155*, 233–252.

[49] O'Neil, M. P.; Niemczyk, M. P.; Svec, W. A.; Gosztola, D.; Gaines, G. L.; Wasielewski, M. R. *Science* **1992**, *257*, 63–65.

[50] Imahori, H.; Hasegawa, M.; Taniguchi, S.; Aoki, M.; Okada, T.; Sakata, Y. *Chemistry Letters* **1998**, *27*, 721–722.

[51] Orazietti, M.; Kuss-Petermann, M.; Hamm, P.; Wenger, O. S. *Angewandte Chemie International Edition* **2016**, *55*, 9407–9410.

[52] Kuss-Petermann, M.; Orazietti, M.; Neuburger, M.; Hamm, P.; Wenger, O. S. *Journal of the American Chemical Society* **2017**, *139*, 5225–5232.

[53] Evans, D. H.; Hu, K. *Journal of the Chemical Society, Faraday Transactions* **1996**, *92*, 3983–3990.

[54] Geske, D. H.; Ragle, J. L.; Bambenek, M. A.; Balch, A. L. *Journal of the American Chemical Society* **1964**, *86*, 987–1002.

[55] Kraiya, C.; Evans, D. H. *Journal of Electroanalytical Chemistry* **2004**, *565*, 29–35.

[56] Evans, D. H. *Chemical Reviews* **2008**, *108*, 2113–2144.

[57] Evans, D. H.; Busch, R. W. *Journal of the American Chemical Society* **1982**, *104*, 5057–5062.

[58] Lehmann, M. W.; Singh, P.; Evans, D. H. *Journal of Electroanalytical Chemistry* **2003**, *549*, 137–143.

[59] Bellec, N.; Boubekeur, K.; Carlier, R.; Hapiot, P.; Lorcy, D.; Tallec, A. *The Journal of Physical Chemistry A* **2000**, *104*, 9750–9759.

[60] Carlier, R.; Hapiot, P.; Lorcy, D.; Robert, A.; Tallec, A. *Electrochimica Acta* **2001**, *46*, 3269–3277.

[61] Benniston, A. C.; Allen, B. D.; Harriman, A.; Llarena, I.; Rostron, J. P.; Stewart, B. *New Journal of Chemistry* **2009**, *33*, 417–427.

[62] Hall, G. B.; Kottani, R.; Felton, G. A. N.; Yamamoto, T.; Evans, D. H.; Glass, R. S.; Lichtenberger, D. L. *Journal of the American Chemical Society* **2014**, *136*, 4012–4018.

[63] Gilbert, H. F. *Advances in Enzymology and Related Areas of Molecular Biology*; John Wiley & Sons, 2006; pp 69–172.

[64] Singh, R.; Whitesides, G. M. *Sulphur-Containing Functional Groups*; John Wiley & Sons, 1993; pp 633–658.

[65] Bulleid, N. J. *Cold Spring Harbor Perspectives in Biology* **2012**, *4*, 1–12.

[66] Depuydt, M.; Messens, J.; Collet, J.-F. *Antioxidants & Redox Signaling* **2011**, *15*, 49–66.

[67] Holmgren, A. *Annual Review of Biochemistry* **1985**, *54*, 237–271.

[68] Otto, H.-H.; Schirmeister, T. *Chemical Reviews* **1997**, *97*, 133–172.

[69] Singh, R.; Whitesides, G. M. *Techniques in Protein Chemistry*; Elsevier, 1995; pp 259–266.

[70] Fernandes, P. A.; Ramos, M. J. *Chemistry - A European Journal* **2004**, *10*, 257–266.

[71] Nagy, P. *Antioxidants & Redox Signaling* **2013**, *18*, 1623–1641.

[72] Whitesides, G. M.; Lilburn, J. E.; Szajewski, R. P. *The Journal of Organic Chemistry* **1977**, *42*, 332–338.

[73] Singh, R.; Whitesides, G. M. *Journal of the American Chemical Society* **1990**, *112*, 1190–1197.

[74] Mislow, K.; Glass, M. A. W.; Hopps, H. B.; Simon, E.; Wahl, G. H. *Journal of the American Chemical Society* **1964**, *86*, 1710–1733.

[75] Hiratsuka, H.; Horiuchi, H.; Furukawa, Y.; Watanabe, H.; Ishihara, A.; Okutsu, T.; Tobita, S.; Yoshinaga, T.; Shinohara, A.; Tokitoh, N.; Oba, M.; Nishiyama, K. *The Journal of Physical Chemistry A* **2006**, *110*, 3868–3874.

[76] Kütt, A.; Leito, I.; Kaljurand, I.; Sooväli, L.; Vlasov, V. M.; Yagupolskii, L. M.; Koppel, I. A. *The Journal of Organic Chemistry* **2006**, *71*, 2829–2838.

[77] Bordwell, F. G.; Hughes, D. L. *The Journal of Organic Chemistry* **1982**, *47*, 3224–3232.

[78] Tsierkezos, N. G. *Journal of Solution Chemistry* **2007**, *36*, 289–302.

[79] Braterman, P. S.; Song, J. I. *The Journal of Organic Chemistry* **1991**, *56*, 4678–4682.

[80] Carlson, C. N.; Kuehl, C. J.; Ogallo, L.; Shultz, D. A.; Thompson, J. D.; Kirk, M. L.; Martin, R. L.; John, K. D.; Morris, D. E. *Organometallics* **2007**, *26*, 4234–4242.

[81] Araujo, R. B.; Banerjee, A.; Panigrahi, P.; Yang, L.; Strømme, M.; Sjödin, M.; Araujo, C. M.; Ahuja, R. *Journal of Materials Chemistry A* **2017**, *5*, 4430–4454.

[82] Mohan, J. *Organic Spectroscopy: Principles and Applications, Second Edition*; Alpha Science International, Ltd, 2004.

[83] Juris, A.; Balzani, V.; Belser, P.; von Zelewsky, A. *Helvetica Chimica Acta* **1981**, *64*, 2175–2182.

[84] Connelly, N. G.; Geiger, W. E. *Chemical Reviews* **1996**, *96*, 877–910.

[85] Pavlishchuk, V. V.; Addison, A. W. *Inorganica Chimica Acta* **2000**, *298*, 97–102.

[86] Willner, I.; Tsfania, T.; Eichen, Y. *The Journal of Organic Chemistry* **1990**, *55*, 2656–2662.

[87] Tucker, J. W.; Narayanam, J. M. R.; Krabbe, S. W.; Stephenson, C. R. J. *Organic Letters* **2010**, *12*, 368–371.

[88] Skaisgirski, M.; Guo, X.; Wenger, O. S. *Inorganic Chemistry* **2017**, *56*, 2432–2439.

[89] Heath, G. A.; Yellowlees, L. J.; Braterman, P. S. *Journal of the Chemical Society, Chemical Communications* **1981**, 287–289.

[90] DeLaive, P. J.; Foreman, T. K.; Giannotti, C.; Whitten, D. G. *Journal of the American Chemical Society* **1980**, *102*, 5627–5631.

[91] Hankache, J.; Niemi, M.; Lemmetyinen, H.; Wenger, O. S. *Inorganic Chemistry* **2012**, *51*, 6333–6344.

[92] Kuss-Petermann, M. Photoinduced formation and decay od charge-separated states in d^6 metal complexes. Ph.D. thesis, University of Basel, 2016.

[93] Antonello, S.; Benassi, R.; Gavioli, G.; Taddei, F.; Maran, F. *Journal of the American Chemical Society* **2002**, *124*, 7529–7538.

[94] Howie, J. K.; Houts, J. J.; Sawyer, D. T. *Journal of the American Chemical Society* **1977**, *99*, 6323–6326.

[95] Christensen, T. B.; Daasbjerg, K.; Valentin-Hansen, P.; Pedersen, E. B.; Rissanen, K.; Shi, W.; Styring, S.; Tommos, C.; Warncke, K.; Wood, B. R. *Acta Chemica Scandinavica* **1997**, *51*, 307–317.

[96] Antonello, S.; Daasbjerg, K.; Jensen, H.; Taddei, F.; Maran, F. *Journal of the American Chemical Society* **2003**, *125*, 14905–14916.

[97] Pellegrin, Y.; Odobel, F. *Comptes Rendus Chimie* **2017**, *20*, 283–295.

[98] DeLaive, P. J.; Lee, J. T.; Sprintschnik, H. W.; Abruna, H.; Meyer, T. J.; Whitten, D. G. *Journal of the American Chemical Society* **1977**, *99*, 7094–7097.

[99] Bausch, M. J.; Guadalupe-Fasano, C.; Gostowski, R. *Energy & Fuels* **1991**, *5*, 419–423.

[100] Santos, R. M. B. D.; Muralha, V. S. F.; Correia, C. F.; Guedes, R. C.; Cabral, B. J. C.; Simões, J. A. M. *The Journal of Physical Chemistry A* **2002**, *106*, 9883–9889.

[101] Nicovich, J. M.; Kreutter, K. D.; Dijk, C. A. V.; Wine, P. H. *The Journal of Physical Chemistry* **1992**, *96*, 2518–2528.

[102] Berkowitz, J.; Ellison, G. B.; Gutman, D. *The Journal of Physical Chemistry* **1994**, *98*, 2744–2765.

[103] Tsukamoto, S.; Ohno, M. *The Journal of Biochemistry* **1978**, *84*, 1625–1632.

[104] AlbeckL, A.; Kliper, S. *Biochemical Journal* **1997**, *322*, 879–884.

[105] Amri, E.; Mamboya, F. *American Journal of Biochemistry and Biotechnology* **2012**, *8*, 99–104.

[106] Llerena-Suster, C. R.; José, C.; Collins, S. E.; Briand, L. E.; Morcelle, S. R. *Process Biochemistry* **2012**, *47*, 47–56.

[107] Gottlieb, H. E.; Kotlyar, V.; Nudelman, A. *The Journal of Organic Chemistry* **1997**, *62*, 7512–7515.

[108] Bandarage, U. K.; Simpson, J.; Smith, R. A.; Weavers, R. T. *Tetrahedron* **1994**, *50*, 3463–3472.

[109] Benniston, A. C.; Hagon, J.; He, X.; Yang, S.; Harrington, R. W. *Organic Letters* **2012**, *14*, 506–509.

[110] Delogu, G.; Fabbri, D.; Dettori, M. A. *Tetrahedron: Asymmetry* **1998**, *9*, 2819–2826.

[111] Wang, D. H.; Shen, Z.; Guo, M.; Cheng, S. Z. D.; Harris, F. W. *Macromolecules* **2007**, *40*, 889–900.

[112] Yadav, G. D.; Lande, S. V. *Advanced Synthesis & Catalysis* **2005**, *347*, 1235–1241.

[113] Keyworth, C. W.; Chan, K. L.; Labram, J. G.; Anthopoulos, T. D.; Watkins, S. E.; McKiernan, M.; White, A. J. P.; Holmes, A. B.; Williams, C. K. *Journal of Materials Chemistry* **2011**, *21*, 11800–11814.

[114] Cho, Y.-H.; Kina, A.; Shimada, T.; Hayashi, T. *The Journal of Organic Chemistry* **2004**, *69*, 3811–3823.

[115] Kuss-Petermann, M.; Wenger, O. S. *The Journal of Physical Chemistry A* **2013**, *117*, 5726–5733.

[116] Hankache, J.; Wenger, O. S. *Chemical Communications* **2011**, *47*, 10145–10147.

[117] Chen, J.; Kuss-Petermann, M.; Wenger, O. S. *Chemistry - A European Journal* **2014**, *20*, 4098–4104.

[118] Kuss-Petermann, M.; Wolf, H.; Stalke, D.; Wenger, O. S. *Journal of the American Chemical Society* **2012**, *134*, 12844–12854.

[119] Al-Rawashdeh, N. A. F.; Chatterjee, S.; Krause, J. A.; Connick, W. B. *Inorganic Chemistry* **2014**, *53*, 294–307.

[120] Kuss-Petermann, M.; Wenger, O. S. *Angewandte Chemie International Edition* **2016**, *55*, 815–819.

Curriculum Vitae

Personal Details

Name	Julia Nomrowski
Date of Birth	December 27th, 1988
Birthplace	Hildesheim, Lower Saxony, Germany

Education

2013 - Present	University of Basel (CH) Supervisor: Prof. Dr. Oliver S. Wenger
2011 - 2013	Georg-August University Göttingen (D) Master thesis: *“Photochemie und Photophysik von ausgewählten Metallkomplexen und organischen Molekülen”* Supervisor: Prof. Dr. Oliver S. Wenger
2008 - 2011	Georg-August University Göttingen (D) Bachelor thesis: *“Synthese eines molekularen Kabels”* Supervisor: Prof. Dr. Oliver S. Wenger
2002 - 2008	Scharnhorst Gymnasium Hildesheim (D) A-level: Chemistry, Mathematics, Physics, German, Politics

Publications

Julia Nomrowski, Oliver S. Wenger
“Photoinduced PCET in Ruthenium–Phenol Systems: Thermo- dynamic Equivalence of Uni- and Bidirectional Reactions”
Inorg. Chem. **2015**, *54*, 3680.

Awards

07/2017	Poster Award, 22st International Symposium on Photochemistry and Photophysics of Coordination Compounds, Oxford, United Kingdom
04/2016	2016 Chemistry Travel Award by SCNAT, SCS and SSFC (awarded with 1000 CHF)

Oral Presentations

08/2017	SCS Fall Meeting 2017 *"Light-driven electron-accumulation in a molecular pentad with potential inversion"* Bern, Switzerland
09/2016	25. Lecture Conference on Photochemistry *"Photoinduced electron accumulation in a molecular triad and thiol-disulfide interchange"* Jena, Germany
03/2015	Koordinationschemie-Tagung 2015 *"Protonengekoppelter Elektronentransfer mit angeregten Ruthenium-Komplexen"* Paderborn, Germany

Poster Presentations

07/2017	22st International Symposium on Photochemistry and Photophysics of Coordination Compounds *"Exploiting potential inversion for photodriven electron-accumulation in a molecular pentad"* Oxford, United Kingdom
09/2016	SCS Fall Meeting 2016 *"Light-induced electron accumulation in a molecular triad"* Zurich, Switzerland
03/2015	21st International Symposium on Photochemistry and Photophysics of Coordination Compounds *"Photoinduced Proton-Coupled Electron Transfer in Ruthenium- Phenol Systems"* Krakow, Poland